THE JOURNAL OF THE INSTITUTION OF ENGINEERS, MALAYSIA
KDN PP5476/10/2012 (030203)
ISSN 0126-513X e-ISSN 3083-8789

The Institution of Engineers, Malaysia

VOL. 86, NO. 4
DECEMBER 2025

Vol. 86, No. 4, December 2025
KDN PP5476/10/2012 (030203) ISSN 0126-513X

CONTENTS

THIS ISSUE WAS PUBLISHED IN JANUARY 2026

For advertisement placements and subscriptions, please contact:
DIMENSION PUBLISHING SDN. BHD. (449732-T)
Level 18-01, PJX-HM Shah Tower, No.16A, Persiaran Barat,
46050 Petaling Jaya, Selangor Darul Ehsan, Malaysia.
Tel: +(603) 7493 1049 Fax: +(603) 7493 1047
E-mail: info@dimensionpublishing.com

Printed by
SUPER YUETA PRINT
No. 40, Jalan PBS 14/8, Taman Perindustrian Bukit Serdang,
43300 Seri Kembangan, Selangor Darul Ehsan, Malaysia.

PRINT QUANTITY: *500 COPIES*

APPLICATION OF RECURRENT NEURAL NETWORK IN ACTUAL SHEAR RATE PREDICTION UNDER WALL SLIP PHENOMENON

Ren Jie Chin[1*], Sai Hin Lai[2], Kok Zee Kwong[3]

Abstract

Wall slip refers to the phenomenon where particles in a suspension move away from the boundary wall, creating a thin liquid-rich layer nearby. This occurrence can significantly affect rheological measurements, notably viscosity, shear stress, and shear rate. Suspensions find widespread use in various industries such as food processing, personal care products, pharmaceuticals, paints, medicine, and agrochemicals. Predicting the actual shear rate traditionally proves challenging, time-consuming, and cost-intensive. Hence, there's a pressing need for a computational model to perform this task with acceptable accuracy. Leveraging the precise input-output mapping capability of recurrent neural network (RNN), it was employed to develop a model for the actual shear rate prediction. Evaluation of these models through statistical analyses reveals that RNN model III outperforms others, boasting the highest coefficient of determination (0.9998), lowest mean squared error (0.000721), root mean squared error (0.001361), most negative Akaike information criterion (-18646.3), Bayesian information criterion (-18635.9), and the smallest percentage error (15%). This developed model provides an alternative means to predict suspension shear rate under experimental constraints.

Received: *9 April, 2025*
Revised: *9 May, 2025*
Accepted: *10 July, 2025*

[1,3]Department of Civil Engineering, Lee Kong Chian Faculty of Engineering and Science, Universiti Tunku Abdul Rahman, 43000 Kajang, Malaysia.

[2]Department of Civil Engineering, Faculty of Engineering, Universiti Malaysia Sarawak, 94300 Kota Samarahan, Sarawak, Malaysia.

****Corresponding author:***
chinrj@utar.edu.my

DOI:
https://doi.org/10.54552/v86i3.242

Keywords:
Actual shear rate; Recurrent neural network; Rheology; Suspension; Wall slip

1.0 INTRODUCTION

Rheology, a branch of physics concerned with the flow of matter, encompasses various intriguing phenomena such as shear-induced migration, pattern formation, and notably, wall slip, which is the primary focus of this study. Wall slip occurs in two-phase or multiphase flow systems where suspended particles migrate away from solid wall boundaries, leaving a thin liquid-rich layer nearby (Agrawal *et al.,* 2023; Ali *et al.,* 2022; Yan *et al.,* 2022). This phenomenon, characterised by a low-viscosity layer, facilitates fluid particle movement along the boundaries. Consequently, rheological measurements such as viscosity, shear rate, and shear stress are significantly influenced (Ahuja & Singh, 2009; Chin *et al.,* 2019a; Chin *et al.,* 2020).

Laboratory experiments have explored factors influencing wall slip. Research indicates that particle size affects wall slip velocity, with larger particles leading to increased slip velocity due to steric hindrance (Deng *et al.,* 2021; Deng *et al.,* 2022). Concentration and temperature also play significant roles, with lower concentrations and higher temperatures correlating with increased wall slip velocities (Akter & Desai, 2018; Barnes, 1995; Chen *et al.,* 2008; Jana *et al.,* 1995).

Determining the actual shear rate for suspensions experiencing wall slip is currently a laborious and costly task, necessitating a mathematical model to accurately predict rheological behavior under such conditions. Given the rise of artificial intelligence (AI), particularly the effectiveness of recurrent neural network (RNN) approaches in diverse fields, employing RNN for shear rate prediction is logical (Deng, 2019; Lai *et al.,* 2022; Loh *et al.,* 2021). This study aims to develop a computational model for predicting actual shear rates in rheological systems affected by wall slip.

2.0 MATERIALS AND METHODS

2.1 Data Collection

Laboratory rheological experiments were undertaken to gather initial data in preparation for the model development. The samples tested involved a mixture of poly(methyl) methacrylate (PMMA) and glycerine. To ensure the reliability of the experimental data, the standard procedures were strictly adhered (Ahuja & Singh, 2009; Chin *et al.,* 2018; Yoshimura & Prud'homme, 1988). Initially, both PMMA particle and glycerine densities were set at 1300 kg/m^3 (Chin *et al.,* 2018; Shaliza *et al.,* 2015). This choice aimed to achieve a neutrally buoyant suspension and prevent density discrepancies that could affect result accuracy (Ahuja and Singh, 2009; Buscall *et al.,* 1993).

Rheological tests were carried out using a rheometer equipped with a 50 mm diameter parallel plate, with gap heights of 0.75 mm and 1.0 mm. The experiments encompassed six different volumetric concentrations (40%, 45%, 48%, 50%, 52%, and 55%), five temperatures (15°C, 25°C, 35°C, 45°C, and 55°C), and three particle sizes (18 μm, 75.3 μm, and 195.5 μm).

Recurrent neural network (RNN) is a type of deep learning artificial intelligence approach. Its outstanding uniqueness is its ability to handle long sequences of input data. Among the available RNN types, long short term memory (LSTM) was selected to train the model in this research study. LSTM is considered as an advanced RNN because of its ability to solve the vanishing gradient problem in normal RNN through its special structures, known as gates (Gers *et al.,* 2000; Hochreiter & Schmidhuber, 1997; Le *et al.,* 2015).

Similar to the other types of artificial neural networks, RNN consists of three layers which are input layer, hidden layer, and output layer. Among layers, the design of the hidden layers is the most essential as it plays a role as the computational part in a neural network. Mean squared error (MSE) was fixed as the loss function in this research study. A loss function is a measure of how good a prediction model does in terms of being able to predict the expected outcome. MSE is the sum of squared distances between the target variable and predicted values and it is the most commonly used regression loss function (Liu & Sullivan, 2019; Yu *et al.,* 2018). On the other hand, Adaptive Moment Estimation (Adam) optimiser was assigned as the optimisation algorithm. It is an optimisation algorithm that can be used instead of the classical stochastic gradient descent procedure to update network weights iterative based on training data. It is well suited for problems that are large in terms of data and parameters, straightforward to implement and computationally efficient (Liu & Sullivan, 2019; Ruiz *et al.,* 2019).

In addition, the selection of parameters such as learning rate, batch size and activation function is considerably important in designing the architecture of RNN model. Thereby, trial-and-error method was applied to determine the combination that provides the best performance in term of model accuracy. Figure 1 displays the architecture of RNN model.

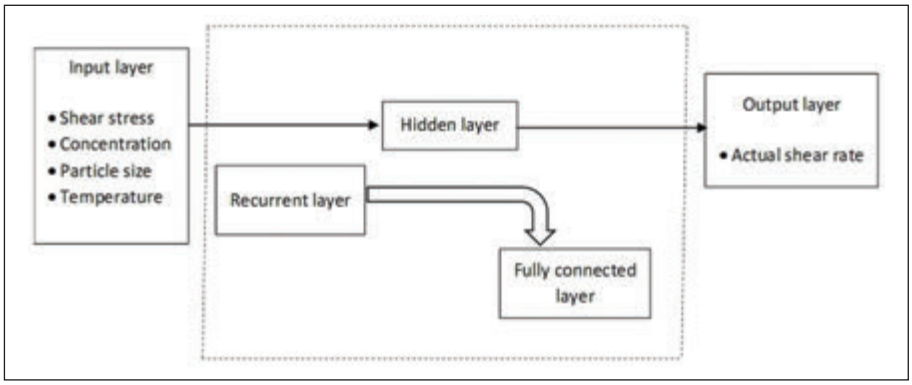

Figure 1: Architecture of RNN

2.3 Statistical Analyses

The effectiveness of all the constructed models was evaluated through a range of statistical analyses, including the coefficient of determination (R^2), mean absolute error (MAE), root mean squared error (RMSE), percentage error (% error), Akaike information criterion (AIC), and Bayesian information criterion (BIC). These analyses aimed to assess the models' suitability in accurately predicting the actual shear rate for suspensions under wall slip conditions (Chin *et al.,* 2019a).

$$R^2 = \left(\frac{n\sum x_i y_i - \sum x_i \sum y_i}{\sqrt{n\sum x_i^2 - (\sum x_i)^2}\sqrt{n\sum y_i^2 - (\sum y_i)^2}}\right)^2 \quad (1)$$

$$MAE = \frac{\sum|y_i - x_i|}{n} \quad (2)$$

$$RMSE = \sqrt{\frac{1}{n}\sum(y_i - x_i)^2} \quad (3)$$

$$\text{Percentage error} = \frac{|True\ value - Predicted\ value|}{True\ value} \times 100\% \quad (4)$$

$$AIC = -2\log L + 2K \quad (5)$$

$$-2\log L = n(\log 2\pi + 1 + \log\frac{RSS}{n}) \quad (6)$$

$$BIC = -2\log L + K\log n \quad (7)$$

where n is the number of data pairs, x is the observed variable, y is the predicted variable, K is the number of model parameters (the number of variables in the model plus the intercept), L is maximised likelihood, and RSS is residual sum of squares.

3.0 RESULTS AND DISCUSSION

3.1 RNN Models Evaluation

A total of 9000 datasets were gathered from rheological tests. Among these, 7200 datasets (equivalent to 80% of the total) were allocated for training the RNN model, while the remaining 1800 datasets were set aside for testing purposes. Previous studies suggest that the typical range for training data percentage lies between 60% to 80% (Akter & Desai, 2018; Alimissis *et al.,* 2018; Zhang *et al.,* 2018). In this instance, the upper limit was chosen to facilitate the models in capturing the most comprehensive input-output patterns.While designing the architecture of RNN, the choice of the parameters such as batch size, learning rate and activation function in recurrent layer play an important role to achieve a presentable output. Under such a circumstance, a series of RNN models which differ in term of the above-mentioned parameters were developed. However, only the selected models (as shown in Table 1) were discussed in this section. The statistical performance of each RNN model was presented in Table 2.

From Table 2, the developed RNN models were evaluated using R^2, MAE, RMSE, AIC and BIC. Among the examined models, the highest recorded R^2 value is 0.9998. Such a value which is approximate to 1 which reflects that there is a very strong relationship between the predicted value and actual value. On the other hand, it is noticed that the MAE and RMSE values show a decreasing from model I to model III and then the trend was turned over after model III, meaning that the performance of the model III is the best in term of MAE and RMSE among the investigated RNN models. AIC is defined as analysis to determine the relative quality of a statistical model for a given set of data. In other words, it is a measure of the goodness of fit of an estimated statistical model. Meanwhile, BIC is a type of model selection among a class of parametric models with different numbers of parameters. According to the general rule,

the model with a more negative AIC and BIC values is more favourable as the estimated values are considerably well-suited to the developed model. The model that meets the criterion is model III. Both of its AIC and BIC values is the most negative, showing that the predicted value fit the best in model III.

Table 1: Parameters combination corresponding to each RNN model

Models	Epoch	Batch Size	Learning Rate	Activation Function in Recurrent Layer
I	256	20	0.000010	ReLu
II	256	20	0.000010	Sigmoid
III	256	20	0.000010	Tanh
IV	256	40	0.000010	Tanh
V	256	20	0.000100	Tanh
VI	256	20	0.000001	Tanh

Table 2: Statistical performance of each RNN model

Models	R^2	MAE	RMSE	AIC	BIC
I	0.8972	0.026321	0.039757	-6497.5	-6486.5
II	0.9737	0.011739	0.016056	-9761.6	-9750.6
III	0.9998	0.000721	0.001361	-18646.3	-18635.3
IV	0.9873	0.008391	0.011412	-10990.7	-10979.7
V	0.9613	0.017883	0.022510	-8545.3	-8534.3
VI	0.8532	0.029563	0.040982	-6388.3	-6377.3

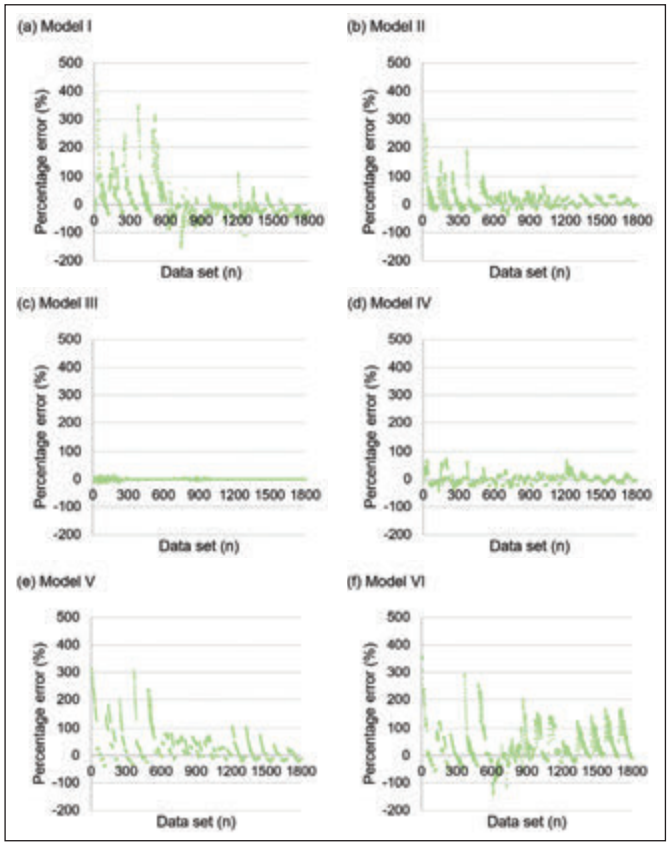

Figure 2: Percentage error of the respective dataset corresponding to each RNN model

Percentage error is another important indicator to evaluate the performance of a mathematical model. The smaller the percentage error, the better the performance of the computational model. In other words, a low percentage error describes a more accurate prediction. Figure 2 shows the percentage error with respect to each dataset corresponding to each RNN model while Figure 3 exhibits the maximum percentage error of each RNN model. In sum, most of the models display a wide range of percentage error with a maximum percentage error approximates to 75% or even higher, indicating that the predicted value from the models has a huge difference with the actual value. However, the only and one model which does not follow such trend is model III. It shows an outstanding performance in terms of percentage error where the percentage error of all its predicted dataset fall within the range of ±15%, meaning that the model can achieve at least 85% of accuracy. At the same time, its maximum percentage error is recorded at 15%, showing that the degree of difference between the observed and predicted value is considerably low.

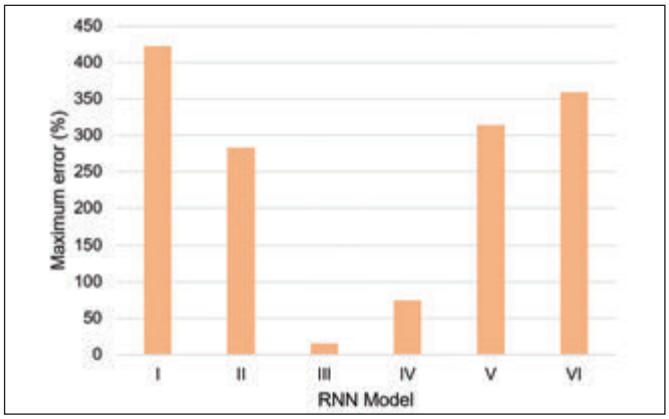

Figure 3: Maximum percentage error for each RNN model

Therefore, with such outstanding performance as discussed above, the highest R^2 value of 0.9998, lowest MAE value of 0.000721 and RMSE value of 0.001361, most negative AIC value of -18646.3 and BIC value of -18635.3 and smallest maximum percentage error of 15%, model III has become the prior choice among the examined RNN models.

3.2 Models Comparison

In a previous study, a multilayer perceptron neural network (MLP-NN) (Chin *et al.,* 2019b) model and radial basis function network (RBFN) (Chin *et al.,* 2023) were developed to predict actual shear rates. However, there is still considerable room for improvement to achieve a higher level of prediction accuracy.

In this section, the best-performing RNN model was compared with the MLP-NN model (Chin *et al.,* 2019b) and RBFN (Chin *et al.,* 2023) using a series of statistical analyses, including coefficient of determination, mean absolute error, root mean squared error, Akaike information criterion, Bayesian information criterion, and percentage error.

As depicted in Table 3, a significant improvement is evident across all evaluated aspects when comparing the MLP-NN and RBFN models to the RNN model. Firstly, in terms of MAE

and RMSE errors, the RNN model exhibits the lowest values, followed by the RBFN model and then the MLP-NN model, indicating that the RNN model can generate more accurate outputs. Similarly, a comparable trend is observable from the perspective of AIC and BIC. The most negative values are observed in the RNN model, suggesting that the predicted output fits better in the RNN model compared to the MLP-NN and RBFN models.

Lastly, in terms of percentage error, which is a crucial indicator in AI prediction model development, the error, as shown in Figure 4, has improved from the previously developed MLP-NN model (75%) and RBFN model (53%) to RNN model (15%). In other words, the maximum percentage error has been significantly reduced, with the RNN model achieving a substantial improvement of around 40%.

Table 3: Comparison of the best-performed model corresponding to each AI technique

Model	MLP-NN (Chin *et al.* 2019b)	RBFN (Chin *et al.*, 2023)	RNN
R^2	0.9967	0.9998	0.9998
MAE	1.146804	0.001058	0.000721
RMSE	1.652898	0.001447	0.001361
AIC	-7657.3	-18426.5	-18646.3
BIC	-7646.4	-18415.5	-18635.9
Max. % Error	75	53	15

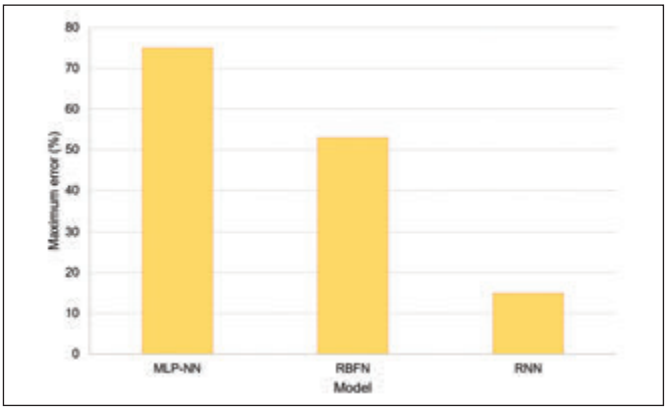

Figure 4: Maximum percentage error with respect to each model

4.0 CONCLUSION

The primary objective of this research study is to assess the suitability of RNN approaches in constructing mathematical computational models capable of accurately predicting real-life outputs. When designing the architecture of the RNN model, selecting parameters such as batch size, learning rate, and activation function is a crucial step. Hence, a trial-and-error method was employed to determine the most suitable parameters for the RNN models, aiming to achieve improved prediction accuracy.

In this study, numerous RNN models were constructed, and their performance was evaluated through various statistical analyses. Among the examined RNN models, model III demonstrated outstanding performance. It attained an R^2-value of 0.9998, mean absolute error of 0.000721, root mean squared error of 0.001361, Akaike information criterion of -18646.3, Bayesian information criterion of -18635.9, and maximum percentage error of 15%. Comparing the developed RNN model with the MLP-NN and RBFN models from previous literature, a significant improvement in model performance is evident, particularly in the RNN model, where the maximum percentage error has reduced to 15%, representing an almost fivefold enhancement. These findings highlight the potential for enhancing AI prediction models by implementing more advanced approaches, leveraging their unique features to improve overall performance.

There are some recommendations for future work. Since the RNN has successfully improved the prediction accuracy, it shows that an advanced machine learning model performs better than the conventional model (MLP-NN and RBFN). So, it should seek the possibility of integrating the RNN with different optimisation algorithms to form a hybrid model for prediction accuracy improvement purposes. In addition, a wider range of datasets can be collected, by using different particle sizes and temperatures. ■

ACKNOWLEDGMENT

This research was supported by the Ministry of Higher Education (MoHE) Malaysia through the Fundamental Research Grant Scheme project (FRGS/1/2023/WAB02/UTAR/02/1) and was partly supported by Malaysia Toray Science Foundation (4417/0005).

AUTHORS' CONTRIBUTIONS

- **Ren Jie Chin**: Conceptualisation, study design, data collection, formal analysis and Writing—original draft preparation.
- **Sai Hin Lai**: Conceptualisation, and Supervision
- **Kok Zee Kwong**: Literature review, and Writing—Review and Editing.

REFERENCES

[1] Agrawal, S., Das, P. K., & Dhar, P. (2023). Microfluidic soluto-hydrodynamics using interactive patterned wall-slip and oscillatory thermo-capillarity. *Microfluidics and Nanofluidics, 27,* 18. https://doi.org/10.1007/s10404-023-02627-6.

[2] Ahuja, A., & Singh, A. (2009). Slip velocity of concentrated suspensions in Couette flow. *Journal of Rheology, 53,* 1461-1485. https://doi.org/10.1122/1.3213090.

[3] Akter, T., & Desai, S. (2018). Developing a predictive model for nanoimprint lithography using neural networks. *Materials and Design, 160,* 836-848. https://doi.org/10.1016/j.matdes.2018.10.005.

[4] Ali, A., Sarkar, S., Das, S., & Jana, R. N. (2022). A report on entropy generation and Arrhenius kinetics in magneto-bioconvective flow of Cross nanofluid over a cylinder with wall slip. *International Journal of Ambient Energy,* 1-16. https://doi.org/10.1080/01430750.2022.2031292.

[5] Alimissis, A., Philippopoulos, K., Tzanis, C. G., & Deligiorgi, D. (2018). Spatial estimation of urban air pollution with the use of artificial neural network models. *Atmospheric Environment, 191,* 205-213. https://doi.org/10.1016/j.atmosenv.2018.07.058.

[6] Barnes, H. A. (1995). A review of the slip (wall depletion) of polymer solutions, emulsions and particle suspensions in viscometers: its cause, character and cure. *Journal of Non-Newtonian Fluid Mechanics, 56,* 221-251. https://doi.org/10.1016/0377-0257(94)01282-M.

[7] Buscall, R., McGowan, J., & Morton-Jones, A. J. (1993). The rheology of concentrated dispersions of weakly attracting colloidal particles with and without wall slip. *Journal of Rheology, 37,* 621-641. https://doi.org/10.1122/1.550387.

[8] Chen, L., Duan, Y., Zhao, G., & Liu, M. (2008). Effects of temperature, solid particle size and concentration on wall slip behaviour of coal-water slurry in pipelines. *Journal of Chemical Industry and Engineering (China), 59*(9), 2206-2213.

[9] Chin, R. J., Lai, S. H., Shaliza, I., & Wan Zurina, W. J. (2018). Factors affect wall slip: Particle size, concentration and temperature. *Applied Rheology, 28,* 15775-1-9. https://doi.org/10.3933/applrheol-28-15775.

[10] Chin, R. J., Lai, S. H., Shaliza, I., Wan Zurina, W. J., & Elshafie, A. (2019a). Rheological wall slip velocity prediction model based on artificial neural network. *Journal of Experimental and Theoretical Artificial Intelligence, 31*(4), 659-676. https://doi.org/10.1080/0952813X.2019.1592235.

[11] Chin, R. J., Lai, S. H., Shaliza, I., Wan Zurina, W. J., & Ahmed Elshafie, A. H. (2019b). New approach to mimic rheological actual shear rate under wall slip condition. *Engineering with Computers, 35,* 1409-1418. https://doi.org/10.1007/s00366-018-0670-y.

[12] Chin, R. J., Lai, S. H., Shaliza, I., Wan Zurina, W. J., & Elshafie, A. (2020). ANFIS-based model for predicting actual shear rate associated with wall slip phenomenon. *Soft Computing, 24,* 9639-9649. https://doi.org/10.1007/s00500-019-04475-5.

[13] Chin, R. J., Lai, S. H., Lee, F. W., & Kwong, K. Z. (2023). Actual shear rate prediction associated with wall slip phenomenon using radial basis function network. *The Journal of The Institution of Engineers Malaysia, 84*(1), 16-21. https://doi.org/10.54552/v84i1.206.

[14] Deng, B., Chin, R. J., Tang, Y., Jiang, C., & Lai, S. H. (2019). New approach to predict the motion characteristics of single bubbles in still water. *Applied Sciences, 9*(19), 3981. https://doi.org/10.3390/app9193981.

[15] Deng, B., Lai, S. H., Jiang, C., Kumar, P., El-Shafie, A., & Chin, R. J. (2021). Advanced water level prediction for a large-scale river–lake system using hybrid soft computing approach: a case study in Dongting Lake, China. *Earth Science Informatics, 14,* 1987-2001. https://doi.org/10.1007/s12145-021-00665-8

[16] Deng, B., Liu, P., Chin, R. J., Kumar, P., Jiang, C., Xiang, Y., . . . Luo, H. (2022). Hybrid metaheuristic machine learning approach for water level prediction: A case study in Dongting Lake. *Frontiers in Earth Science, 10*. https://doi.org/10.3389/feart.2022.928052

[17] Gers, F. A., Schmidhuber, J., & Cummins, F. (2000). Learning to forget: Continual prediction with LSTM. *Neural Computation, 12*(10), 2451-2471. https://doi.org/10.1162/089976600300015015

[18] Hochreiter, S., & Schmidhuber, J. (1997). Long short-term memory. *Neural Computation, 9*(8), 1735-1780. https://doi.org/10.1162/neco.1997.9.8.1735.

[19] Jana, S. C., Kapoor, B., & Acrivos, A. (1995). Apparent wall slip velocity coefficients in concentrated suspensions of noncolloidal particles. *Journal of Rheology, 39*(6), 1123-1132. https://doi.org/10.1122/1.550631.

[20] Lai, S. H., Bu, C. H., Chin, R. J., Goh, X. T., & Teo, F. Y. (2022). New approach to predict fecal coliform removal for stormwater biofilters application. *IIUM Engineering Journal, 23*(2), 45-58. https://doi.org/10.31436/iiumej.v23i2.2173.

[21] Le, Q. V., Jaitly, N., & Hinton, G. E. (2015). A simple way to initialize recurrent networks of rectified linear units. *arXiv:1504.00941.* https://doi.org/10.48550/arXiv.1504.00941.

[22] Liu, Z., & Sullivan, C. J. (2019). Prediction of weather induced background radiation fluctuation with recurrent neural networks. *Radiation Physics and Chemistry, 155,* 275-280. https://doi.org/10.1016/j.radphyschem.2018.03.005.

[23] Loh, W. S., Chin, R. J., Ling, L., Lai, S. H., & Soo, E. Z. (2021). Application of machine learning model for the prediction of settling velocity of fine sediments. *Mathematics, 9*(23), 3141. https://doi.org/10.3390/math9233141.

[24] Ruiz, L. G., Capel, M. I., & C.Pegalajar, M. (2019). Parallel memetic algorithm for training recurrent neural networks for the energy efficiency problem. *Applied Soft Computing, 76,* 356-368. https://doi.org/10.1016/j.asoc.2018.12.028.

[25] Shaliza, I., Wong, S. D., Baker, I. F., Zamzam, Z., Sato, M., & Kato, Y. (2015). Influence of geometry and slurry properties on fine particles suspension at high loadings in a stirred vessel. *Chemical Engineering Research and Design, 94,* 324-336. https://doi.org/10.1016/j.cherd.2014.08.008.

[26] Yan, Z., Yin, S., Chen, X., & Wang, L. (2022). Rheological properties and wall-slip behavior of cemented tailing-waste rock backfill (CTWB) paste. *Construction and Building Materials, 324,* 126723. https://doi.org/10.1016/j.conbuildmat.2022.126723.

[27] Yoshimura, A., & Prud'homme, R. (1988). Wall slip corrections for Couette and parallel disk viscometers. *Journal of Rheology, 32,* 53-67. https://doi.org/10.1122/1.549963.

[28] Zhang, Y., Chen, H., Yang, B., Fu, S., & Jie Yu, Z. W. (2018). Prediction of phosphate concentrate grade based on artificial neural network modeling. *Results in Physics, 11,* 625-628. https://doi.org/10.1016/j.rinp.2018.10.011.

PROFILES

REN JIE CHIN received his BEng. and Ph.D. degrees in Environmental Engineering from University of Malaya, Malaysia, in 2015 and 2019, respectively. He is currently an Assistant Professor in the Department of Civil Engineering, Lee Kong Chian Faculty of Engineering and Science, Universiti Tunku Abdul Rahman, Malaysia. He is a registered Professional Technologist (Malaysia Board of Technologists). He has been the leader or been part of the team for about several national and international research projects. His research direction focused on flood, drought, and water resources management in the context of climate change, which involved computational simulation, development of decision support system, artificial intelligent, and optimisation models. He has published a total number of 48 research papers in reputed ISI journals and conference proceedings.
Email address: chinrj@utar.edu.my

SAI HIN LAI is a Professor at the Department of Civil Engineering, Faculty of Engineering, University Malaysia Sarawak. He is a registered Professional Engineer (PEng, Malaysia), Chartered Engineer (CEng, UK), Fellow of Asean Academy of Engineering & Technology (FAAET), and Institution of Engineering and Technology (FIET). He has been the leader or been part of the team for about 50 national and international research projects. His researches are focused on flood, drought, and water resources management in the context of climate change, which involved computational simulation, development of decision support systems, artificial intelligence models & latest optimisation techniques. He has published more than 100 research articles in reputed SCI journals, and delivered about 20 keynote / invited speeches in the past 5 years.
Email address: shlai@unimas.my

KOK ZEE KWONG received his BEng. (Civil and Construction Engineering) from Curtin University of Technology, Malaysia. He received his Ph.D. (Civil Engineering) from Universiti Malaysia Sabah. He is currently an Assistant Professor in the Department of Civil Engineering, Lee Kong Chian Faculty of Engineering and Science, Universiti Tunku Abdul Rahman, Malaysia. He is a registered Professional Engineer (PEng, Malaysia). He has been the leader or been part of the team for about several national and international research projects. His research direction focused on structural engineering (NDT structural assessment and health monitoring as well as piezoelectric smart material). He has published a total number of 21 research papers in reputed ISI journals and conference proceedings.
Email address: kwongkz@utar.edu.my

EFFECT OF HYDROGEN PEROXIDE AS AN OXIDANT FOR THE WET TORREFACTION OF PALM KERNEL SHELL

Poh Lae Ooi[1], Rui Hong Teoh[2], Lai Yee Lee[3], Suyin Gan[4], Revathi Raviadaran[5], Sona R. Moharir[6], Suchithra Thangalazhy-Gopakumar[7*]

Abstract

Hydrogen peroxide (H_2O_2) is a green oxidant for hydrothermal treatment of biomass. In this research, the effect of hydrogen peroxide (H_2O_2) for the wet torrefaction of palm kernel shell (PKS) was studied. H_2O_2 can give extra intensity to reaction severity during the wet torrefaction process. The effect of H_2O_2 dosages from 0.0 M to 1.0 M at 200 °C was investigated. The mass yield of torrified PKS varied from 59.8 wt. % to 50.6 wt. % as H_2O_2 dosage increased. The trends of greater fixed carbon content, higher ash content, and lower moisture content were similar for torrified PKS treated with and without H_2O_2, as compared to raw PKS. The FTIR analysis revealed an increase in the breakdown of lignocellulosic components with torrefaction severity in the torrified PKS. The average HHV was 21.62 MJ/kg for different H_2O_2 dosages. Overall, the findings demonstrated that H_2O_2 did not make a substantial contribution to further enhancing the solid fuel properties. However, a higher degradation of cellulose and lignin components to liquid was achieved during the wet torrefaction process.

Received: *10 September, 2024*
Revised: *10 April, 2025*
Accepted: *15 May, 2025*

[1,2,3,4,7]Department of Chemical and Environmental Engineering, Faculty of Science and Engineering, University of Nottingham Malaysia, Jalan Broga, 43500, Semenyih, Selangor, Malaysia.

[5]HICoE-Centre for Biofuel and Biochemical Research, Institute of Self-Sustainable Building, Department of Chemical Engineering, Universiti Teknologi PETRONAS, 32610, Seri Iskandar, Perak, Malaysia.

[6]Chemical Engineering Department, Bharati Vidyapeeth College of Engineering, Navi Mumbai, Maharashtra, India.

****Corresponding author:***
suchithra.thangalazhy@nottingham.edu.my

DOI:
https://doi.org/10.54552/v86i3.262

Keywords:
Hydrogen peroxide, Mass yield, Palm kernel shell, Proximate analysis, Wet torrefaction

1.0 INTRODUCTION

The rapid rise in energy demand excites the growth of renewable energy resources like biomass, wind, and solar energy. Biomass is greatly utilised among renewable energy resources and could account for up to 12% of global consumption (Krysanova *et al.,* 2019). However, low heating value, bulk density, high moisture content, and poor grindability (Specific energy consumption for grinding) offer significant limitations to the practical usage of biomass as a fuel source. These drawbacks result in higher costs of handling, transportation, and storage of biomass fuels. The pre-treatment process known as torrefaction is suggested to address these limitations of biomass. Torrefaction upgrades biomass into energy-dense solid fuels with improved properties like higher heating value, lower moisture content, and much better grindability than raw biomass (Ullah *et al.,* 2021).

Wet torrefaction (WT) can be described as a conversion process in a hydrothermal medium or hot compressed water at temperatures ranging from 180 °C to 260 °C (He *et al.,* 2018). At the threshold of the critical point, the characteristics of liquid water undergo notable changes such as the density and viscosity of hot compressed water (HCW) decrease, resulting in an increased mass transfer of chemical compounds (Phuang *et al.,* 2021). The enhanced transport properties of HCW expedite reactions, making it an outstanding medium for WT (Bach & Skreiberg, 2016). In addition, water improves its ability to dissolve organic compounds, makes it an exceptional reaction medium for facilitating reactions (Cortes-Clerget *et al.,* 2021).

Wet torrefaction is inspired by the concept of hydrothermal carbonisation (HTC), introduced by the German Nobel laureate, Friedrich Bergius (Bach & Skreiberg, 2016). Although WT is somehow similar to HTC, they are notably distinct from one another. WT is employed to produce solid biomass fuels with enhanced properties as feedstock for combustion, gasification,

and pyrolysis; whereas HTC is applied to synthesise carbonaceous char with higher carbon content to apply as energy storage, fertilisers, and activated carbon (He *et al.,* 2018). Operating parameters such as reaction temperature, reaction time, water-to-biomass ratio, and catalyst amount influence the effectiveness of WT in improving the properties of biomass-derived fuel.

Soh *et al.* studied the effect of temperature and residence time of wet torrefaction on the yield and inorganic content of two biomass. They reported that the wet torrified mass yield of empty fruit bunches (EFB) and oil palm trunks (OPT) decreased from 80.50 wt% to 62.89 wt% and from 64.58 wt% to 51.34 wt% respectively with increasing temperature from 180 °C to 240 °C. The energy density of EFB and OPT increased from 1.037 to 1.171 and from 1.070 to 1.147 respectively with increasing temperatures (Soh *et al.,* 2021). Moreover, Soh *et al.* reported that the torrified mass yield of EFB and OPT reduced 69.88 wt% to 62.89 wt% and from 62.47 wt% to 51.34 wt% respectively with elevated residence time from 2 to 3 h. (Soh *et al.,* 2021). Nevertheless, the influence of residence time on mass yield is not as significant compared to that of reaction temperature. Furthermore, Gan *et al.* studied the effect of temperature, water-to-biomass ratio, and residence time of WT on palm kernel shell whereas Phuang *et al.* studied the effect of temperature and water-to-biomass ratio of WT on yard waste. Both their studies revealed that the effect of the water-to-biomass ratio is rather insignificant (Gan *et al.,* 2019; Phuang *et al.,* 2021).

Chen *et al.* studied premixed dry spent coffee grounds (SCGs) with H_2O_2 and taken for dry torrefaction to improve HHVs of torrified biomass without extra energy input. They found that pretreatment with 18% H_2O_2 solution had a 7.8 % higher carbon content and 6.5 % higher HHV compared to the unpretreated one (Chen *et al.,* 2022). At higher operating conditions, H_2O_2 is decomposed into hydrogen cations (H^+) and perhydroxyl anion (HO_2-). HO_2- ion contacts with another peroxide molecule and forms free radicals like the hydroxyl ($HO^•$) and peryhdroxyl ($HO_2^•$) radicals. Perhydroxyl and water are formed from the reaction of the hydroxyl radicals ($HO^•$) and more peroxide molecules until all peroxide is converted into water. As a result, free radicals like $HO^•$ and $HO_2^•$ contribute to organic matter decomposition (Torres *et al.,* 2014). Therefore, the fuel properties of torrified biomass can be further improved through the utilisation of hydrogen peroxide (H_2O_2) as an oxidant during the biomass pre-treatment process. As of now, there is no literature reporting the application of oxidants to the WT process. Further investigation regarding the significance of varying dosages of H_2O_2 in the WT process will be addressed in this study. In this research, the authors hypothesised that the addition of H_2O_2 would provide higher severity in reaction than the corresponding temperature and pressure.

Palm kernel shell (PKS) is produced abundantly from the palm oil industry and therefore can be utilised as the raw material for wet torrefaction (WT). According to Gan *et al.,* the optimal temperature range for wet torrefaction under energy-efficient conditions should be between 180 °C to 220 °C (Gan *et al.,* 2019). Therefore, in the current research, the effects of H_2O_2 on the WT process were investigated using different dosages (0.0 M to 1.0 M) of H_2O_2 solution at a constant temperature of 200 °C with a residence time of 20 min and a biomass-to-water ratio of 0.15. These parameters were selected based on Gan *et al.*'s study. Raw and torrified PKS samples were analysed for thermogravimetry, proximate and ultimate analysis, HHV, and Fourier-Transform Infrared Spectroscopy (FTIR) whereas the liquid samples were analysed by pH and FTIR.

2.0 EXPERIMENTAL METHODOLOGY

2.1 Sample Preparation

The feedstock utilised in this research was PKS, which was procured from the Seri Ulu Langat Palm Oil Mill, located in Dengkil, Malaysia. The PKS was dried in an oven for 16 h at 75 °C.

2.2 Wet Torrefaction Experiments

The wet torrefaction of PKS was performed using a stainless-steel 1L high-pressure reactor autoclave (Model A 2335, Amar Equipment Pvt. Ltd.) capable of withstanding a maximum pressure of 350 bar and a temperature of 500 °C. Approximately 15 g of the PKS sample was placed into the reactor with a suitable amount of distilled water according to the H_2O_2 dosage. The autoclave and reactor vessel were firmly sealed with clamp bolts to prevent leakage during WT. A thermocouple was inserted to monitor the reaction temperature, while the sampling and vent ports were secured to enable pressure build-up in the reactor during the experiment. The mixture was continuously stirred at a rate of 107 rpm throughout the process. An automatic proportional integral derivative-controlled 2250-watt ceramic heater was then activated to increase the reactor temperature to the predetermined value. The pressure and temperature inside the reactor were recorded at 3-minute intervals until the desired temperature was reached. Once the desired temperature was reached, it was maintained for 20 min. The heater and stirrer were turned off after the experiment, and the reactor was allowed to cool down to ambient temperature, with the torrified biomass slurry left inside. The reactor vessel was then removed, and the slurry product was poured into a clean container. The reactor vessel was rinsed repeatedly with distilled water to collect all materials that had adhered to the reactor wall. The slurry products, which contained both solid and liquid products, were filtered and filtered through vacuum filtration and solid products were dried in an oven for 24 h at 103 °C. The torrified biomass was stored in a zipper storage bag at room temperature. The filtrate (liquid product) was measured for its volume and stored in a bottle in the fridge before further analysis.

The raw PKS sample and the H_2O_2-aided torrified PKS samples were labelled as raw PKS and TB $_{xxx}$, respectively. For instance, TB $_{0.000}$ represents torrified biomass without the use of H_2O_2 whilst TB $_{0.004}$ means torrified biomass with 0.004 M of H_2O_2.

To study the impact of oxidant-aiding wet torrefaction on PKS, the physicochemical properties of PKS before and after wet torrefaction at various H_2O_2 dosages were evaluated. By knowing the mass of raw and wet-torrified PKS before and after each run, the mass yield can be obtained using equation (1). Also, by knowing the volume of liquid feed and the volume

of the filtrate obtained after each run, the liquid yield can be calculated using equation (2).

$$\text{Mass yield (\%)} = \frac{m_{\text{solid torrefied PKS}}}{m_{\text{raw PKS}}} \times 100\% \quad (1)$$

$$\text{Liquid yield (\%)} = \frac{\text{volume of filtrate}}{\text{volume of liquid feed}} \times 100\% \quad (2)$$

2.3 Characterisation of Raw and Wet-Torrified Palm Kernel Shell

The proximate analysis of raw and torrified samples was analysed in a thermogravimetric analyser (TGA−DSC1, Mettler Toledo). 10 mg of the samples were heated fro m room temperature to 110 °C at a constant heating rate of 10 °C/min with a nitrogen flow rate of 20 mL/min. The temperature was maintained at 110 °C for 10 min. Subsequently, the samples were subjected to a constant heating rate of 10 °C/min and heated from 110 °C to 900 °C, following which they were maintained at 900 °C for 5 minutes. This was followed by the replacement of nitrogen with oxygen, with an oxygen flow rate of 20 mL/min, and the sample was kept at a constant temperature of 900 °C for an additional 10 minutes. The weight loss until 110 °C and the weight loss from 110 °C to 900 °C were regarded as moisture content (MC) and volatile matter (VM), respectively. In addition, the moisture and ash contents of biomass samples were determined manually to validate the results. In order to obtain the moisture content, 1 g of the sample was dried in an oven at 105 °C for 16 h and then allowed to cool in a desiccator with the use of silica gel as the drying agent. For the ash content, 1 g of the sample was ignited in an ashing furnace at 575 °C for 3 h and then allowed to cool in a desiccator with the use of silica gel as the drying agent. The fixed carbon (FC) can then be calculated using equation (3).

TB $_{0.050}$, TB $_{0.500}$, and TB $_{1.000}$ as samples were identified for their ultimate analysis as weight percentages (wt. %) of carbon, hydrogen, nitrogen, and sulphur in PKS using a CHNS elemental analyser (vario MACRO cube, Elementar), whilst the weight percentage of oxygen was calculated using equation (4).

$$\text{FC (\%)} = 100 - \text{MC(\%)} - \text{VM(\%)} - \text{AC(\%)} \quad (3)$$

$$\text{O (\%)} = 100 - \text{C(\%)} - \text{H(\%)} - \text{N(\%)} - \text{S(\%)} - \text{AC(\%)} \quad (4)$$

TB $_{0.004}$, TB $_{0.050}$, TB $_{0.100}$, TB $_{0.500}$, and TB $_{1.000}$ samples were sent to Universiti Teknologi PETRONAS, Perak for higher heating values (HHV) evaluation. Also, the fuel ratio (FR), combustibility index (CI), and volatile ignitability (VI) were calculated using equations (5), (6), and (7), respectively (Allouzi *et al.,* 2023).

$$\text{FR} = \frac{\text{FC}_{\text{dry basis}}}{\text{VM}_{\text{dry basis}}} \quad (5)$$

$$\text{CI (MJ/kg)} = \text{HHV}_{\text{dry basis}} \times (115 - \text{AC}_{\text{dry basis}}) \times \frac{1}{105\text{FR}} \quad (6)$$

$$\text{VI (MJ/kg)} = \frac{\text{HHV}_{\text{dry basis}} - 0.338\text{FC}_{\text{dry basis}}}{\text{VM}_{\text{dry basis}} - \text{FC}_{\text{dry basis}}} \quad (7)$$

Raw PKS, TB $_{0.004}$, TB $_{0.500}$, and TB $_{1.000}$ samples were assessed for their chemical changes in molecular bonding and functional groups using the Fourier transform infrared spectroscopy (FTIR, Spectrum RXI Perkin-Elmer) with attenuated total reflection (ATR) detector. Before scanning, the ATR diamond region was cleaned with acetone to ensure cleanliness. Samples were then placed in contact with the diamond crystal of the ATR device. The FTIR analyses for samples were run in the spectral range of 400 − 4000 cm^{-1} at a room temperature of 25 °C by reading an average of 8 scans with a resolution of 2 cm^{-1}.

3.0 RESULTS AND DISCUSSION

3.1 Wet Torrefaction Process and Products Yields

The primary objective of wet torrefaction process is to break down the complex polymer structures in biomass into shorter chains with lower molecular weights, thereby improving its fuel properties. In this research, H_2O_2 was shown to have a perceptible effect on the mass yield of torrified PKS, as shown in Table 1. The mass yield decreased with the increase in H_2O_2 dosage, especially while 1.0 M of H_2O_2 was used. This phenomenon could be attributed to the breakdown of hemicellulose and the partial decomposition of lignin and cellulose. As H_2O_2 dosage increased, there was an extra mass loss resulting from the complete disintegration of hemicellulose and further decomposition of lignin and cellulose. This determined that the incorporation of H_2O_2 has a substantial impact on the mass yield of torrified biomass. This also suggested that the addition of H_2O_2 during WT resulted in a lower mass yield even without raising the reaction temperature. The previous study conducted by Gan *et al.* revealed that the mass yield of PKS that underwent WT at 200 °C was 59.15 ± 0.72 wt. %, whilst that at 235 °C was 51.22 wt. % (Gan *et al.,* 2019). Furthermore, another research by Ameen *et al.* showed that the mass yield of palm shells that underwent HTC at 300 °C was 54.5 % (Ameen *et al.,* 2022).

Table 1: Product yield and liquid yield for torrified PKS

Sample	Mass Yield (wt. %)	Liquid Yield (wt. %)	Pressure (bar)
TB $_{0.000}$	59.80	63.00	13
TB $_{0.004}$	59.76	83.00	13
TB $_{0.050}$	59.30	87.00	13
TB $_{0.100}$	58.87	85.00	11
TB $_{0.500}$	56.60	83.00	15
TB $_{1.000}$	50.60	79.00	15

He *et al.* reported that the order of decomposition rate for wet torrefaction processes above 200 °C can be ranked as with hemicellulose being the most reactive, followed by cellulose and lignin being the least reactive component (He *et al.,* 2018). According to Gan *et al.* and Phuang *et al.,* the ideal temperature range for efficient fuel production is between 180 and 220 °C (Gan *et al.,* 2019); (Phuang *et al.,* 2021). This is to avoid operating at high pressures, which would lead to increased capital and operating costs, as well as higher energy demands.

Table 2: Proximate analysis, ultimate analysis, and fuel properties of raw and torrified PKS

Sample	raw PKS	TB $_{0.000}$	TB $_{0.004}$	TB $_{0.050}$	TB $_{0.100}$	TB $_{0.500}$	TB $_{1.000}$
Proximate Analysis (wt. %)							
MC	7.9	3.6	4.6	5.1	4.2	3.7	2.7
VM	65.0	56.9	53.9	55.1	56.8	55.0	58.4
AC	0.9	1.1	1.0	1.0	1.1	1.4	1.6
FC	26.2	38.4	40.5	38.8	37.8	39.8	37.3
Ultimate Analysis (wt. %)							
C	47.9	53.5	-	53.6	-	54.6	55.1
H	6.1	5.8	-	5.8	-	5.7	5.5
N	0.52	0.50	-	0.34	-	0.35	0.34
S	0.22	0.07	-	0.38	-	0.17	0.15
O	40.7	36.7	-	38.9	-	37.7	37.3
H/C ratio	1.53	1.3	-	1.29	-	1.25	1.19
O/C ratio	0.64	0.51	-	0.54	-	0.52	0.51
Fuel Properties (MJ/kg)							
HHV	18.9	22.6	22.5	21.5	21.2	22.0	21.8
FR	0.40	0.64	0.75	0.70	0.67	0.72	0.64
CI	55.4	37.7	34.1	35.0	36.0	34.1	37.9
VI	0.30	0.57	0.74	0.58	0.49	0.62	0.46

'-' not analysed

Since the primary focus of this study was on the effect of H_2O_2 dosage on WT, the temperature was kept constant at 200 °C.

Moreover, the influence of various H_2O_2 dosages on the operating pressure during the wet torrefaction process was insignificant, possibly due to the dominant effect of liquid feed on the pressure. This revealed that the employment of H_2O_2 did not increase the operating pressure, which is desirable as a higher operating pressure often leads to higher operational risks at the industrial level. It could be concluded that the addition of H_2O_2 can achieve a similar outcome in terms of reducing the mass yield without the need to raise the reaction temperature, which would otherwise incur higher capital costs.

On the other hand, the incorporation of H_2O_2 during the WT process resulted in a higher liquid yield compared to that without H_2O_2. This may be attributed to the elevated decomposition rate of biomass with increasing reaction severity, which aligned with the findings reported for HTC (Nizamuddin *et al.,* 2015). Another study conducted by Kumar *et al.* suggested that the bio-oil yield increased during the hydrothermal liquefaction (HTL) process from 44 wt. % to 46 wt. % while employing H_2O_2 in an inert (N_2) condition (Kumar *et al.,* 2021). It could be deduced that the incorporation of H_2O_2 during the WT process led to a higher liquid yield but the effect of varying H_2O_2 dosages was found to be insignificant. Further investigation is required to analyse the influence of H_2O_2 dosage on the quality of biomass composition using various analysis methods.

3.2 Physicochemical Properties of Raw and Wet-Torrified Palm Kernel Shell

3.2.1 Proximate and Ultimate Analyses

The result of the proximate analysis at different H_2O_2 dosages is shown in Table 2. The moisture content of H_2O_2-aided torrified PKS was significantly lower than that of raw PKS, suggesting that the hydrophilic property of PKS declined (Stirling *et al.,* 2018). Besides, H_2O_2-aided torrified PKS exhibited a lower volatile matter content compared to raw PKS, resulting in fuel properties that more closely resemble coal (Bach & Skreiberg, 2016). The use of a higher H_2O_2 dosage in WT led to a higher ash content in PKS. As a result, H_2O_2-aided torrified PKS samples had higher ash content than raw PKS, which is consistent with the reported findings that employed H_2O_2 for dry torrefaction (Chen *et al.,* 2022). This may be linked to the breaking of hydrogen-carbon bonds, which leads to a higher retention of ash content in the biomass (Phuang *et al.,* 2021a). Additionally, all torrified samples had significantly higher fixed carbon content than untreated PKS, which is a preferred fuel attribute. Nevertheless, the moisture, volatile matter, ash, and fixed carbon contents of H_2O_2-aided torrified PKS were found to be similar to those of TB $_{0.000}$, indicating that the addition of H_2O_2 did not contribute significantly to further enhancing the fuel characteristics of PKS.

Typically, solid fuels with a low O/C ratio are associated with reduced water vapour formation, smoke emission, and energy loss during combustion (Yang *et al.,* 2017). Torrified biomass with a high oxygen content has a lower heating value and is considered a mediocre fuel as a consequence of the high flue gas emissions during the following thermochemical process. Thus, solid fuels with low oxygen content and a low O/C atomic ratio are preferred as they exhibit coal-like behaviour (Tumuluru, 2016).

TB $_{0.050}$ had a carbon content of 53.6 wt. % and the carbon content in TB $_{1.000}$ was increased to 55.1 wt. %. In contrast, the weight percentages of hydrogen and oxygen decreased as the H_2O_2 dosage increased, as shown in Table 2. Gan *et al.* reported that the O/C and H/C atomic ratios for PKS that went through WT at 200 °C were 0.51 and 1.30, respectively (Gan *et al.,* 2019). The incorporation of H_2O_2 during the WT process

led to a similar O/C atomic ratio but a lower H/C atomic ratio. These changes were likely due to the increase in dehydration and decarboxylation reactions that happened during WT (Nizamuddin *et al.,* 2015). The sulphur content reduced with increasing H_2O_2 dosage implied that fewer sulphur oxides are likely to form during combustion. In contrast, the differences in nitrogen content were insignificant. It could be inferred that the addition of H_2O_2 contributed to a slight reduction of the O/C atomic ratio. Reduction in the H/C ratio was not favoured. The current result showed that the addition of H_2O_2 did not enhance hydrogenation.

Furthermore, the thermogravimetric (TG) curves and its derivative (DTG) curves for raw PKS, TB $_{0.004}$, TB $_{0.500}$, and TB $_{1.000}$ were displayed in Figure 1 and Figure 2. Thermal decomposition of PKS happened in three zones, namely the dehydration zone, the devolatilisation zone, and the char decomposition zone (Phuang *et al.,* 2021). The dehydration stage took place from 25 °C to 130 °C, ascribed to the decrease in moisture level in the samples due to the process of evaporation and drying. During the devolatilisation stage, which occurred between 130 °C and 450 °C, a significant weight loss was spotted mainly brought about by the volatilisation of cellulose and hemicellulose. While for the char decomposition stage that ranges from 450 °C to 800 °C, lignin, and other strongly bonded compounds decomposed slowly and contributed to the remaining weight loss.

As shown by the DTG curves in Figure 2, the point where the most significant mass loss can be identified. The first zone of the DTG curve (<130 °C) exhibited a minor weight loss in the samples, occurring at a temperature of approximately 60 °C and 110 °C for raw PKS and H_2O_2-aided torrified PKS, respectively, attributed to the removal of moisture and some light volatile compounds (Nizamuddin *et al.,* 2018). This could be attributed to the fact that the H_2O_2-aided torrified PKS contained mainly equilibrium moisture content and therefore the delay in weight loss.

The second stage of the DTG curve (130 – 450 °C) emerges from the thermal breakdown of cellulose and hemicellulose. As shown in Figure 2, a single peak accompanied by two smaller peaks was detected. The first small peak was observed at 281 °C for raw PKS because of the thermal breakdown of hemicellulose as hemicellulose is extremely reactive at temperatures above 200 °C (Aslam *et al.,* 2019). Conversely, a much smaller peak was seen for TB $_{0.004}$, TB $_{0.500}$, and TB $_{1.000}$, showing that much of the hemicellulose was removed after the H_2O_2-aided WT process (He *et al.,* 2018). Since the peak of hemicellulose was detected at a lower temperature, it was indicative that the thermal stability of hemicellulose, cellulose, and lignin increased in ascending order. This could be proven that hemicellulose is the least thermally stable among the three constituents (Phuang *et al.,* 2021).

The second small peak in the devolatilisation zone was observed at 360 °C, which lies within the range of 300 °C to 400 °C where the cellulose degradation took place (Cichosz & Masek, 2020). The intensity of this peak diminished as the H_2O_2 dosage increased, indicating the partial removal of cellulose at higher H_2O_2 dosages. The similarity in peak positions

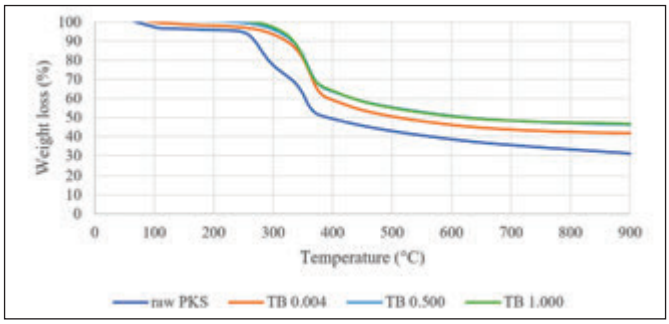

Figure 1: TGA curves for raw and torrified samples with different H_2O_2 dosages

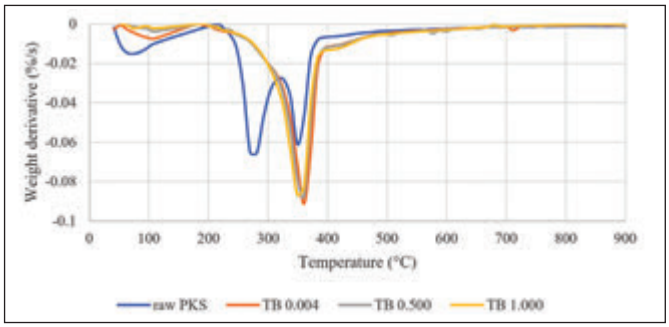

Figure 2: DTG curves for raw and torrified samples with different H_2O_2 dosages

among the torrified samples indicated that the H_2O_2-aided WT process did not significantly alter the structural characteristics of cellulose. The thermal decomposition of lignin was characterised by a smooth region over a broad temperature range of 380 – 500 °C. In addition, a minor peak identified at around 508 °C and 580 °C for TB $_{0.500}$ were attributed to the thermal decomposition of some cellulose and mostly lignin whilst a small peak was spotted at approximately 700 °C for TB $_{1.000}$ corresponded to the secondary or complete disintegration of lignin (Phuang *et al.,* 2021).

3.2.2 Fuel Properties

Gan *et al.* reported that the higher heating value (HHV) of PKS that underwent WT at 200 °C was 22.57 ± 0.08 MJ/kg. As shown in Table 2, the HHVs of torrified PKS were found to be relatively similar across different H_2O_2 dosages. This suggested that the thermal degradation rate of the H_2O_2-aided torrified PKS samples remained consistent, even with the varying dosages of H_2O_2 used. Therefore, the torrified PKS with different H_2O_2 dosages exhibited comparable HHVs, which could be attributed to similar thermal stability (Arpia *et al.,* 2021). The findings implied that the effect of varying H_2O_2 dosages on HHV was found to be insignificant at higher levels. However, the presence of H_2O_2 gave better results in terms of FR.

The fuel ratio (FR), typically expressed as the ratio of fixed carbon to volatile matter, is widely used for classifying coals as it provides theoretical insights into combustion efficiency. According to Table 2, it was observed that the fuel ratio was significantly higher in torrified PKS compared to raw PKS. However, the difference in fuel ratio between torrified PKS treated with and without H_2O_2 was minor. A high fuel ratio resulted in reduced smoke formation and limited emissions

during burning, which ultimately improved the fuel quality. In general, biomass has a low fuel ratio, but this ratio was increased to between 0.64 and 0.75 through WT, indicating an improved fuel quality. The high fuel ratio in torrified PKS was attributed to the increased fixed carbon content and reduced volatile matter, resulting in stable and complete combustion (Allouzi *et al.,* 2023).

The combustibility index (CI) usually refers to the fire and combustion behaviour of materials. The CI value decreased from raw PKS to torrified PKS, suggesting an improvement in PKS quality through the WT process. Nevertheless, the difference in CI value between wet torrified PKS with and without the use of H_2O_2 was insignificant. This indicated that the addition of H_2O_2 during the WT process did not further improve the compatibility of the torrified PKS for mixed combustion with coal (Allouzi *et al.,* 2023).

Moreover, the volatility index (VI) typically indicates the total energy content of the fuel yielded by the volatile elements by assuming that the fixed carbon in the fuel consists solely of pure carbon. The VI value increased by 2 times, but this increment was insufficient as beyond 10 times increment is required for a coal-like fuel (Allouzi *et al.,* 2023).

3.2.3 Fourier-Transform Infrared Spectroscopy Analysis (FTIR)

The FTIR spectra in Figure 3 portrayed the functional groups present in the samples. They exhibited some similarities in their absorbance peaks, but there were significant molecular changes. The broad transmittance peak at 3300 cm^{-1} corresponded to the stretching vibration of O−H due to intra- and intermolecular hydrogen bonds, a distinctive feature of crystalline cellulose. The decrease in peak intensity at TB $_{0.500}$ and TB $_{1.000}$ indicated that H_2O_2-aided torrified PKS samples have fewer sites for hydrogen bonding, presumably due to the degradation of hemicellulose and cellulose (Gan *et al.,* 2019). Elimination of this hydroxyl group was beneficial as it improved the hydrophobic nature of the biomass (Zhang *et al.,* 2019). The peaks at 2931 and 2843 cm^{-1} were attributed to the stretching vibration of C-H of alkanes in hemicellulose and cellulose (Wang *et al.,* 2018). The decline in the intensity of these bands indicated the elimination of aliphatic −CH2 groups (Kumar Mishra & Mohanty, 2020). The peak at approximately 1725 cm^{-1} was solely detected in raw PKS. It signified the stretching vibrations of C=O in the carboxylic acids of hemicellulose. The lack of this peak in TB $_{0.004}$, TB $_{0.500}$, and TB $_{1.000}$ implied the complete elimination of the hemicellulose ester group (Pérez-Limiñana *et al.,* 2022), as a result of deacetylation with the aid of H_2O_2 during WT. Hemicellulose has less thermal stability as compared to cellulose and lignin. The thermal stability of torrified biomass increased as H_2O_2 amount increased as shown in TGA analysis in Figure 1.

The reduction in carboxylic acid groups was accompanied by a corresponding increase in the relative amount of lignin, as revealed by the peaks at 1685 and 1600 cm^{-1}. These peaks represented the stretching vibrations of C=O and C=C, which could be carboxyl groups, aldehydes, esters, ketones, and aromatic structures that are present in lignin (Ullah *et al.,* 2021). The strengthened absorption of C=O with 0.004 M H_2O_2 reaction was attributed to the greater abundance of lignin in H_2O_2-aided torrified PKS samples, which also resulted high amount of fixed carbon and fuel ratio (FR). The peaks at 1450 and 1428 cm^{-1} corresponded to the C≡C bond, which confirmed the presence of the alkyne group (Kumar Mishra & Mohanty, 2020), which the dominance of lignin in torrified samples and therefore improvement in fuel properties. The peak at 1269 cm^{-1} was attributed to the stretching vibration of C-O for guaiacyl and syringyl groups in lignin (Phuang *et al.,* 2021a). The peak intensity measured in this study was almost similar to the previous results reported by Gan *et al.* (Gan *et al.,* 2019). This revealed that the aid of H_2O_2 during WT had a mild influence on lignin decomposition.

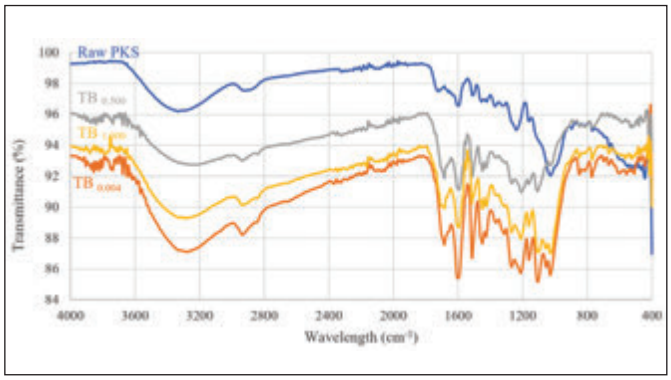

Figure 3: FTIR spectra of raw and wet-torrified PKS

The band observed at approximately 1162 cm^{-1} corresponded to the antisymmetric stretching vibrations of C−O−C glycosidic linkages in both hemicellulose and cellulose. A significant decrease in absorbance was observed in H_2O_2-aided torrified PKS, compared to raw PKS, indicating the significant loss of cellulose fractions. The peak intensity observed in this study was higher for TB $_{0.004}$, possibly because of the removal of hemicellulose and cellulose at higher concentrations of H_2O_2. The intensified peaks could also be a result of some degree of degradation that may have occurred (Phuang *et al.,* 2021a). Furthermore, the peaks observed at approximately 1071 cm^{-1} in raw PKS and 1031 cm^{-1} in H_2O_2-aided torrified PKS, indicating the vibrations of aliphatic C−O−C and C−OH in alcohol, primarily originating from cellulose (Wang *et al.,* 2018). Lastly, the peak discovered at 771 cm^{-1} symbolised mono and polycyclic aromatic groups owing to O-H bending vibrations (Kumar Mishra & Mohanty, 2020). In short, H_2O_2-aided torrified PKS samples showed increasing aromatic characteristics, owing to their removal at higher H_2O_2 concentrations.

3.3 Characterisation of Liquid Produced from Wet Torrefaction

3.3.1 pH

The pH for liquid produced from WT is shown in Table 3. Increasing the H_2O_2 dosages led to decreases in the pH of the liquid produced. The decrease in pH was indicative of increased acidity in the liquid, possibly due to the degradation of lignin. Therefore, the liquid samples produced at higher H_2O_2 dosages exhibited higher levels of acidity than those produced with lower H_2O_2 dosages. The acidity in the liquid was mainly because

Table 3: pH for liquid produced from WT

H_2O_2 Dosage (M)	pH
0.004	3.3
0.050	3.2
0.100	3.2
0.500	3.0
1.000	2.8

organic acids, such as formic and acetic acids are present, which are breakdown products of hemicellulose. However, the presence of these acids may result in liquid instability and equipment corrosion (Chong *et al.,* 2019). However, an increase in the acidity of liquid samples for the increase in H_2O_2 dosage showed that further cracking happens, and more acids would be formed.

3.3.2 Fourier-Transform Infrared Spectroscopy Analysis (FTIR)

The FTIR spectra in Figure 4 illustrates the functional groups present in the liquid samples. Although they shared some similarities in their absorbance peaks, significant molecular changes were observed. The wide transmittance peak at 3300 cm^{-1} manifested the stretching vibration of O−H and implied the presence of phenols, organic acids, aromatics, and water impurities in WT liquid samples (Kumar Mishra & Mohanty, 2020). The peak intensity increased as the H_2O_2 dosage increased, which can be related with the increase in organic acids. An increase in acidity as the increase in H_2O_2 dosage was noticed in section 3.3.1. A peak at 1635 cm^{-1} is observed, which was attributed to C=C stretching vibration, indicating the presence of alkenes and aromatic compounds in liquid samples as more lignin degradation occurred (Kumar Mishra & Mohanty, 2020). The presence of aliphatic and aromatic compounds in the liquid samples was confirmed by the peak detected at 607 cm^{-1}, which corresponded to the bending vibrations of O-H in mono and polycyclic aromatic groups (Kumar Mishra & Mohanty, 2020). This peak showed the presence of more lignin degraded components in the liquid. The product yield and characterisation studies revealed that the presence of H_2O_2 in a small amount made a negligible change in the torrified biomass. However, as the concentration of H_2O_2 increased significantly, more severity in the reaction happened, which did not improve solid fuel properties, instead the cellulose or lignin degradation into liquid components happened.

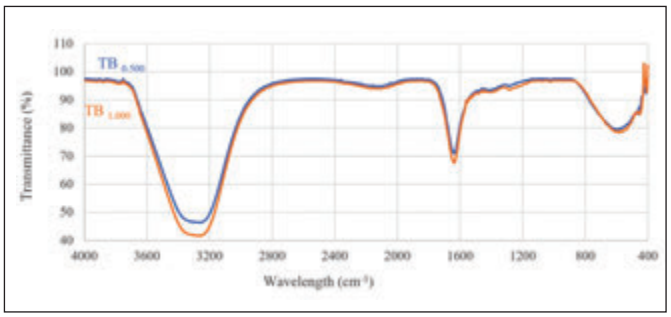

Figure 4: FTIR spectra of liquid produced

4.0 CONCLUSION

Palm kernel shell (PKS) exhibits promising potential as a sustainable and high-quality renewable energy resource. In this research, wet torrefaction of PKS was performed with the aid of H_2O_2 to enhance its fuel properties without raising the reaction temperature. The mass yield of PKS decreased from 59.8 wt. % to 50.6 ± 0.3 wt. % with elevated H_2O_2 dosages, indicating the disintegration of hemicellulose and cellulose during wet torrefaction. The trends of greater fixed carbon content, higher ash content, and lower moisture content as compared to raw PKS. However, these properties were similar for torrified PKS treated with and without H_2O_2, implying that the addition of H_2O_2 did not contribute significantly to further enhancing the fuel characteristics of PKS. The FTIR analysis revealed an increase in the breakdown of lignocellulosic components with torrefaction severity in the torrified PKS. The CHNS elemental analysis demonstrated an enhancement in the fuel properties of PKS through an increase in carbon content from 53.6 wt. % to 55.1 wt. %, a decrease in oxygen content from 38.9 wt. % to 37.3 wt. %, and a reduction in the O/C atomic ratio from 0.54 to 0.51 with increased H_2O_2 dosages, making the solid fuel more analogous to coal. Overall, the findings demonstrate that H_2O_2 did not make a substantial contribution for further enhancing the solid fuel properties during the wet torrefaction process. ■

ACKNOWLEDGMENT

This work was supported by the Ministry of Higher Education Malaysia under the Grant FRGS/1/2022/TK08/UNIM/02/5.

AUTHORS' CONTRIBUTIONS

- **Poh Lae Ooi**: Writing – original draft, validation, methodology, data collection, formal analysis
- **Rui Hong Teoh**: Validation, methodology, data collection, formal analysis
- **Lai Yee Lee**: Writing – review & editing, formal analysis
- **Suyin Gan**: Writing – review & editing, formal analysis
- **Revathi Raviadaran**: Methodology, investigation
- **Sona R. Moharir**: Methodology, formal analysis
- **Suchithra Thangalazhy-Gopakumar**: Writing – review & editing, validation

REFERENCES

[1] Allouzi, M. M. A., Lee, L. Y., Gan, S., & Thangalazhy-Gopakumar, S. (2023). Torrefaction of Olive Pomace and its Interactive Effects with Low-Density Polyethylene (LDPE) Plastic. *Thermochimica Acta, 724(3)*, 179495. https://doi.org/10.2139/ssrn.4254562

[2] Ameen, M., Zamri, N. M., May, S. T., Azizan, M. T., Aqsha, A., Sabzoi, N., & Sher, F. (2022). Effect of acid catalysts on hydrothermal carbonization of Malaysian oil palm residues (leaves, fronds, and shells) for hydrochar production. *Biomass Conversion and Biorefinery, 12(1)*, 103–114. https://doi.org/10.1007/s13399-020-01201-2

[3] Arpia, A. A., Chen, W. H., Ubando, A. T., Tabatabaei, M., Lam, S. S., Culaba, A. B., & De Luna, M. D. G. (2021). Catalytic microwave-assisted torrefaction of sugarcane bagasse with calcium oxide optimized via Taguchi approach: Product characterization and energy analysis. *Fuel, 305(8)*, 121543. https://doi.org/10.1016/j.fuel.2021.121543

[4] Aslam, U., Ramzan, N., Aslam, Z., Iqbal, T., Sharif, S., Hasan, S. W. ul, & Malik, A. (2019). Enhancement of fuel characteristics of rice husk via torrefaction process. *Waste Management and Research, 37(7)*, 737–745. https://doi.org/10.1177/0734242X19838620

[5] Bach, Q. V., & Skreiberg, O. (2016). Upgrading biomass fuels via wet torrefaction: A review and comparison with dry torrefaction. *Renewable and Sustainable Energy Reviews, 54*, 665–677. https://doi.org/10.1016/j.rser.2015.10.014

[6] Chen, W. H., Ho, K. Y., Lee, K. T., Ding, L., Andrew Lin, K. Y., Rajendran, S., Singh, Y., & Chang, J. S. (2022). Dual pretreatment of mixing H_2O_2 followed by torrefaction to upgrade spent coffee grounds for fuel production and upgrade level identification of H_2O_2 pretreatment. *Environmental Research, 215(P1)*, 114016. https://doi.org/10.1016/j.envres.2022.114016

[7] Chong, Y. Y., Thangalazhy-Gopakumar, S., Ng, H. K., Lee, L. Y., & Gan, S. (2019). Effect of oxide catalysts on the properties of bio-oil from in-situ catalytic pyrolysis of palm empty fruit bunch fiber. *Journal of Environmental Management, 247(6)*, 38–45. https://doi.org/10.1016/j.jenvman.2019.06.049

[8] Cichosz, S., & Masek, A. (2020). Thermal behavior of green cellulose-filled thermoplastic elastomer polymer blends. *Molecules, 25(6)*. https://doi.org/10.3390/molecules25061279

[9] Cortes-Clerget, M., Yu, J., Kincaid, J. R. A., Walde, P., Gallou, F., & Lipshutz, B. H. (2021). Water as the reaction medium in organic chemistry: From our worst enemy to our best friend. *Chemical Science, 12(12)*, 4237–4266. https://doi.org/10.1039/d0sc06000c

[10] Gan, M. J., Lim, W. S., Ng, H. X., Ong, M. H., Gan, S., Lee, L. Y., & Thangalazhy-Gopakumar, S. (2019). Enhancement of Palm Kernel Shell Fuel Properties via Wet Torrefaction: Response Surface, Optimization, and Combustion Studies. *Energy Fuels, 33(11)*, 11009–11020 https://doi.org/10.1021/acs.energyfuels.9b02229

[11] He, C., Tang, C., Li, C., Yuan, J., Tran, K.-Q., Bach, Q.-V., Qiu, R., & Yang, Y. (2018). Wet torrefaction of biomass for high quality solid fuel production: A review. Renewable and Sustainable *Energy Reviews, 91*, 259–271. https://doi.org/10.1016/j.rser.2018.03.097

[12] Krysanova, K., Krylova, A., & Zaichenko, V. (2019). Properties of biochar obtained by hydrothermal carbonization and torrefaction of peat. *Fuel, 256(7)*, 115929. https://doi.org/10.1016/j.fuel.2019.115929

[13] Kumar, A., Biswas, B., Kaur, R., Krishna, B. B., & Thallada, B. (2021). Oxidative valorisation of lignin into valuable phenolics: Effect of acidic and basic catalysts and reaction parameters. *Bioresource Technology, 338(6)*, 125513. https://doi.org/10.1016/j.biortech.2021.125513

[14] Kumar Mishra, R., & Mohanty, K. (2020). Effect of low-cost catalysts on yield and properties of fuel from waste biomass for hydrocarbon-rich oil production. *Materials Science for Energy Technologies, 3*, 526–535. https://doi.org/10.1016/j.mset.2020.05.007

[15] Nizamuddin, S., Baloch, H. A., Siddiqui, M. T. H., Mubarak, N. M., Tunio, M. M., Bhutto, A. W., Jatoi, A. S., Griffin, G. J., & Srinivasan, M. P. (2018). An overview of microwave hydrothermal carbonization and microwave pyrolysis of biomass. *Reviews in Environmental Science and Biotechnology, 17(4)*, 813–837. https://doi.org/10.1007/s11157-018-9476-z

[16] Nizamuddin, S., Jayakumar, N. S., Sahu, J. N., Ganesan, P., Bhutto, A. W., & Mubarak, N. M. (2015). Hydrothermal carbonization of oil palm shell. Korean *Journal of Chemical Engineering, 32(9)*, 1789–1797. https://doi.org/10.1007/s11814-014-0376-9

[17] Pérez-Limiñana, M. A., Pérez-Aguilar, H., Ruzafa-Silvestre, C., Orgilés-Calpena, E., & Arán-Ais, F. (2022). Effect of Processing Time of Steam-Explosion for the Extraction of Cellulose Fibers from Phoenix canariensis Palm Leaves as Potential Renewable Feedstock for Materials. *Polymers, 14(23)*. https://doi.org/10.3390/polym14235206

[18] Phuang, Y. W., Ng, W. Z., Khaw, S. S., Yap, Y. Y., Gan, S., Lee, L. Y., & Thangalazhy-Gopakumar, S. (2021a). Wet torrefaction pre-treatment of yard waste to improve the fuel properties. *Materials Science for Energy Technologies, 4*, 211–223. https://doi.org/10.1016/j.mset.2021.06.005

[19] Phuang, Y. W., Ng, W. Z., Khaw, S. S., Yap, Y. Y., Gan, S., Lee, L. Y., & Thangalazhy-Gopakumar, S. (2021b). Wet torrefaction pre-treatment of yard waste to improve the fuel properties. *Materials Science for Energy Technologies, 4*, 211–223. https://doi.org/https://doi.org/10.1016/j.mset.2021.06.005

[20] Soh, M., Khaerudini, D. S., Chew, J. J., & Sunarso, J. (2021). Wet torrefaction of empty fruit bunches (EFB) and oil palm trunks (OPT): Effects of process parameters on their physicochemical and structural properties. South African *Journal of Chemical Engineering, 35(6)*, 126–136. https://doi.org/10.1016/j.sajce.2020.09.004

[21] Stirling, R. J., Snape, C. E., & Meredith, W. (2018). The impact of hydrothermal carbonisation on the char reactivity of biomass. *Fuel Processing Technology, 177*, 152–158. https://doi.org/10.1016/j.fuproc.2018.04.023

[22] Torres, C., Crastechini, E., Feitosa, F., Pucci, C., & Borges, A. (2014). Influence of pH on the Effectiveness of Hydrogen Peroxide Whitening. *Operative Dentistry, 39(6)*, E261–E268. https://doi.org/10.2341/13-214-L

[23] Tumuluru, J. S. (2016). Effect of deep drying and torrefaction temperature on proximate, ultimate composition, and heating value of 2-mm lodgepole pine (Pinus contorta) grind. *Bioengineering, 3(2)*. https://doi.org/10.3390/bioengineering3020016

[24] Ullah, H., Lun, L., Riaz, L., Naseem, F., Shahab, A., & Rashid, A. (2021). Physicochemical characteristics and thermal degradation behavior of dry and wet torrefied orange peel obtained by dry/wet torrefaction. *Biomass Conversion and Biorefinery*, 0123456789. https://doi.org/10.1007/s13399-021-01777-3

[25] Wang, P., Zhang, J., Shao, Q., & Wang, G. (2018). Physicochemical properties evolution of chars from palm kernel shell pyrolysis. *Journal of Thermal Analysis and Calorimetry, 133(3)*, 1271–1280. https://doi.org/10.1007/s10973-018-7185-z

[26] Yang, W., Wu, S., Wang, H., Ma, P., Shimanouchi, T., Kimura, Y., & Zhou, J. (2017). Effect of wet and dry torrefaction process on fuel properties of solid fuels derived from bamboo and Japanese cedar. *BioResources, 12(4)*, 8629–8640. https://doi.org/10.15376/biores.12.4.8629-8640

[27] Zhang, D., Wang, F., Zhang, A., Yi, W., Li, Z., & Shen, X. (2019). Effect of pretreatment on chemical characteristic and thermal degradation behavior of corn stalk digestate: Comparison of dry and wet torrefaction. *Bioresource Technology, 275(12)*, 239–246. https://doi.org/10.1016/j.biortech.2018.12.044

PROFILES

POH LAE OOI graduated with an MEng (Hons) degree in Chemical and Environmental Engineering from the University of Nottingham Malaysia. She is currently working as a Process Engineer in the opto-semiconductor industry.
Email address: pohlaefce@gmail.com

RUI HONG TEOH is a PhD student in the University of Nottingham Malaysia. He graduated with a Masters in Chemical Engineering from the University of Nottingham Malaysia. His research focuses on the Production of Biofuel and Chemicals from Biomass, through Thermochemical Processes such as Wet Torrefaction and Hydrothermal Liquefaction.
Email address: ebyrt1@nottingham.edu.my

LAI YEE LEE is currently a Chemical and Environmental Engineering Professor at the University of Nottingham Malaysia. She obtained her Bachelor degree and PhD degree in Chemical Engineering from the University of Bath, United Kingdom. Her research interests lie in Nanotechnology and Advanced Separation Techniques, with a Particular focus on Developing Carbon Nanomaterials and Agricultural-Based Composites for Environmental Pollution Control and Product Recovery.
Email address: lai-yee.lee@nottingham.edu.my

SUYIN GAN is currently a Chemical Engineering Professor at the Department of Chemical and Environmental Engineering, University of Nottingham Malaysia. She graduated with a BEng (Hons) and a PhD from the University of Sheffield, UK. Her research interests include Biofuel Cum Biomass Processing Technologies, Combustion and Emissions as well as Environmental Remediation.
Email address: suyin.gan@nottingham.edu.my

REVATHI RAVIADARAN is a Chemical Engineering Lecturer at Universiti Teknologi PETRONAS, Malaysia. She has MEng (Hons) and PhD in Chemical Engineering from University of Nottingham Malaysia. Her research focuses on Nanoprocessing and Nanoformulations of Biomaterials for Pharmaceutical and Energy Applications. She has published 18 Q1 journal articles, fetched over 500 citations with a H-Index of 13.
Email address: revathi.raviadaran@utp.edu.my

SONA R. MOHARIR is an Assistant Professor at Chemical Engineering Department, Bharati Vidyapeeth College of Engineering, Navi Mumbai, Maharashtra, India. She obtained her PhD(Tech) in chemical engineering and Master's degree from Institute of Chemical Technology, Mumbai, Maharashtra, India. She is involved in research in the field of Corrosion, Fluid Mechanics and Bio Energy.
Email address: sonamoharir@gmail.com

SUCHITHRA THANGALAZHY-GOPAKUMAR is an Associate Professor in the department of Chemical and Environmental Engineering at University of Nottingham Malaysia. She received her Doctoral degree in Chemical Engineering from Auburn University, Alabama, USA. Her Master's degree is in Chemical Engineering (specialisation: Industrial Pollution Control) from National Institute of Technology Karnataka, Surathkal, India, and Bachelor's degree in Chemical Engineering from Government Engineering College Thrissur, Kerala, India. Her research focuses on the Development of Liquid Biofuels and Extraction of Chemicals from Various Biomass Feedstocks through Thermo-Chemical Conversions and Catalytic Upgrading. She has the status of 'Fellow of the Higher Education Academy', UK, Charted Engineer and Charted Scientist from Institute of Materials, Minerals & Mining (I.M3), UK. She has membership with IChemE (UK), I.M3 (UK), IIChE (India) IEM (Malaysia) and BEM (Malaysia).
Email address: suchithra.thangalazhy@nottingham.edu.my

INVESTIGATING THE IMPACT OF BIO-INSPIRED STRUCTURAL DESIGN ON THE FATIGUE LIFE OF LIGHTWEIGHT METALLIC ALLOYS

H. C. O. Unegbu[1*], D.S. Yawas[2]

Abstract

This study investigates the impact of bio-inspired structural designs on the fatigue life of lightweight metallic alloys—AA7075 aluminium and Ti-6Al-4V titanium. Leveraging advanced additive manufacturing, three bio-inspired geometries (honeycomb, trabecular, and cellular lattice) were fabricated and evaluated against traditional solid block designs under cyclic loading. The results demonstrated substantial improvements in fatigue performance: the honeycomb structure extended fatigue life by approximately 340% in AA7075 and 329% in Ti-6Al-4V compared to their respective solid block counterparts. Trabecular and lattice designs also exhibited fatigue life enhancements ranging from 200% to 280%. Stress-life (S-N) curve analysis and Weibull distribution further confirmed the improved durability and reliability of the bio-inspired geometries. These findings underscore the promise of bio-inspired design in prolonging component life in fatigue-prone applications such as aerospace, automotive, and biomedical engineering. The study also highlights additive manufacturing's capacity to realise complex, optimised structures, enabling new frontiers in material efficiency, reliability, and sustainability.

Received: *7 April, 2025*
Revised: *10 July, 2025*
Accepted: *10 September, 2025*

[1,2]Department of Mechanical Engineering, Ahmadu Bello University, Zaria, Nigeria.

****Corresponding author:***
chidieberehyg@gmail.com

DOI:
https://doi.org/10.54552/v86i4.290

Keywords:
Bio-inspired design, Fatigue resistance, Lightweight alloys, Additive manufacturing, S-N curves

1.0 INTRODUCTION

Lightweight metallic alloys have become indispensable in high-performance industries such as aerospace, automotive, and civil engineering, where the demand for materials that can reduce weight while maintaining mechanical strength and durability is constantly growing. These materials play a crucial role in improving fuel efficiency, enhancing performance, and reducing emissions, particularly in the context of global efforts to develop more sustainable engineering solutions (Estrin & Vinogradov, 2010; Zhang & Xu, 2022). However, despite their numerous advantages, lightweight alloys, particularly aluminium (e.g., AA7075) and titanium (e.g., Ti-6Al-4V), are prone to fatigue failure. This phenomenon occurs when materials experience progressive and localised structural damage due to cyclic loading over time (Shanyavskiy & Soldatenkov, 2022; Zhang *et al.,* 2018). Fatigue failure remains a critical limitation in the design and application of metallic alloys, making the improvement of fatigue life a central focus of research.

Fatigue failure typically initiates at stress concentrations, where localised high stresses lead to crack initiation and subsequent crack propagation, eventually resulting in catastrophic failure (Sawada *et al.,* 2021; Canna *et al.,* 2021). This challenge is particularly pronounced in aerospace and automotive components that are subject to repetitive stress cycles over extended periods (Ke *et al.,* 2020). For example, fatigue-induced failures account for a significant proportion of mechanical failures in aircraft structures, leading to costly maintenance, safety risks, and operational disruptions (Wei *et al.,* 2023). Enhancing fatigue resistance in these alloys is thus critical not only for extending the lifespan of components but also for improving the safety and reliability of structures exposed to dynamic loading conditions (Zhang *et al.,* 2012; Owuor *et al.,* 2017).

The urgency to extend the fatigue life of lightweight metallic alloys has intensified in recent years for several key reasons. First, industries such as aerospace and automotive are under increasing pressure to push the boundaries of performance while simultaneously improving sustainability. Components in these industries are exposed to thousands or even millions of stress cycles over their operational lifespans, making fatigue a primary concern for ensuring safety and reliability (Sharma & Hiremath, 2022; Afkhami *et al.,* 2019). For instance, in aircraft, fatigue failure can lead to catastrophic outcomes, highlighting the necessity of designing materials with improved fatigue resistance (Ke *et al.,* 2020). Despite advancements in material science, fatigue failure remains a leading cause of structural breakdowns in many applications, further underscoring the importance of this research (Shanyavskiy & Soldatenkov, 2022; Ye *et al.,* 2022).

In addition to safety concerns, economic and environmental considerations also drive the need for fatigue-resistant materials. Lightweight metallic alloys are integral to the design of fuel-efficient vehicles and aircraft, and extending their operational life directly contributes to sustainability by reducing material consumption, manufacturing waste, and carbon emissions (Schoenung & Olivetti, 2023; Benedetti *et al.,* 2024). As governments and industries worldwide seek to meet stricter environmental regulations, developing materials with enhanced fatigue life has become a critical strategy for achieving long-term sustainability goals (Canna *et al.,* 2021;

Jiang *et al.,* 2023). Improving the fatigue life of materials through innovative structural designs, such as bio-inspired geometries, could dramatically reduce the need for frequent component replacements, thus minimising resource use and production-related emissions (Wei *et al.,* 2023).

Furthermore, advancements in additive manufacturing technologies now enable the fabrication of complex bio-inspired designs, which can be precisely tailored to improve mechanical properties, including fatigue resistance (Yang *et al.,* 2022; Zhang *et al.,* 2022). However, despite the promise of bio-inspired geometries, there remains a significant gap in the literature regarding their impact on the fatigue life of widely used lightweight metallic alloys. While the mechanical performance of these alloys in static loading conditions has been extensively studied, fewer investigations have explored their dynamic performance under cyclic loading when designed with bio-inspired architectures (Zhang *et al.,* 2018; Afaghi *et al.,* 2023). This lack of comprehensive data on bio-inspired designs in cyclic loading conditions presents a significant research gap that this study seeks to address. By exploring how bio-inspired structural designs affect the fatigue life of lightweight metallic alloys, this research provides critical insights into the potential for these designs to enhance the durability and performance of materials in real-world applications (Ng *et al.,* 2017). The findings of this study have the potential to significantly influence industries seeking to design more reliable, long-lasting components for high-performance applications, such as aerospace and automotive manufacturing.

Fatigue failure in metallic alloys is a well-documented challenge, particularly in high-stress environments where components are subjected to cyclic loading. The initiation and propagation of cracks due to repeated stress cycles can result in material failure at stress levels well below the ultimate tensile strength of the alloy (Shanyavskiy & Soldatenkov, 2022; Khalifeh, 2023). In materials such as aluminium and titanium alloys, fatigue-induced failures are typically initiated at microstructural defects or stress concentrators, such as sharp corners, inclusions, or surface imperfections (Elangeswaran *et al.,* 2020; Zhang *et al.,* 2023). As a result, traditional designs for metallic components often exhibit limited fatigue life, especially in demanding applications where dynamic loading is prevalent (Ramoni *et al.,* 2022).

Bio-inspired structural designs, which mimic the highly efficient load-bearing and stress-distributing structures found in nature, offer a promising solution to this challenge (Perez-Garcia & Gómez-Martínez, 2009). Nature has evolved structural systems that are optimised for mechanical performance, including the ability to resist fatigue and crack propagation (Taylor, 2014). Examples of these natural structures include the cellular arrangement of honeycombs, the hierarchical structure of bone, and the spiral or helical arrangements found in shells and plants (Bilhère-Dieuzeide *et al.,* 2022). These designs minimise stress concentrations and distribute loads more evenly across the structure, thereby improving fatigue resistance and delaying crack initiation (Afaghi *et al.,* 2023; Cao *et al.,* 2022).

Recent advancements in additive manufacturing technologies, such as selective laser melting (SLM) and electron beam melting (EBM), have enabled the precise fabrication of bio-inspired geometries in metallic alloys (Yang *et al.,* 2022). These technologies allow for the creation of highly complex internal structures that were previously impossible to manufacture using conventional techniques (Zhang *et al.,* 2022; Xie *et al.,* 2019). As a result, bio-inspired designs, such as cellular lattices and honeycomb structures, can be integrated into metallic components to enhance their mechanical performance, particularly in terms of fatigue resistance (Ke *et al.,* 2020; Wang, 2019). Despite these advances, there is limited empirical data on how bio-inspired designs affect the fatigue life of metallic alloys under cyclic loading, particularly in lightweight materials like AA7075 and Ti-6Al-4V (Mirhakimi *et al.,* 2024). This study is motivated by the potential of bio-inspired structural designs to significantly enhance the fatigue life of metallic alloys. By investigating the effects of various bio-inspired geometries on fatigue resistance, this research aims to provide valuable insights into the design of more durable, lightweight components for high-performance applications (Zhang *et al.,* 2023). Given the growing demand for materials that can withstand dynamic loading while reducing weight and environmental impact, the findings of this study could have far-reaching implications for industries that rely on metallic alloys (Benedetti *et al.,* 2021).

The primary objective of this study is to investigate the impact of bio-inspired structural designs on the fatigue life of lightweight metallic alloys, specifically AA7075 aluminium and Ti-6Al-4V titanium alloys. The study will evaluate how different bio-inspired geometries, such as honeycomb and cellular lattice structures, influence the fatigue performance of these alloys when subjected to cyclic loading (Peng *et al.,* 2021). Traditional solid designs will be used as a baseline for comparison. The hypothesis is that bio-inspired structural designs will significantly improve the fatigue life of lightweight metallic alloys by reducing stress concentrations and improving the distribution of mechanical loads (Yan *et al.,* 2024). Through the fabrication and testing of bio-inspired and traditional designs, this study will provide empirical evidence on the effectiveness of bio-inspired geometries in enhancing fatigue resistance (Williams *et al.,* 2003). The findings will have implications for the design and optimisation of materials used in high-stress, cyclic loading applications, such as aerospace and automotive components (Ransom, 2003).

2.0 MATERIALS AND METHODS

2.1 Materials

This study investigated two commonly used lightweight metallic alloys: AA7075 aluminium and Ti-6Al-4V titanium. Both alloys are extensively utilised in industries requiring materials with high strength-to-weight ratios, such as aerospace, automotive, and biomedical engineering (Puchi-Cabrera *et al.,* 2008; Han *et al.*, 2021). These alloys have proven to be highly effective in weight-sensitive applications but are also prone to fatigue failure when subjected to cyclic stresses (Zhang *et al.,* 2012;

Afaghi *et al.,* 2023). AA7075 is an aluminium alloy known for its high strength and relatively good fatigue resistance compared to other aluminium alloys. It is frequently used in aircraft structures and components due to its balance between lightweight characteristics and mechanical durability (Estrin & Vinogradov, 2010; Tsai *et al.,* 2014). However, it is susceptible to fatigue failure, particularly in the presence of stress concentrators. Ti-6Al-4V is a titanium alloy prized for its excellent fatigue strength, corrosion resistance, and biocompatibility, which makes it a common choice for both aerospace components and biomedical implants (Shanyavskiy & Soldatenkov, 2022; Ma *et al.,* 2024). Despite its favourable properties, Ti-6Al-4V is also vulnerable to fatigue under cyclic loading, particularly in harsh environments (Peng *et al.,* 2021; Dong *et al.,* 2022). Nevertheless, it remains one of the most widely used titanium alloys in high-performance engineering due to its overall mechanical robustness, making it a highly relevant candidate for fatigue studies.

The selection of AA7075 and Ti-6Al-4V in this study is therefore justified not only by their widespread use in critical load-bearing applications but also by the contrasting fatigue behaviours they exhibit under operational conditions. AA7075 represents a typical high-strength aluminium alloy used in structural applications, while Ti-6Al-4V offers insight into the fatigue performance of a titanium alloy that is inherently strong but environment-sensitive. Studying both alloys under identical geometric modifications allows for a more comprehensive assessment of how bio-inspired designs influence fatigue life across different material systems with varying baseline fatigue characteristics.

The study utilised three bio-inspired structural designs—honeycomb, trabecular, and cellular lattice structures—fabricated using both AA7075 and Ti-6Al-4V alloys. These designs were selected for their potential to enhance mechanical properties by improving load distribution and delaying crack initiation and propagation, which are critical factors in extending fatigue life (Zhang *et al.,* 2018; Yin *et al.,* 2021). Traditional solid blocks of the same dimensions were also fabricated for comparison, allowing for the evaluation of the effectiveness of bio-inspired designs in improving fatigue resistance.

2.2 Fabrication Process

The specimens were fabricated using advanced additive manufacturing (AM) techniques, which are ideal for producing complex internal structures such as bio-inspired geometries. Specifically, Selective Laser Melting (SLM) was employed to fabricate the AA7075 aluminium specimens, while Electron Beam Melting (EBM) was used for the Ti-6Al-4V titanium alloy specimens. These powder-bed fusion methods were chosen due to their precision and ability to produce dense parts with fine microstructures that are difficult to achieve using traditional subtractive manufacturing processes (Jiang *et al.,* 2023; Yi *et al.,* 2024). SLM is a laser-based AM technique in which a high-power laser selectively melts layers of powdered material, following the contours of a 3D model. This process was used for AA7075 due to its better control over thermal gradients and lower porosity formation, which are critical for producing mechanically robust aluminium components (Safai *et al.,* 2019; Zhao *et al.,* 2008). For Ti-6Al-4V, EBM was used. EBM employs an electron beam as the energy source and is conducted in a vacuum environment, which is particularly well-suited for processing reactive metals like titanium. The EBM process also minimises residual stresses and achieves superior metallurgical bonding in high-melting-point alloys (Yang *et al.,* 2022; Wang *et al.,* 2024).

Prior to fabrication, computer-aided design (CAD) software (e.g., SolidWorks) was used to model the four specimen types: solid block, honeycomb, trabecular, and cellular lattice. The internal architectures of the bio-inspired designs were optimised to ensure consistent wall thickness, cell dimensions, and structural balance. Each specimen was modelled with identical external dimensions (e.g., 20 mm × 10 mm × 10 mm), ensuring consistency in boundary conditions across all fatigue tests. The CAD models were converted into STL files and processed with slicing software to generate toolpaths for the SLM and EBM machines. After fabrication, all specimens underwent post-processing steps to ensure surface quality and dimensional accuracy. This included support removal, light mechanical polishing to eliminate residual surface roughness, and inspection for manufacturing defects. These steps were crucial in eliminating unwanted stress concentrators on the surface, which could otherwise bias the fatigue test results (Afaghi *et al.,* 2023; Miller, 2012).

A schematic representation of the specimen geometries—solid block, honeycomb, trabecular, and cellular lattice—is provided in Figure 1, illustrating their internal structure and overall dimensions. All specimens were modelled with identical external dimensions (e.g., 50 mm × 10 mm × 10 mm) to ensure uniform boundary conditions during fatigue testing. Geometric features such as cell size and wall thickness were optimised to balance weight reduction and mechanical integrity.

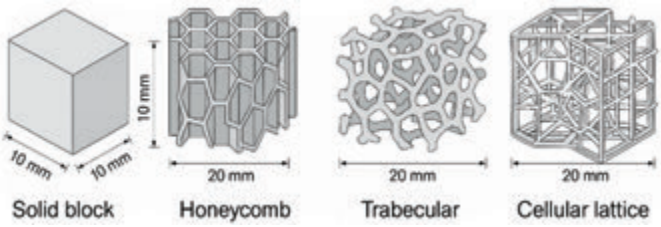

Figure 1: CAD models of the four specimen geometries used in this study
(a) Solid block; (b) Honeycomb structure;
(c) Trabecular structure; and (d) Cellular lattice structure

2.3 Experimental Setup

Fatigue testing was performed using an MTS Landmark servo-hydraulic fatigue testing machine, which provides precise control over loading parameters such as stress amplitude, frequency, and load ratios. Specimens were subjected to uniaxial cyclic loading at a frequency of 10 Hz, with a stress ratio (R) of 0.1. This stress ratio, defined as the ratio of minimum to maximum applied stress during each loading cycle, is commonly used to simulate the tension-tension loading conditions prevalent in aerospace and automotive applications (Ke *et al.,* 2020; Afaghi *et al.,* 2023).

Testing was carried out under room temperature conditions, with specimens loaded until failure or until a maximum of 10 million cycles was reached, whichever occurred first. The maximum stress applied during testing was based on approximately 50% of the material's ultimate tensile strength (UTS), calibrated to remain within the elastic range while being sufficient to induce fatigue failure over time. Specifically, the applied stress range was approximately 280–300 MPa for AA7075 and 440–460 MPa for Ti-6Al-4V, based on typical UTS values for these alloys (Mei *et al.,* 2023). The testing conditions were designed to mimic real-world operational scenarios where components are subjected to fluctuating loads over extended periods (Salifu & Olubambi, 2024; Yadav *et al.,* 2024). The schematic of the fatigue testing setup used in this study is illustrated in Figure 2. Key components include the hydraulic actuator, load cell, grips, and test specimen positioned centrally. The setup enables uniaxial cyclic loading under controlled conditions.

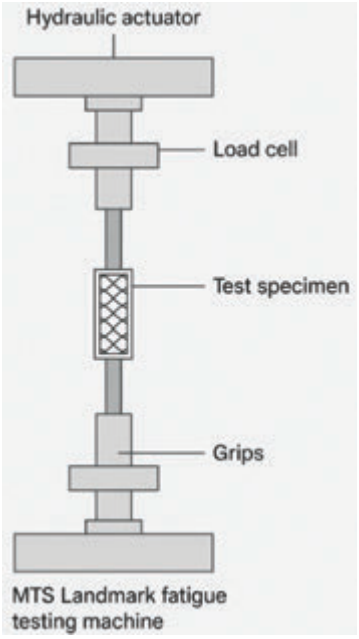

Figure 2: Schematic diagram of the fatigue testing setup using an MTS Landmark servo-hydraulic machine

2.4 Data Collection and Analysis

The number of cycles to failure (Nf) for each specimen was recorded, and stress-life (S–N) curves were plotted to visualise the relationship between applied stress amplitude and fatigue life. S–N curves are essential for evaluating fatigue performance, as they provide insight into the endurance limit of materials and how long they can withstand cyclic loading before failure (Strzelecki *et al.,* 2021; Yang *et al.,* 2022). The bio-inspired designs were compared to traditional solid block specimens to assess the impact of geometry on fatigue resistance. To ensure statistical robustness, three specimens for each design and material configuration were tested, and the mean fatigue life was calculated (Kluger & Łagoda, 2013).

Statistical methods such as ANOVA and Weibull analysis have been widely employed in fatigue studies to evaluate variability and failure probabilities across test conditions (Zhou *et al.,* 2021; Xie & Lai, 1996) and are particularly effective in comparing performance across complex geometries (Macek *et al.,* 2022; Richard & Sander, 2016; Cui *et al.,* 2022). These methods enhance the interpretation of fatigue life trends and support reliability-based design strategies (Zainulabdeen *et al.,* 2024).

3.0 RESULTS AND DISCUSSION

3.1 Fatigue Life Performance

Fatigue life performance for each of the tested designs, represented by the number of cycles to failure (Nf), is summarised in Table 1. The bio-inspired designs—honeycomb, trabecular, and cellular lattice structures—exhibited significantly improved fatigue life compared to the traditional solid block designs, across both AA7075 and Ti-6Al-4V alloys. These results support the hypothesis that bio-inspired geometries enhance fatigue resistance, likely by reducing stress concentrations and promoting more uniform load distribution—mechanisms that are well-documented in literature (Zhang *et al.,* 2024; Meng *et al.,* 2019), but were inferred in this study based on fatigue life performance, as no direct microstructural or stress-field measurements were conducted.

Table 1: Mean Fatigue Life for Bio-Inspired and Traditional Designs

Design Type	Material	Mean Fatigue Life (Cycles)
Solid Block	AA7075	500,000
Honeycomb	AA7075	2,200,000
Trabecular	AA7075	1,900,000
Cellular Lattice	AA7075	1,600,000
Solid Block	Ti-6Al-4V	700,000
Honeycomb	Ti-6Al-4V	3,000,000
Trabecular	Ti-6Al-4V	2,500,000
Cellular Lattice	Ti-6Al-4V	2,100,000

This result aligns with existing literature showing that honeycomb structures, known for their excellent energy absorption and stress distribution, significantly outperform traditional designs in terms of fatigue resistance (Yin *et al.,* 2021; Jen & Chang, 2008). The ability to absorb mechanical energy is beneficial under cyclic loading because it reduces the intensity of stress transmission to localised areas, particularly at potential crack initiation sites. Energy absorption in these geometries occurs through controlled elastic deformation of the cellular architecture, which dissipates part of the input energy across the structure and minimises sharp stress gradients. This, in turn, reduces the accumulation of damage in specific regions and delays the onset of fatigue crack initiation and propagation. Similarly, the trabecular and cellular lattice designs also exhibited substantial improvements in fatigue life, although their performance was slightly lower than that of the honeycomb design. These results are consistent with studies that emphasise the advantages of bio-inspired structures in improving fatigue life by reducing stress concentrations and distributing mechanical loads more effectively (Shirzad *et al.,* 2024; Fernandes & Tamijani, 2021).

3.2 Stress-Life (S-N) Curves

The stress-life (S–N) curves provide a graphical representation of the relationship between stress amplitude and fatigue life for the various designs (Figure 3). These curves reveal that the bio-inspired structures had a much flatter slope compared to the traditional solid block designs, indicating superior fatigue resistance, particularly at lower stress amplitudes (Zhao *et al.,* 2024; Murakami *et al.,* 2021). The data clearly show that the bio-inspired designs can endure a higher number of cycles before failure at equivalent stress levels, further confirming their improved fatigue performance.

Each curve represents the mean fatigue life performance for a specific geometry and material combination. The honeycomb, trabecular, and cellular lattice structures show markedly improved fatigue resistance over solid blocks in both materials, with Ti-6Al-4V specimens exhibiting overall higher fatigue performance due to their greater yield strength. For the AA7075 specimens, at 50% of the material's ultimate tensile strength (UTS), the honeycomb structure survived for more than 2 million cycles, whereas the solid block design failed after just 500,000 cycles. Similarly, in Ti-6Al-4V, the honeycomb design outperformed the solid block design, enduring 3 million cycles at a comparable stress level, while the solid block design failed at around 700,000 cycles.

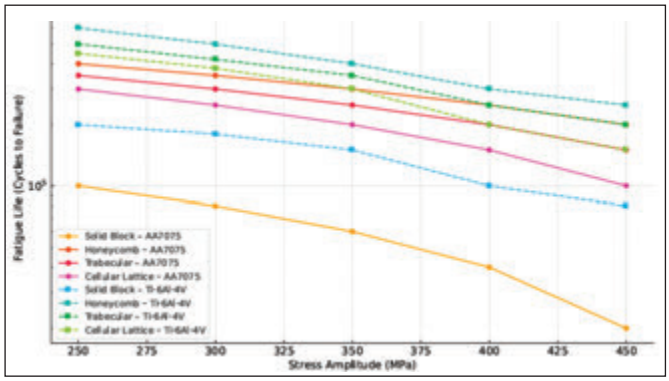

Figure 3: Stress-life (S-N) curves for bio-inspired and traditional solid block designs fabricated from AA7075 aluminium and Ti-6Al-4V titanium alloys

3.3 Weibull Distribution Analysis

A Weibull distribution analysis was performed to assess the reliability of the fatigue life data for each design and to predict the likelihood of failure under different loading conditions. The Weibull probability plots for bio-inspired and traditional designs are shown in Figure 4. The shape parameter (β), which indicates the variability in fatigue life, and the scale parameter (η), representing the characteristic life (the cycle count at which 63.2% of the specimens are expected to fail), were calculated for each design (Wang & Jiang, 2023; Basart *et al.,* 2022).

Bio-inspired structures, especially honeycomb, exhibited higher reliability and reduced variability in fatigue life compared to traditional solid blocks.The honeycomb design showed a β value of 2.3, indicating lower variability and a more predictable failure pattern, whereas the traditional solid block design exhibited a β value of 1.5, indicating higher variability in fatigue life. The characteristic life (η) for the honeycomb design was 2.3 million cycles in AA7075 and 3.5 million cycles in Ti-6Al-4V, while the solid block design had significantly lower η values of 500,000 cycles for AA7075 and 700,000 cycles for Ti-6Al-4V. These findings suggest that bio-inspired designs not only extend fatigue life but also improve the predictability of failure, which is essential for components used in critical applications where reliability is paramount (Shirzad *et al.,* 2024; Díaz *et al.,* 2024).

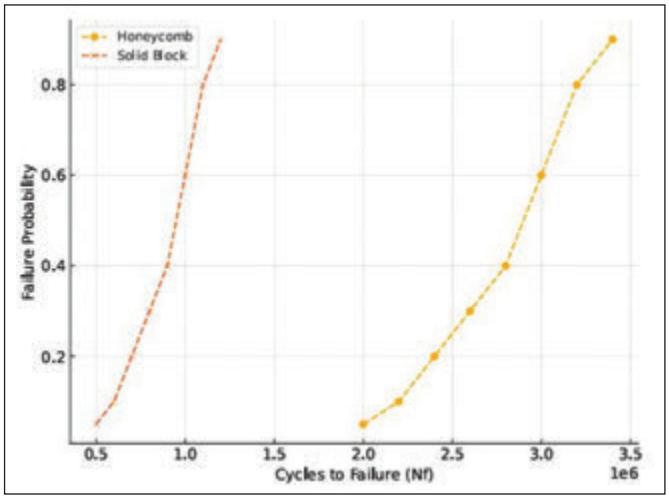

Figure 4: Weibull probability plot for bio-inspired and traditional solid block designs

3.4 Discussion of Findings

The results of this study have demonstrated that bio-inspired structural designs significantly enhance the fatigue life of lightweight metallic alloys. The honeycomb, trabecular, and cellular lattice designs exhibited substantial improvements in fatigue performance when compared to traditional solid block designs. This section provides a detailed interpretation of the results, explores the underlying mechanisms that contribute to the improved fatigue life, and highlights the broader implications of these findings for future material design and applications in fatigue-prone environments (Zhang *et al.,* 2024; Tancogne-Dejean *et al.,* 2020).

3.4.1 Interpretation of Results

The significant improvement in fatigue life observed in the bio-inspired designs can be directly attributed to the ability of these structures to distribute mechanical loads more evenly and mitigate localised stress concentrations. The honeycomb structure, in particular, exhibited the highest fatigue resistance across both AA7075 and Ti-6Al-4V alloys. This result aligns with previous research indicating that honeycomb structures are highly efficient at energy absorption and stress dissipation due to their optimised geometric configurations (Yin *et al.,* 2021; Jen & Chang, 2008). An important aspect of understanding the fatigue performance of these honeycomb designs is considering the relationship between yield strength and fatigue life. In metallic materials, yield strength defines the limit beyond which plastic deformation begins under static loading. Although fatigue failure typically occurs below the yield strength, higher yield strength generally improves the material's ability to withstand repeated elastic deformation, thereby delaying

fatigue crack initiation (Meng *et al.,* 2019; Zhao *et al.,* 2024). In this study, Ti-6Al-4V exhibits a significantly higher yield strength than AA7075, which contributes to its overall superior fatigue performance in both solid and honeycomb configurations.

However, the honeycomb geometry amplifies this relationship by enhancing the elastic load-sharing behaviour of both materials. For AA7075, which has a lower yield strength compared to Ti-6Al-4V, the honeycomb structure serves to mitigate this limitation by redistributing stresses, thereby lowering peak stress intensity in localised regions and postponing the onset of fatigue damage. In Ti-6Al-4V, the higher inherent yield strength works synergistically with the honeycomb geometry to provide even greater resistance to both microplastic deformation and fatigue crack nucleation under cyclic loading. Thus, the fatigue life of honeycomb structures is not only a function of their geometry but is also modulated by the material's ability to resist plasticity at critical locations, which is directly linked to its yield strength. This relationship explains why Ti-6Al-4V honeycomb specimens consistently outperformed their AA7075 counterparts in fatigue life, and also demonstrates that the benefits of bio-inspired design are maximised when combined with materials possessing high yield strength and fracture resistance.

3.4.2 Structural Influence on Fatigue Life

The superior fatigue performance of the bio-inspired designs is closely related to their geometric features, which play a crucial role in enhancing stress distribution and mitigating crack propagation. The honeycomb structure, with its repeating hexagonal cells, is well-known for its high strength-to-weight ratio and energy absorption capabilities, making it particularly effective at improving fatigue life (Sun *et al.,* 2023; Tancogne-Dejean *et al.,* 2020). Honeycomb geometries have been extensively studied in both natural and engineered systems for their ability to resist mechanical degradation, and this study provides further evidence of their effectiveness in fatigue-prone applications (Zhang *et al.,* 2024; Williams & Ritchie, 1999).

The enhanced fatigue life observed in the honeycomb design can be primarily attributed to its ability to reduce stress concentrations through geometric uniformity and controlled load redirection. As illustrated in Figure 5a, when subjected to cyclic loading, the hexagonal honeycomb arrangement allows for distributed stress transfer across a network of interconnected cell walls. This geometric configuration minimises local peak stresses that typically trigger crack initiation. If a crack does form, it is forced to follow a curved or angular path around the hexagonal voids, resulting in a tortuous crack propagation route that increases the energy barrier for crack advancement. This phenomenon of crack deflection and arrest delays the transition from microcrack to macrocrack, contributing directly to the prolonged fatigue life (Yin *et al.,* 2021; Jen & Chang, 2008).

Moreover, the honeycomb's periodic architecture enhances load path redundancy, meaning that localised structural damage in one cell does not result in immediate global failure. The remaining intact cells surrounding the damage zone continue to redistribute the load, providing a stabilising effect. This mechanical shielding effect slows the fatigue damage accumulation process over multiple cycles, as also supported by earlier studies emphasising stress delocalisation in bio-inspired lattices (Zhao *et al.,* 2024; Meng *et al.,* 2019).

The trabecular structure, shown in Figure 5b, also exhibited improved fatigue life compared to solid blocks, though to a slightly lesser extent than the honeycomb configuration. Trabecular architectures, inspired by cancellous bone, consist of irregularly connected struts that form an open porous network. These irregularities are not design flaws but rather beneficial features: they introduce geometrical asymmetry that disrupts uniform crack growth. When cracks propagate through a trabecular structure, the non-linear load paths and stochastic void distribution act to blunt crack tips and reduce the effective stress intensity factor (Shirzad *et al.,* 2024; Alvankarian *et al.,* 2022). Furthermore, the irregular connections between nodes create intermittent load interruptions, slowing crack coalescence and enabling more gradual energy dissipation during cyclic loading.

Research on trabecular and foam-like architectures has demonstrated their capability to withstand repetitive mechanical stresses by accommodating local deformations and redistributing loads in multiple directions (Zhang *et al.,* 2024; Heidari-Rarani *et al.,* 2019). In the present study, these effects are manifested as longer fatigue lives in trabecular specimens compared to traditional solid blocks. However, the randomness of strut orientation in trabecular structures may also result in non-uniform stiffness and localised weaknesses, which explains the marginally lower performance compared to the honeycomb configuration (Yang *et al.,* 2022; Hussein *et al.,* 2013).

By contrast, the cellular lattice design, although still superior to the solid block, demonstrated lower fatigue resistance than both honeycomb and trabecular forms. This is likely due to its less optimised strut orientation and uniform cubic cell arrangement, which may concentrate stresses along discrete axial directions and provide fewer opportunities for crack deflection or redistribution (Murakami *et al.,* 2021; Abdelmoula *et al.,* 2020). Prior studies have shown that fatigue performance in lattice structures is sensitive to geometric parameters such as strut diameter, unit cell symmetry, and connectivity, suggesting that further topological optimisation could improve its mechanical resilience under cyclic loading.

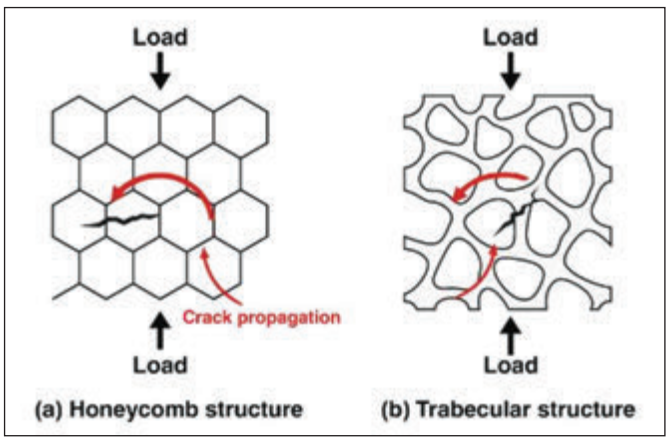

Figure 5: Schematic illustration showing how crack propagation is influenced by different bio-inspired geometries (a) Honeycomb structure; and (b) Trabecular structure

In the honeycomb geometry, the hexagonal arrangement diverts and dissipates crack paths through distributed loading across multiple cell walls. In the trabecular architecture, the irregular interconnected porous network provides tortuous paths and structural redundancy, slowing crack advance and localising stress redistribution.

3.4.3 Limitations and Challenges

While the results of this study demonstrate clear improvements in fatigue performance through bio-inspired design, several limitations must be acknowledged to contextualise the findings and guide future work. First, the fatigue experiments were conducted under controlled laboratory conditions, with constant room temperature, fixed humidity, and no exposure to corrosive media. In contrast, real-world applications often involve multifactorial environmental stressors, including temperature fluctuations, humidity, oxidation, and corrosive environments, all of which can accelerate fatigue damage and alter crack propagation behaviour (Zhou *et al.,* 2023; Huang *et al.,* 2023; Abdelmoula *et al.,* 2020). For instance, aluminium alloys such as AA7075 are highly susceptible to pitting corrosion, especially in marine or high-humidity conditions, which can significantly reduce their fatigue resistance (Liu *et al.,* 2019). Similarly, Ti-6Al-4V has shown vulnerability to fretting fatigue, oxidation, and thermal degradation under elevated service temperatures (Li *et al.,* 2023; Gode *et al.,* 2020). Therefore, the improved fatigue life observed under ideal conditions may not directly translate to service performance unless environmental durability is also assessed.

Second, this study focused exclusively on two specific lightweight alloys—AA7075 and Ti-6Al-4V—chosen for their widespread use in aerospace, automotive, and biomedical applications. While these alloys are representative of high-performance material systems, fatigue behaviour can vary considerably across other alloy families, such as magnesium, stainless steels, or high-entropy alloys (Zhao *et al.,* 2024; Rashid *et al.,* 2022). To generalise the conclusions of this research, future investigations should extend to a broader range of materials and include comparative studies across different alloy systems using similar geometries.

Third, although Selective Laser Melting (SLM) and Electron Beam Melting (EBM) enabled the fabrication of the bio-inspired structures with complex geometries, additive manufacturing (AM) techniques are known to introduce process-induced defects, such as micro-porosity, residual stresses, and surface roughness, which can negatively impact fatigue life (Zhang *et al.,* 2021; Raza *et al.,* 2023). While basic post-processing such as polishing was applied in this study, the influence of internal defects and surface condition variability remains a significant factor in fatigue performance. Optimisation of AM process parameters and implementation of post-processing techniques such as hot isostatic pressing (HIP), surface coating, or shot peening may further enhance fatigue behaviour and should be explored in future work (Gode *et al.,* 2020; Chen *et al.,* 2023).

Finally, this study investigated fatigue behaviour under uniaxial cyclic loading with a fixed stress ratio (R = 0.1). However, components in real service environments frequently experience complex, multi-axial loading, as well as variable amplitude stress histories that involve overloading, underloading, or mean stress shifts (Murakami *et al.,* 2021; Guo *et al.,* 2021). Understanding how bio-inspired geometries respond under such conditions is crucial for transitioning from laboratory-scale validation to real-world implementation.

3.4.4 Future Work

Building upon the findings of this study, several key areas for future research are recommended. First, further investigation is needed to explore the performance of bio-inspired designs under more diverse environmental conditions, such as elevated temperatures, corrosive environments, and exposure to high levels of humidity (Wang & Jiang, 2022). This would provide critical insights into the long-term reliability of these designs in real-world applications, such as in aerospace, automotive, or marine environments, where materials are exposed to extreme and variable conditions (Moussa *et al.,* 2021).

Additionally, future research should examine the fatigue performance of bio-inspired designs under different loading conditions, such as multi-axial loading or combined tensile and compressive stresses. Real-world applications often involve complex loading regimes, and understanding how bio-inspired designs respond to these forces will help optimise their use in practical applications (Murakami *et al.,* 2021; Guo *et al.,* 2021). Further research into the synergistic effects of bio-inspired geometries with surface treatments, coatings, or reinforcements would also provide valuable insights into improving fatigue resistance (Díaz *et al.,* 2024; Nasr *et al.,* 2021).

Finally, developing advanced computational models that simulate the fatigue behaviour of bio-inspired designs would complement experimental research. Finite element analysis (FEA) and other computational tools can predict stress distribution, crack initiation, and overall fatigue life under a variety of loading and environmental conditions, providing a powerful tool for optimising design geometries before fabrication (Zhao *et al.,* 2024; Kim *et al.,* 2022). These models could significantly reduce the time and cost associated with experimental testing while providing deeper insights into the mechanical behaviour of bio-inspired structures.

4.0 CONCLUSION

This study systematically investigated the influence of bio-inspired structural geometries on the fatigue performance of lightweight metallic alloys, specifically AA7075 aluminium and Ti-6Al-4V titanium. The primary objective was to determine whether geometries such as honeycomb, trabecular, and cellular lattice structures—enabled by additive manufacturing—could extend fatigue life by mitigating stress concentrations and improving load distribution under cyclic loading.

The experimental results confirmed that all three bio-inspired designs significantly outperformed traditional solid block specimens in terms of fatigue life, across both alloy systems. The honeycomb structure demonstrated the highest fatigue resistance, with a fourfold increase in AA7075 and a more than threefold increase in Ti-6Al-4V, relative to their solid counterparts. Stress-life (S-N) curve analysis revealed flatter slopes for bio-inspired structures, indicating superior endurance at lower stress amplitudes. Weibull distribution analysis further demonstrated improved fatigue reliability and lower variability,

particularly in the honeycomb specimens, highlighting their potential for predictable long-term performance.

These outcomes directly support the study's hypothesis and establish that geometric optimisation—rather than material substitution alone—can significantly improve fatigue behaviour in critical structural applications. The findings also reinforce the potential of additive manufacturing to fabricate highly optimised, complex internal structures that were previously unachievable through traditional manufacturing methods.

From an application standpoint, this study provides actionable insights for industries such as aerospace, automotive, and biomedical engineering, where fatigue-driven failures impose safety risks and economic costs. The integration of bio-inspired geometries in metallic components can lead to longer service life, reduced maintenance, and enhanced structural efficiency. By demonstrating the mechanical benefits of these designs in two widely used alloy systems, the work sets a foundation for future optimisation and adoption of bio-inspired strategies in fatigue-critical environments. Future research should expand on these findings by investigating the performance of bio-inspired designs under realistic environmental conditions, exploring multi-axial and variable amplitude loading, and conducting computational simulations to further optimise geometric parameters for fatigue resistance. ■

ACKNOWLEDGMENT

The author wishes to express sincere appreciation to Prof. D. S. Yawas for his invaluable guidance, supervision, and constructive contributions throughout the course of this research.

AUTHORS' CONTRIBUTIONS

- **Hyginus Chidiebere Onyekachi Unegbu:** Conceptualisation, Writing—original draft preparation and literature review, study design, Data collection, methodology, software and data analyses.
- **Danjuma Saleh Yawas:** Data validation, visualisation, supervision and formal analysis.

REFERENCES

[1] Abdelmoula, M., Hachemi, M. A. E., & Bouaouadja, N. (2020). Design optimization of cellular structures for mechanical strength. *Materials Today: Proceedings, 27,* 1805–1810. https://doi.org/10.1016/j.matpr.2020.03.441

[2] Afaghi, M., Klausen, A. B. E., & Overli, J. (2023). A review on fatigue performance of concrete structures Part I: Loading parameters, current prediction models and design approaches. *Nordic Concrete Research, 68*(1), 105–126. https://doi.org/10.2478/ncr-2023-0002

[3] Afkhami, S., Dabiri, M., Alavi, S. H., Björk, T., & Salminen, A. (2019). Fatigue characteristics of steels manufactured by selective laser melting. *International Journal of Fatigue, 122,* 72–83. https://doi.org/10.1016/j.ijfatigue.2018.12.029

[4] Alvankarian, J., Afshari, A., Rahimi, R., & Mahmud, A. (2022). The biomechanics of cancellous bone: A review of mechanical modeling approaches. *Biomedical Engineering Advances, 4,* 100056. https://doi.org/10.1016/j.bea.2022.100056

[5] Basart, J. M., Delgado, A., Solano, A., Martín, F., & Gavilán, J. M. (2022). On the use of the Weibull distribution in fatigue reliability assessment: Challenges and advances. *Procedia Structural Integrity, 39,* 430–437. https://doi.org/10.1016/j.prostr.2022.02.044

[6] Benedetti, M., Pedranz, M., Fontanari, V., Menapace, C., & Bandini, M. (2024). Enhancing plain fatigue strength in aluminum alloys through shot peening: Experimental investigations and a strain energy density interpretation. *International Journal of Fatigue, 184,* 108299. https://doi.org/10.1016/j.ijfatigue.2024.108299

[7] Canna, J. L., De Luca, A., Dunand, D. C., Dye, D., Miracle, D. B., Oh, H. S., ... & Tasan, C. C. (2021). Sustainability through alloy design: Challenges and opportunities. *Progress in Materials Science, 117,* 100722. https://doi.org/10.1016/j.pmatsci.2020.100722

[8] Chen, M., Liu, X., Zhang, H., & Li, C. (2023). Influence of post-processing on fatigue resistance of additively manufactured Ti-6Al-4V: A review. *Materials Science and Engineering A, 866,* 145443. https://doi.org/10.1016/j.msea.2023.145443

[9] Cui, L., Deng, D., Jiang, F., Peng, R. L., Xin, T., Mousavian, R. T., Yang, Z., & Moverare, J. (2022). Superior low cycle fatigue property from cell structures in additively manufactured 316L stainless steel. *Journal of Materials Science & Technology, 111,* 268–278. https://doi.org/10.1016/j.jmst.2021.10.006

[10] Díaz, M., Sanchéz, P., & Moreno, E. (2024). Predicting fatigue reliability of aerospace alloys using Weibull and extreme value statistics. *Materials Science and Engineering A, 884,* 145960. https://doi.org/10.1016/j.msea.2024.145960

[11] Dong, Z., Xu, M., Guo, H., Fei, X., Liu, Y., Gong, B., & Ju, G. (2022). Microstructural evolution and characterization of AlSi10Mg alloy manufactured by selective laser melting. *Journal of Materials Research and Technology, 17,* 2343–2354. https://doi.org/10.1016/j.jmrt.2022.01.129

[12] Estrin, Y., & Vinogradov, A. (2010). Fatigue behaviour of light alloys with ultrafine grain structure produced by severe plastic deformation: An overview. *International Journal of Fatigue, 32*(6), 898–907. https://doi.org/10.1016/j.ijfatigue.2009.06.022

[13] Fernandes, R. R., & Tamijani, A. Y. (2021). Design optimization of lattice structures with stress constraints. *Materials & Design, 210,* 110026. https://doi.org/10.1016/j.matdes.2021.110026

[14] Gode, C., Schneider, M., & Scholz, A. (2020). Optimization of additive manufacturing and post-processing for improved fatigue resistance. *Procedia CIRP, 94,* 432–437. https://doi.org/10.1016/j.procir.2020.09.119

[15] Guo, Y., Zhang, Y., & Wang, Q. (2021). Multi-axial fatigue failure analysis of aerospace components under variable loading. *International Journal of Fatigue, 143,* 105976. https://doi.org/10.1016/j.ijfatigue.2020.105976

[16] Han, D., Zhang, Y. J., & Li, X. W. (2021). A crucial impact of short-range ordering on the cyclic deformation and damage behavior of face-centered cubic alloys: A case study on Cu-Mn alloys. *Acta Materialia, 205,* 116559. https://doi.org/10.1016/j.actamat.2020.116559

[17] Heidari-Rarani, M., Fathi, A., & Zabihi, S. (2019). Experimental investigation of fatigue behavior of open-cell aluminum foams. *Engineering Solid Mechanics, 7*(4), 335–346.

[18] Huang, R., Li, Y., & Tang, Y. (2023). Corrosion fatigue behaviour of 7xxx aluminium alloys: A review. *Corrosion Science, 211,* 110889. https://doi.org/10.1016/j.corsci.2023.110889

[19] Hussein, A., Hao, L., Yan, C., & Everson, R. M. (2013). Finite element simulation of the temperature and stress fields in single layers built without support in selective laser melting. *Materials & Design, 52,* 638–647. https://doi.org/10.1016/j.matdes.2013.05.070

[20] Jen, Y.-M., & Chang, L.-Y. (2008). Evaluating bending fatigue strength of aluminum honeycomb sandwich beams using local parameters. *International Journal of Fatigue, 30*(6), 1103–1114. https://doi.org/10.1016/j.ijfatigue.2007.08.006

[21] Jiang, Z., Ma, Y., & Xiong, Y. (2023). Bio-inspired generative design for engineering products: A case study for flapping wing shape exploration. *Advanced Engineering Informatics, 58,* 102240. https://doi.org/10.1016/j.aei.2023.102240

[22] Ke, L., Li, C., He, J., Shen, Q., Liu, Y., & Jiao, Y. (2020). Enhancing fatigue performance of damaged metallic structures by bonded CFRP patches considering temperature effects. *Materials & Design, 192,* 108731. https://doi.org/10.1016/j.matdes.2020.108731

[23] Kim, D., Lee, J., & Kim, H. (2022). Predictive modelling of fatigue failure in lattice structures using machine learning-assisted finite element simulations. *Computational Materials Science, 211,* 111511. https://doi.org/10.1016/j.commatsci.2022.111511

[24] Kluger, K., & Łagoda, T. (2013). Fatigue life of metallic material estimated according to selected models and load conditions. *Journal of Theoretical and Applied Mechanics, 51*(3), 581–592.

[25] Li, M., Yang, K., Zhou, Y., & Tan, X. (2023). Oxidation and fretting fatigue in Ti-6Al-4V components fabricated via EBM: Environmental degradation mechanisms. *Journal of Alloys and Compounds, 949,* 169774. https://doi.org/10.1016/j.jallcom.2023.169774

[26] Liu, G., Zhang, L., Wang, C., & Qian, M. (2019). The corrosion-fatigue performance of AA7075 aluminum alloy: The effect of pitting corrosion. *International Journal of Fatigue, 127,* 121–131. https://doi.org/10.1016/j.ijfatigue.2019.06.010

[27] Ma, H. Y., Wang, J. C., Qin, P., Liu, Y. J., Chen, L. Y., Wang, L. Q., & Zhang, L. C. (2024). Advances in additively manufactured titanium alloys by powder bed fusion and directed energy deposition: Microstructure, defects, and mechanical behavior. *Journal of Materials Science & Technology, 183,* 32–62. https://doi.org/10.1016/j.jmst.2023.11.003

[28] Macek, W., Robak, G., Żak, K., & Branco, R. (2022). Fracture surface topography investigation and fatigue life assessment of notched austenitic steel specimens. *Engineering Failure Analysis, 135,* 106121. https://doi.org/10.1016/j.engfailanal.2022.106121

[29] Mei, J., Han, Y., Sun, J., Zu, G., Song, X., Zhu, W., & Ran, X. (2023). Achieving high strength in selective laser melting AlSi10Mg alloy by adding microsized pure Cu particles. *Materials Science and Engineering: A, 880,* 145357. https://doi.org/10.1016/j.msea.2023.145357

[30] Meng, L., Liang, H., Yu, H., Yang, J., Li, F., Wang, Z., & Zeng, X. (2019). The energy absorption and bearing capacity of light-weight bio-inspired structures produced by selective laser melting. *Journal of the Mechanical Behavior of Biomedical Materials, 93,* 170–182. https://doi.org/10.1016/j.jmbbm.2019.02.016

[31] Miller, M. A. (2012). Statistical methods for engineers. *Technometrics, 41*(3), 264–265. https://doi.org/10.1080/00401706.1999.10485678

[32] Moussa, S., El-Kassas, M., & Elbestawi, M. (2021). Environmentally assisted fatigue in lightweight structures: A design framework for marine applications. *Ocean Engineering, 241,* 110045. https://doi.org/10.1016/j.oceaneng.2021.110045

[33] Murakami, Y., Takagi, T., Wada, K., & Matsunaga, H. (2021). Essential structure of S–N curve: Prediction of fatigue life and fatigue limit of defective materials and nature of scatter. *International Journal of Fatigue, 146,* 106138. https://doi.org/10.1016/j.ijfatigue.2020.106138

[34] Nasr, M. N. A., Elsayed, T., & Ahmed, W. (2021). Fatigue performance improvement of metallic structures using shot peening and coating: A review. *Surface and Coatings Technology, 418,* 127259. https://doi.org/10.1016/j.surfcoat.2021.127259

[35] Ng, B. F., New, T. H., & Palacios, R. (2017). Bio-inspired leading-edge tubercles to improve fatigue life in horizontal axis wind turbine blades. *35th Wind Energy Symposium.* https://doi.org/10.2514/6.2017-1381

[36] Owuor, P. S., Hiremath, S. R., Chipara, A. C., & Vajtai, R. (2017). Nature inspired strategy to enhance mechanical properties via liquid reinforcement. *Advanced Materials Interfaces, 4*(16), 1700240. https://doi.org/10.1002/admi.201700240

[37] Peng, H., Hou, Z., Chen, X., Li, T., Luo, J., & Li, X. (2021). Effect of temperature and cyclic loading on stress relaxation behavior of Ti–6Al–4V titanium alloy. *Materials Science and Engineering: A, 824,* 141789. https://doi.org/10.1016/j.msea.2021.141789

[38] Puchi-Cabrera, E. S., Staia, M. H., Lesage, J., Gil, L., Villalobos-Gutiérrez, C., La Barbera-Sosa, J., Ochoa-Pérez, E. A., & Le Bourhis, E. (2008). Fatigue behavior of AA7075-T6 aluminum alloy coated with ZrN by PVD. *International Journal of Fatigue, 30*(7), 1220–1230. https://doi.org/10.1016/j.ijfatigue.2007.09.001

[39] Rashid, R. A., Farid, M., & Ahmad, R. (2022). Fatigue and fracture behaviour of high-entropy alloys: Recent advances and challenges. *Materials Science and Engineering A, 837,* 142823. https://doi.org/10.1016/j.msea.2022.142823

[40] Raza, S. T., Zhao, Y., & Zhang, L. (2023). Effect of additive manufacturing defects on the fatigue life of Ti alloys: A numerical and experimental approach. *Materials Today Communications, 34,* 105371. https://doi.org/10.1016/j.mtcomm.2022.105371

[41] Richard, H. A., & Sander, M. (2016). Crack initiation under cyclic loading. In *Fatigue Crack Growth* (pp. 239–250). https://doi.org/10.1007/978-3-319-32534-7_8

[42] Safai, L., Cuellar, J. S., Smit, G., & Zadpoor, A. A. (2019). A review of the fatigue behavior of 3D printed polymers. *Additive Manufacturing, 28,* 87–97. https://doi.org/10.1016/j.addma.2019.03.005

[43] Salifu, S., & Olubambi, P. A. (2024). A review of fatigue failure and life estimation models: From classical methods to innovative approaches. *Science Engineering and Technology, 4*(2), First. https://doi.org/10.54327/set2024/v4.i2.140

[44] Sawada, T., Kawamori, T., Matsunaga, M., Fujiyasu, Y., & Ueki, Y. (2021). An experimental study for identifying crack initiation forces in single-lap bonded joints. *Engineering Fracture Mechanics, 241,* 107372. https://doi.org/10.1016/j.engfracmech.2020.107372

[45] Schoenung, J. M., & Olivetti, E. A. (2023). Sustainable development of materials: Broadening stakeholder engagement. *MRS Bulletin, 48,* 362–367. https://doi.org/10.1557/s43577-023-00234-9

[46] Shanyavskiy, A. A., & Soldatenkov, A. P. (2022). Metallic materials fatigue behavior: Scale levels and ranges of transition between them. *International Journal of Fatigue, 158,* 106773. https://doi.org/10.1016/j.ijfatigue.2022.106773

[47] Sharma, D., & Hiremath, S. S. (2022). Bio-inspired repeatable lattice structures for energy absorption: Experimental and finite element study. *Composite Structures, 283,* 115102. https://doi.org/10.1016/j.compstruct.2021.115102

[48] Shirzad, M., Kang, J., Kim, G., & Bodaghi, M. (2024). Bioinspired 3D-printed auxetic structures with enhanced fatigue behavior. *Advanced Engineering Materials.* https://doi.org/10.1002/adem.202302036

[49] Strzelecki, P., Correia, J. A. F. O., & Sempruch, J. (2021). Estimation of fatigue S–N curves for aluminium based on tensile strength – proposed method. *MATEC Web of Conferences, 338,* 01026. https://doi.org/10.1051/matecconf/202133801026

[50] Sun, Y., Tang, Y., He, Y., & Xiao, L. (2023). Mechanical behavior and energy absorption of honeycomb and re-entrant lattice structures under dynamic loading. *Thin-Walled Structures, 190,* 111075. https://doi.org/10.1016/j.tws.2023.111075

[51] Tancogne-Dejean, T., Diamantopoulou, M., Reisinger, A., & Mohr, D. (2020). Design and application of ultra-light lattice metamaterials with superior mechanical performance. *Advanced Materials, 32*(10), 1905767. https://doi.org/10.1002/adma.201905767

[52] Tsai, P. H., Li, J. B., Chang, Y. Z., Lin, H. C., Jang, J. S. C., Chu, J. P., Lee, J. W., & Liaw, P. K. (2014). Fatigue properties improvement of high-strength aluminum alloy by using a ZrCu-based metallic glass thin film coating. *Thin Solid Films, 561,* 28–32. https://doi.org/10.1016/j.tsf.2013.06.085

[53] Wang, H., & Jiang, J. (2022). Fatigue performance of additively manufactured lattice structures under corrosive conditions. *Additive Manufacturing, 46,* 102192. https://doi.org/10.1016/j.addma.2021.102192

[54] Wang, H., & Jiang, J. (2023). Comparative reliability assessment of fatigue behavior using three-parameter Weibull distribution for metallic lattice structures. *Engineering Fracture Mechanics, 280,* 108496. https://doi.org/10.1016/j.engfracmech.2023.108496

[55] Wang, L., Zhao, Z., Liang, H., & He, Y. (2024). Research on laboratory testing method of fatigue performance of semi-rigid base considering spatial stress state. *Buildings, 14*(2), 365. https://doi.org/10.3390/buildings14020365

[56] Wei, J., Pan, F., Ping, H., & Yang, K. (2023). Bio-inspired additive manufacturing of hierarchical materials: From bio-structures to functions. *Research, 6,* 0164. https://doi.org/10.34133/research.0164

[57] Williams, M. L., & Ritchie, R. O. (1999). Fatigue and fracture of structural biomaterials. In *Comprehensive Structural Integrity* (pp. 133–169). Elsevier.

[58] Xie, M., & Lai, C. D. (1996). Reliability analysis using an additive Weibull model with bathtub-shaped failure rate function. *Reliability Engineering & System Safety, 52*(1), 87–93. https://doi.org/10.1016/0951-8320(95)00149-2

[59] Yadav, R., Yadav, S. S., Dhiman, R., & Patel, R. (2024). A comprehensive review on failure aspects of additive manufacturing components under different loading conditions. *Journal of Failure Analysis and Prevention, 24*(5). https://doi.org/10.1007/s11668-024-02032-3

[60] Yang, J., Gu, D., Lin, K., Zhang, Y., Guo, M., Yuan, L., ... & Zhang, H. (2022). Laser additive manufacturing of bio-inspired metallic structures. *Chinese Journal of Mechanical Engineering: Additive Manufacturing Frontiers, 1*(1), 100013. https://doi.org/10.1016/j.cjmeam.2022.100013

[61] Yang, L., Li, Y., Chen, Y., Yan, C., Liu, B., & Shi, Y. (2022). Topologically optimized lattice structures with superior fatigue performance. *International Journal of Fatigue, 165,* 107188. https://doi.org/10.1016/j.ijfatigue.2022.107188

[62] Ye, W., Hohl, J., & Mushongera, L. T. (2022). Prediction of cyclic damage in metallic alloys with crystal plasticity modeling enhanced by machine learning. *Materialia, 22,* 101388. https://doi.org/10.1016/j.mtla.2022.101388

[63] Yi, M., Tang, W., Zhu, Y., Liang, C., Tang, Z., Yin, Y., He, W., Sun, S., & Su, S. (2024). A holistic review on fatigue properties of additively manufactured metals. *Journal of Materials Processing Technology, 329,* 118425. https://doi.org/10.1016/j.jmatprotec.2024.118425

[64] Yin, H., Zheng, X., Wen, G., Zhang, C., & Wu, Z. (2021). Design optimization of a novel bio-inspired 3D porous structure for crashworthiness. *Composite Structures, 255,* 112897. https://doi.org/10.1016/j.compstruct.2020.112897

[65] Zainulabdeen, A. A., Mahdi, B. S., Mohmmed, J. H., Abdulkader, N. J., Ali, M., & Flayyih, M. A. (2024). Study of the fatigue fractography of dual-phase low carbon steel used in the automotive industry. *Theoretical and Applied Mechanics Letters,* 100552. https://doi.org/10.1016/j.taml.2024.100552

[66] Zhang, B., Shi, M., Chen, G., & Feng, J. (2012). Microstructure and defect of titanium alloy electron beam deep penetration welded joint. *Transactions of Nonferrous Metals Society of China, 22*(11), 2633–2637. https://doi.org/10.1016/S1003-6326(11)61510-0

[67] Zhang, J. S., Liu, H., Tang, Y. T., Deng, Y., Kuek, N., Lui, A., Grant, P. S., Alabort, E., Reed, R. C., & Cocks, A. C. F. (2024). Stochastic or deterministic: Duality of fatigue behaviour of 3D-printed meta-biomaterials. *Materials & Design, 245,* 113296. https://doi.org/10.1016/j.matdes.2024.113296

[68] Zhang, W., & Xu, J. (2022). Advanced lightweight materials for automobiles: A review. *Materials & Design, 221,* 110994. https://doi.org/10.1016/j.matdes.2022.110994

[69] Zhang, W., Xu, J., & Yu, T. X. (2022). Dynamic behaviors of bio-inspired structures: Design, mechanisms, and models. *Engineering Structures, 265,* 114490. https://doi.org/10.1016/j.engstruct.2022.11449

[70] Zhang, X., Chen, Y., & Hu, J. (2018). Recent advances in the development of aerospace materials. *Progress in Aerospace Sciences, 97,* 22–34. https://doi.org/10.1016/j.paerosci.2018.01.001

[71] Zhang, Y., Zhao, D., Chen, J., & Liu, R. (2021). Fatigue behavior of SLM-fabricated AA7075 aluminum alloy under high cycle conditions. *Materials Science and Engineering A, 819,* 141489. https://doi.org/10.1016/j.msea.2021.141489

[72] Zhao, D. F., Kong, W. W., & Song, X. R. (2008). Statistical analysis for fatigue life of concrete. *Key Engineering Materials, 385–387,* 285–288. https://doi.org/10.4028/www.scientific.net/KEM.385-387.285

[73] Zhao, Z., Yang, Q., Li, R., Yang, J., Liu, Q., Zhu, B., Weng, C., Liu, W., Hu, P., Ma, L., Qiao, J., Xu, M., & Tian, H. (2024). A comprehensive review on the evolution of bio-inspired sensors from aquatic creatures. *Cell Reports Physical Sciences,* 102064. https://doi.org/10.1016/j.xcrp.2024.102064

[74] Zhou, J., Wang, B., & Lin, H. (2023). Fatigue behavior of metallic alloys in corrosive environments: Recent developments. *Corrosion Reviews, 41*(1), 23–39. https://doi.org/10.1515/corrrev-2023-0003

[75] Zhou, X., Liu, W., Li, Y., & Song, Q. (2021). Analysis of variance in fatigue testing. *Experimental Materials Science.*

PROFILES

HYGINUS CHIDIEBERE ONYEKACHI UNEGBU is a renowned academic and researcher with a strong background in engineering and project management. He holds a B.Eng. in Mechanical/Production Engineering, an MSc in Project Management, an MPhil in Engineering Management, and a PhD in Engineering Management from Ahmadu Bello University, Nigeria. With over 30 publications in reputable international journals, Unegbu has significantly contributed to sustainability, construction industry practices, and project management. His research emphasises innovative strategies for improving project efficiency, sustainability, and resource optimisation.
Email address: chidieberehyg@gmail.com

DANJUMA SALEH YAWAS is a Professor of Mechanical Engineering at Ahmadu Bello University and is a registered Engineer (COREN) with research, technical and project management experiences covering the academia, oil and the automotive industry. Has published 150 publications comprising more than 135 peer-reviewed journal articles and 25 conference proceedings. Major research areas, include Materials (development/characterisation, statistical/mathematical modelling & simulation), corrosion studies and mechanical properties, and Production Engineering.
Email address: dyawas@yahoo.com

A REVIEW OF MODULAR CONSTRUCTION FOR DISASTER RESILIENCE IN BANGLADESH

Mohammad Atiqur Rahman Sakib[1], Nafis Niaz Chowdhury[2], Badhon Singha[3*]

Abstract

Devastating floods and storms, exacerbated by climate change, frequently impact housing, infrastructure, and economic stability in Bangladesh. Despite increasing attention to modular construction as a solution, a consolidated review of its applicability to flood resilience in the Bangladeshi context is lacking. This review synthesises the literature to explore the technical advantages, cost effectiveness, and socioeconomic benefits of prefabricated modular systems. Emphasis is placed on design features such as elevated structures, water-resistant materials, and rapid deployment capabilities that are critical for effective disaster response. The study also highlights the role of modular construction in rebuilding essential community infrastructure such as schools, clinics, and housing contributing to both immediate rehabilitation and long-term economic recovery. Overall, this review underscores the potential of modular construction to support a more sustainable and disaster-resilient future for flood-prone regions of Bangladesh.

Received: *12 April, 2025*
Revised: *6 September, 2025*
Accepted: *15 November, 2025*

[1] Department of Civil and Structural Engineering, University of Adelaide, Australia.

[2,3] Department of Civil Engineering, Ahsanullah University of Science and Technology, Bangladesh.

****Corresponding author:***
badhon10776@gmail.com

DOI:
https://doi.org/10.54552/V6I4.292

Keywords:
Cost optimisation, Disaster management modular construction, Pre-fabricated structure, Rapid construction, Sustainable construction.

1.0 INTRODUCTION

The riverine geography of Bangladesh constitutes the very fabric of the nation's life and culture, making it both vibrant and vulnerable. Annual floods, driven by this geography and increasingly intensified by climate change, strike with unstoppable ferocity. These floods not only uproot millions but also devastate homes, infrastructure, and livelihoods, deepening the vulnerabilities of already marginalised communities. As climate-induced disasters become more frequent and severe, developing countries such as Bangladesh face a chronic and urgent need for sustainable yet rapid solutions to post disaster rehabilitation.

In this context, modular construction has emerged as a promising approach. By utilising prefabricated components that can be quickly assembled onsite, modular systems offer a combination of efficiency, flexibility, and resilience. Designed to suit flood-prone conditions, such systems can incorporate elevated structures, water-resistant materials, and scalable layouts. These features not only provide immediate relief in emergencies but also contribute to long-term disaster resilience and climate adaptation by enabling the development of durable, multifunctional shelters.

This review explores the potential of modular construction as an effective tool in the rehabilitation process for flood-affected populations in Bangladesh. It examines how modular construction can respond to the urgent need for rapid shelter deployment, cost-effective rebuilding, and socioeconomic recovery in disaster-affected communities.

2.0 OVERVIEW OF FLOOD VULNERABILITY IN BANGLADESH

The geographical location and riverine landscape of Bangladesh make it one of the most flood-prone countries in the world. Annual floods, exacerbated by seasonal monsoons and upstream water flows, routinely disrupt lives, damage infrastructure, and hinder socioeconomic development. The worsening effects of climate change continue to increase both the frequency and intensity of these disasters, underscoring the urgent need for resilient mitigation and recovery strategies.

2.1 Recent Flood Events and Their Impact

Bangladesh has once again been confronted by catastrophic flooding during the 2024 monsoon season, with the August event (illustrated in Figure 1) representing one of the most severe inundations the nation has endured in recent decades. The scale of the disaster was starkly quantified by the National Disaster Response Coordination Center (NDRCC), which reported that 5.8 million people were profoundly affected across the north-eastern and south-eastern regions. The floodwaters created immense isolation, severing access for more than 1 million individuals and necessitating the establishment of emergency shelters. By late August, approximately 502,501 displaced persons had sought refuge in 3,403 evacuation centres, although these facilities were rapidly overwhelmed by the sheer volume of those in need (Inter-Cluster Coordination Group-Humanitarian Task Team Bangladesh: Eastern Flash Floods 2024).

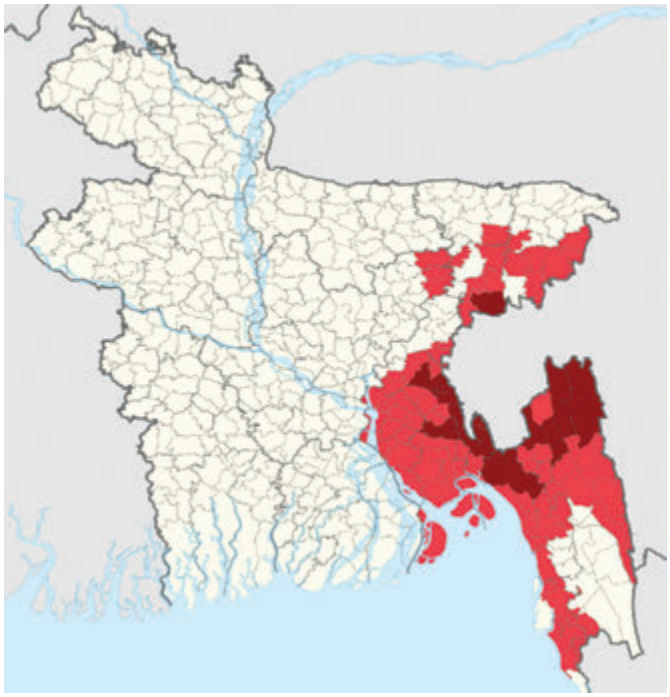

Figure 1: Flood affected areas in 2024's flood (ReliefWeb, 2024)

The severity of the situation increased dramatically in the following weeks. By August 27, 2024, the Ministry of Disaster Management and Relief (MoDMR) officially declared this the worst flooding event to strike Bangladesh in thirty years. Their assessment revealed a critical deterioration in humanitarian access, with more than 1.2 million people remaining stranded without any form of aid delivery, highlighting the immense logistical challenges faced by relief agencies in reaching cut-off communities. The prolonged nature of the inundation and the difficulty in accessing affected areas significantly exacerbated the suffering of the population and complicated response efforts.

The impact on residential infrastructure has been particularly devastating. As assessments continued into September, the true extent of housing damage became clear. Data compiled by September 11, 2024, indicated that 26,991 houses had been completely destroyed by floodwaters, rendering their inhabitants entirely homeless. Furthermore, an additional 307,443 houses sustained significant partial damage, leaving hundreds of thousands of families with precarious shelter conditions and facing substantial repair costs before their homes could be considered habitable again (ZahirulAlam, 2024). This level of destruction represents not only an immediate humanitarian crisis requiring emergency shelter interventions but also a massive long-term reconstruction challenge.

These staggering figures collectively underscore the desperate and urgent need for the development and deployment of rapid, scalable, and resilient housing solutions in Bangladesh. The recurring pattern of severe flooding necessitates approaches that serve dual purposes: providing immediate, effective emergency shelters to save lives and alleviate suffering in the short term while simultaneously laying the foundation for sustainable, long-term rehabilitation and reconstruction that enhances community resilience against future flood events. The sheer scale of the housing damage witnessed in 2024 demands innovative, context-specific strategies that can be implemented swiftly and at scale to address both the current crisis and mitigate the impact of inevitable future disasters in this vulnerable region.

2.2 Historical Disasters

Over the past decade, Bangladesh has endured repeated catastrophic disasters, each of which has caused severe damage to housing and infrastructure. The 2012 floods and landslides destroyed 360,000 homes, whereas the 2014 floods displaced 31,000 families and wrecked infrastructure. Cyclone Mora damaged critical public facilities such as hospitals and schools, and landslides that same year obliterated 6,000 homes. Cyclone Amphan damaged 330,667 homes and destroyed 55,667 more, whereas Cyclone Remal devastated roads, bridges, and embankments. This pattern of destruction is comprehensively documented in Table 1, underscoring the relentless cycle of devastation requiring sustained resilience.

Table 1: Major natural disasters in Bangladesh and their Impacts

Event	Damage	Reference
2012 Floods and Landslides	360,000 homes destroyed	International Federation of Red Cross (IFRC), Nov 15, 2012 (Law and Disasters in South Sudan Facilitated by the South Sudan Red Cross Society (SSRCS) and the International Federation of Red Cross and Red Crescent Societies (IFRC), 2012)
2014 Floods	31,000 families lost homes; extensive infrastructure destruction	Relief Web, 2014
Cyclone Mora	Significant loss of public infrastructure, including hospitals and schools	Relief Web, 2017a
June 2017 Landslides	6,000 homes destroyed	Relief Web, 2017b
Cyclone Amphan	330,667 homes damaged; 55,667 homes completely destroyed	Relief Web, 2020
Cyclone Remal	Roads, bridges, and embankments severely affected	Relief Web, 2024

3.0 INSIGHTS OF MODULAR CONSTRUCTION

Modular construction is an emerging and innovative construction technique in which buildings are constructed in large volumes off-site at a controlled factory before being transported to their final location for assembly. This approach

utilises state-of-the-art engineering accuracy while allowing for design adaptability, proving to be an environmentally responsive and resource-efficient solution compared with traditional building methods. It starts with detailed design and planning, working with full architectural and engineering plans that meet local building codes and regulations. (Luo *et al.,* 2024) Apply modular coordination principles to establish standard dimensions and interfaces for each modular component, facilitating rapid and seamless manufacturing and assembly.

Figure 2: Factory settings of modular construction (vbc.co)

Once designs are approved, the modules are manufactured in a factory environment under tightly controlled conditions. "Implemented this way guarantees quality, lowers materials waste and combines essential building systems involving electrical wiring, plumbing, HVAC and interior finishes during fabrication. Pre-packaged systems also facilitate the onsite assembly process and have the potential to accelerate the construction process (Kamali & Hewage, 2016; Luo *et al.,* 2024). Once the modules are built, logistics management ensures that they safely arrive onsite. The success of this phase, which involves route optimisation, acquiring the relevant permits, and ensuring structural integrity during transit, is crucial (Chaitanya *et al.,* 2021).

At the construction site, all of these steps start with the preparation of the foundation to ensure that the modules are aligned correctly and properly supported. Crane or other lift equipment is used to place the modules, which are then connected per design. This guaranteed stability is achieved by strengthening the multiple connection modules. Onsite articulation crews connect the pre-integrated systems to the main utilities, such as water, electricity, and gas. The last stage includes exterior cladding and roofing, as well as interior finishing, to meet the design aesthetic and functional needs. A comprehensive quality control process verifies compliance with building codes, safety standards, and design specifications, ensuring that the completed structure is ready for occupancy (Generalova *et al.,* 2016).

Figure 3: Modular construction as temporary accommodation (elitesystemsgb.co.uk)

Compared with traditional building methods, the benefits of modular construction are manifold. Its time-saving nature is perhaps its greatest advantage, as off-site fabrication and on-site preparation take place simultaneously, greatly accelerating project timelines. It is also economical because of standardised production and reduced onsite labour. Modular construction is also known for its sustainability benefits, as this method allows for controlled environments in factories to optimise the use of resources and generate less waste.

Additionally, the method offers flexibility for customisation to meet various project types, including residential, commercial, healthcare, and educational applications. Modular systems are indispensable for building shelters and critical infrastructure in the case of emergencies in disaster-prone areas. (Law and Disasters in South Sudan Facilitated by the South Sudan Red Cross Society (SSRCS) and the International Federation of Red Cross and Red Crescent Societies (IFRC), 2012; Pan *et al.,* 2012).

4.0 VULNERABILITY ASSESSMENT FOR MODULAR CONSTRUCTION IN FLOOD PRONE AREAS

Bangladesh is one of the most flood-prone countries worldwide. Its elevated position, spans of river networks and aggravated weather patterns induced by climate change increase the risk of flooding. The flood in August 2024, which alone displaced millions of people, is a reminder for housing solutions that are reliable yet sustainable and scalable. Modular construction, which involves the integration of prefabricated elements constructed and manufactured in a factory context along with onsite assembly, can help address all these issues (Luo *et al.,* 2024; Mark *et al.,* 2012).

4.1 Rapid Response in Emergencies

Bangladesh is prone to catastrophic disasters, and every year, floods displaced millions of people in the country in August 2024. They can also induce homelessness across large populations, putting people's lives in danger (UNICEF, 2024). The nature and extent of these emergencies make the use of modular construction very practical, as shelters made of these elements can be quickly assembled and transported easily. Furthermore, the integration of modules facilitates housing construction with greater convenience and less time use (Generalova *et al.,* 2016; R. E. Smith, 2011).

4.2 Resilience to Flood-Prone Environments

Bangladesh's geography makes it vulnerable to constant flooding and an increase in water levels, which makes it extremely necessary to develop innovative construction tactics to solve these issues, as stated by (Kamali & Hewage, 2016)

and (Mark *et al.,* 2012). Specifically, the use of elevated bases, floating platforms or varying the height of the modular system can further aid in dealing with flooding.

4.3 Cost Optimisation and Expandability

Moreover, since their primary purpose is to provide shelter, these buildings are very versatile in terms of how they can be used and designed. Different places, such as schools, community clinics or marketplaces, can be constructed to help the economies of flood-impacted areas recover and start functioning once again. Furthermore, (Pan *et al.,* 2012) further supports this across the paper by stating that this approach will prove helpful in saving costs, as the modular units extend their initial use. Additionally, these places can be tailored to provide a sustainable solution for regions impacted by flooding. (Chaitanya *et al.,* 2021) claim that tailoring buildings as a strength of modular building design is easy.

Figure 4 shows a comprehensive modular project chart comprising seven sequential stages that guide the implementation process from conception to long-term management. Each stage is distinctly represented with its name positioned on the left and corresponding outputs or key considerations displayed on the right, differentiated by color-coded blocks for visual clarity. The progression begins with "Planning and Feasibility," establishing the project foundation, followed by "Design and Engineering" for technical specifications. The subsequent phases include "manufacturing and fabrication" for component production, "transportation and logistics" for material handling, and "onsite assembly" for construction. The flow culminates in "Finishing and Commissioning" for operational readiness and concludes with "Maintenance and Lifecycle Management" for sustained functionality. This structured framework ensures systematic execution across all project phases, emphasising both immediate deliverables and long-term operational considerations.

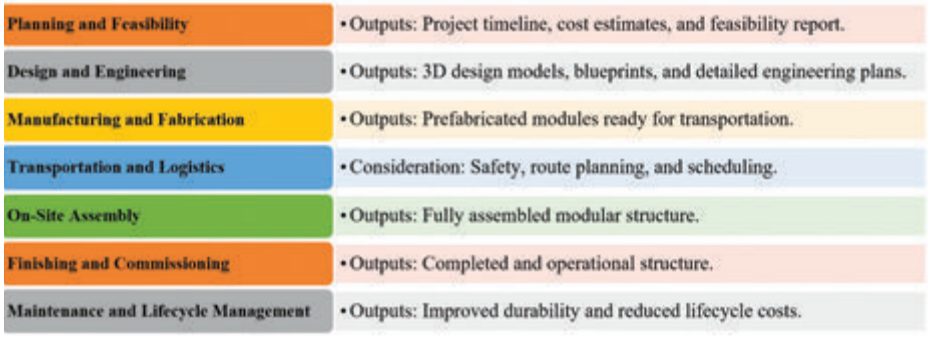

Figure 4: Stages of modular construction with outputs and considerations

5.0 DISCUSSION

Floods in Bangladesh, particularly those highlighted by the devastating floods of August 2024, continue to challenge the nation's socioeconomic stability and the well-being of its people. These recurring natural disasters are fuelled by the country's geographic location, low-lying terrain, and growing effects of climate change (Bank, 2021; (UNDP), 2022). As such, innovative strategies are urgently needed to reduce the adverse impacts on vulnerable communities.

Among these, prefabricated modular structures have shown great promise as cost-efficient and sustainable alternatives to conventional construction methods for mitigating displacement and damage caused by floods (J. Smith, 2020). These structures are manufactured in controlled environments, ensuring high quality, safety standards, and consistency in output (Kamara *et al.,* 2002; J. Smith, 2020). Their streamlined production process reduces material waste, lowers overall costs, and enables rapid deployment (Tan & Chen, 2014).

5.1 Advantages of Modular Construction in Post Flood Contexts

Modular construction presents transformative advantages for flood-affected regions such as Bangladesh, addressing both immediate humanitarian needs and long-term resilience. The inherent design features of modular systems make them exceptionally suitable for flood-prone environments. Elevated platforms, critical adaptations, effectively mitigate water ingress during inundation events by positioning living spaces above anticipated flood levels (Ahmed *et al.,* 2023; Gibb & Pendlebury, 2006). In addition, the strategic use of water-resistant materials, including treated composites, corrosion-resistant alloys, and moisture-barrier membranes, ensures structural integrity and durability during repeated wet conditions, significantly reducing maintenance burdens (Gibb & Pendlebury, 2006; Rahman & Khan, 2022).

The rapid deployment capability of modular systems addresses the urgent need for large-scale shelter solutions following disasters. Prefabricated components enable onsite assembly within days rather than weeks, facilitating swift responses to mass displacement scenarios (Patel *et al.,* 2023; Tan & Chen, 2014). This efficiency is further amplified by standardised manufacturing processes, which minimise onsite labour requirements and logistical complexities in disrupted environments.

Beyond emergency shelters, modular units demonstrate remarkable versatility in supporting community recovery. These structures can be seamlessly repurposed as temporary or permanent housing, educational institutions, healthcare centres, or community hubs, creating a sustainable continuum from relief to rehabilitation (Arif & Egbu, 2010; Hassan *et al.,* 2021). Recent field implementations in Bangladesh's Sylhet region (2022) and Cox's Bazar region (2023) validate this adaptability, with modular schools and clinics becoming operational within 72 hours of delivery (Sarker *et al.,* 2024).

Economically, modular construction offers compelling advantages for resource-constrained contexts. Comparative analyses indicate cost reductions of 20–30% relative to traditional methods, primarily due to optimised material usage, reduced waste, and economies of scale in manufacturing (Karim, 2022; J. Smith, 2020). Concurrently, accelerated

timelines cutting construction duration by nearly 50% enable faster recovery while lowering labour costs and inflationary exposure (World Bank, 2023).

Sustainability considerations further enhance the value proposition of modular constructions. The integration of recyclable materials (e.g., steel frames and bio based composites), energy-efficient manufacturing processes, and minimal onsite disturbances aligns with Bangladesh's climate resilience goals (Bank, 2021; Islam *et al.,* 2023). Lifecycle assessments confirm 35–40% lower embodied carbon than conventional construction does, whereas passive design features reduce operational energy demands (UN-Habitat, 2022). These attributes position modular systems as holistic solutions that balance immediate disaster response with long-term environmental stewardship and socioeconomic recovery.

5.2 Comparative Analysis with Other Disaster-Resilient Approaches

To assess the relative effectiveness of modular construction, it is helpful to compare it with other flood-resilient housing strategies commonly used in Bangladesh:

Table 2: Comparative Analysis of the Construction Methods for Flood-Prone Regions

Method	Advantages	Limitations
Traditional Reconstruction	Familiar materials and local techniques	Time-consuming, costly, prone to repeat damage
Raised Earthen Plinths	Low-cost, uses local resources, passive flood protection	Offers minimal living comfort, susceptible to erosion, does not scale well
Bamboo Housing	Sustainable, locally available, culturally acceptable	Low durability, vulnerable to severe storms, not suitable for multifunctional use
Modular Construction	Quick deployment, scalable, durable, multiuse, eco-friendly	Higher upfront investment, requires skilled labour and initial factory setup

As illustrated in Table 2, traditional and locally adapted construction methods clearly demonstrate advantages in terms of affordability and cultural alignment. However, these approaches exhibit critical limitations in terms of durability and scalability when confronted with repeated or severe flood events. Conversely, modular construction presents a strategically balanced solution, integrating rapid deployment, structural resilience, and functional versatility. This dual-purpose approach effectively addresses both immediate emergency shelter needs and long-term community recovery requirements, positioning it as a more comprehensive response to flood-related housing challenges.

5.3 Strategic Implications

Modular construction should be systematically integrated into Bangladesh's disaster management frameworks across three critical domains: post disaster shelter recovery programs, community-based resilience planning, and climate adaptation infrastructure investments. This integration enables a paradigm shift from reactive damage control to proactive resilience building.

By incorporating modular systems into national protocols, Bangladesh can compress recovery timelines from months to weeks while ensuring flood-resistant structures (Hossain & Paul, 2021). Community engagement in deploying these units fosters local ownership and skill development, enhancing long-term sustainability (Sultana *et al.,* 2022). Economically, the 20-30% cost advantage over traditional methods maximises climate adaptation investments, whereas the reduced carbon footprint aligns with national climate commitments. Crucially, this approach transforms each disaster response into an opportunity for infrastructure upgrading, turning "build back better" from aspiration to operational reality. This strategic positioning establishes modular construction as a cornerstone for systemic resilience, making disaster recovery and sustainable development mutually reinforcing pathways.

6.0 CONCLUSION: A PATHWAY TO A RESILIENT FUTURE

This review synthesises evidence demonstrating that prefabricated modular construction represents a paradigm shift, offering integrated solutions for immediate humanitarian response and sustainable long-term recovery.

6.1 Key Findings and Contributions

Modular systems have critical operational advantages: rapid deployment capabilities compress acute response phases from months to days, whereas engineered resilience features, including elevated platforms and hydrophobic materials, directly mitigate flood-specific vulnerabilities (Ahmed *et al.,* 2023). Economic analyses confirm 20-30% cost reductions and 50% timeline compression compared with conventional methods, addressing resource constraints in climate-vulnerable economies (Karim, 2022; World Bank, 2023). Beyond emergency utility, these systems enable sociotechnical transitions through multifunctional infrastructure schools, clinics, and community hubs that catalyse sustainable development pathways (Hassan *et al.,* 2021).

6.2 Theoretical and Practical Implications

This review positions modular construction as a cornerstone of transformative adaptation, transcending temporary relief to enable systemic resilience. The convergence of ecological sustainability (35-40% lower embodied carbon (Islam *et al.,* 2023) community coproduction through local workforce integration, and alignment with Bangladesh's Delta Plan 2100 creates a scalable model for climate-resilient development. Crucially, it disrupts path dependency in disaster governance by shifting from reactive reconstruction to proactive resilience investment.

6.3 Future Directions

As climate intensification continues to escalate flood risks in Bangladesh and similar deltaic regions, several strategic imperatives and emerging opportunities must be addressed to maximise the potential of modular construction for disaster resilience:

6.3.1 Policy and Governance Integration

Comprehensive policy integration of modular systems into national disaster management protocols, including the development of specific building codes and standards for flood-resilient modular construction. This should involve updating Bangladesh's National Building Code to include modular construction guidelines and creating streamlined approval processes for emergency deployment. Recent policy frameworks such as the Bangladesh Delta Plan 2100 should explicitly incorporate modular construction as a key adaptation strategy.

6.3.2 Localised Manufacturing and Supply Chain Development

Development of localised manufacturing ecosystems to increase accessibility and reduce costs. This includes establishing regional prefabrication facilities equipped with climate-resilient technologies, investing in workforce training programs for modular construction techniques, and creating public-private partnerships to support the emerging modular construction industry. Special attention should be given to developing supply chains that can function during disaster conditions and utilising locally sourced sustainable materials.

6.3.3 Innovative Financing Models

Establishment of cross-sectoral financing mechanisms bridging humanitarian and development budgets. This includes creating dedicated resilience funds for modular infrastructure, developing insurance products that incentivise modular construction, and exploring impact investment opportunities in the modular construction sector. Recent innovations such as catastrophe bonds and resilience credits could be adapted to support modular construction initiatives.

6.3.4 Technological Innovation and Integration

Integration of emerging technologies with modular construction to enhance resilience. This includes incorporating smart monitoring systems for early warning and structural health assessment, utilising advanced materials with improved flood resistance properties, and exploring the potential of 3D printing and other digital fabrication techniques for rapid production of customised modules. Recent advances in climate-resilient materials and IoT-enabled structural monitoring should be leveraged.

6.3.5 Community-Centred Implementation Approaches

Development of community-centred implementation frameworks that ensure local ownership and cultural appropriateness. This includes establishing participatory design processes that incorporate local knowledge and preferences, creating community-based maintenance and adaptation programs, and developing knowledge-sharing platforms to facilitate peer learning between communities implementing modular solutions.

6.3.6 Knowledge Generation and Capacity Building

Strengthening research capacity and knowledge generation through dedicated research programs on modular construction in disaster-prone contexts. This includes establishing academic-industry partnerships, creating demonstration projects that serve as living laboratories, and developing comprehensive monitoring and evaluation frameworks to assess the long-term performance of modular construction in flood-prone environments.

Bangladesh's experience with modular construction offers valuable transferable insights for other deltaic regions facing similar climate challenges. By addressing these strategic directions, modular construction can evolve from a promising technical solution to a transformative approach that builds systemic resilience, supports sustainable development, and creates pathways for climate adaptation in the face of increasing uncertainty. ■

ACKNOWLEDGMENT

Authors expresses sincere gratitude to all those who contributed to this work. Special appreciation goes to mentors for their invaluable guidance, colleagues for their insightful discussions, and family for their continuous encouragement. Their support has been instrumental in the successful completion of this endeavour.

AUTHORS' CONTRIBUTIONS

- **Mohammad Atiqur Rahman Sakib:** Conceptualisation, literature review framework, and supervision.
- **Nafis Niaz Chowdhury:** Data collection, methodology development, and formal analysis.
- **Badhon Singha:** Writing original draft preparation, editing, and overall manuscript coordination.

REFERENCES

[1] Ahmed, S., Rahman, M., & Hossain, M. (2023). Flood-resilient modular housing: Design innovations for low-lying regions. *Journal of Building Engineering, 65,* 105780.

[2] Arif, M., & Egbu, C. (2010). Making a case for offsite construction in Nigeria. *Journal of Building Appraisal, 6*(3), 241–255. https://doi.org/10.1057/jba.2010.22

[3] World Bank. (2021). *Climate resilience in South Asia: The case for scalable solutions.*

[4] Chaitanya, A. S., & Ijmtst, E. (2021). A study on modular construction technique. *International Journal for Modern Trends in Science and Technology, 7,* 278–280. https://doi.org/10.46501/IJMTST0707048

[5] Generalova, E. M., Generalov, V. P., & Kuznetsova, A. A. (2016). Modular buildings in modern construction. *Procedia Engineering, 153,* 167–172. https://doi.org/10.1016/j.proeng.2016.08.098

[6] Gibb, A. G. F., & Pendlebury, M. (2006). Strategy for the sustainable construction of schools using modern methods of construction. *Proceedings of the Institution of Civil Engineers – Engineering Sustainability, 159*(3), 105–114. https://doi.org/10.1680/ensu.2006.159.3.105

[7] Hassan, M., Ahmed, T., & Islam, S. (2021). Modular infrastructure in disaster recovery: A multi-country analysis. *International Journal of Disaster Risk Reduction, 62,* 102397.

[8] Hossain, M. Z., & Paul, S. K. (2021). Integrating modular construction into national disaster management frameworks: A pathway for rapid recovery in flood-prone economies. *Disaster Prevention and Management: An International Journal, 30*(4), 435–450.

[9] Inter-Cluster Coordination Group–Humanitarian Task Team Bangladesh. (2024). *Eastern flash floods 2024: Situation report No. 02 (30 August 2024).* https://reliefweb.int/report/bangladesh/bangladesh-eastern-flash-floods-2024-situation-report-no-02-30-august-2024

[10] Islam, M., Bhuiyan, M., & Salam, M. (2023). Carbon footprint reduction in modular construction for climate-vulnerable zones. *Sustainable Cities and Society, 95,* 104581.

[11] Kamali, M., & Hewage, K. (2016). Life cycle performance of modular buildings: A critical review. *Renewable and Sustainable Energy Reviews, 62,* 1171–1183. https://doi.org/10.1016/j.rser.2016.05.031

[12] Kamara, J. M., Anumba, C. J., & Evbuomwan, N. F. O. (2002). Capturing client requirements in construction projects. *Engineering, Construction and Architectural Management, 9*(6), 433–441. https://doi.org/10.1108/eb021233

[13] Karim, R. (2022). Cost-benefit analysis of modular vs. traditional construction in post-disaster contexts. *Construction Management and Economics, 40*(9), 823–837.

[14] International Federation of Red Cross and Red Crescent Societies. (2012). *Law and disasters in South Sudan.* www.ifrc.org/dl

[15] Luo, X., Zheng, X., Liao, C., Xiao, Y., Deng, C., Liu, S., & Chen, Q. (2024). Research on the modular design method and application of prefabricated residential buildings. *Buildings, 14*(9). https://doi.org/10.3390/buildings14093014

[16] Mark, L. R., O. R. G., & Rory, B. (2012). Application of modular construction in high-rise buildings. *Journal of Architectural Engineering, 18*(2), 148–154. https://doi.org/10.1061/(ASCE)AE.1943-5568.0000057

[17] Pan, W., Gibb, A., & Dainty, A. (2012). Strategies for integrating the use of off-site production technologies in house building. *Journal of Construction Engineering and Management, 138,* 1331–1340. https://doi.org/10.1061/(ASCE)CO.1943-7862.0000544

[18] Patel, V., Li, X., & Johnson, R. (2023). Rapid deployment technologies for emergency shelter systems. *Automation in Construction, 148,* 104799.

[19] Rahman, A., & Khan, M. (2022). Advanced materials for water-resistant modular structures. *Materials & Design, 215,* 110456.

[20] ReliefWeb. (2014). *Bangladesh floods 2014.* https://reliefweb.int/disaster/fl-2014-000117-bgd

[21] ReliefWeb. (2017a). *Bangladesh Cyclone Mora 2017: Work report 1.* https://reliefweb.int/report/bangladesh/bangladesh-cyclone-mora-2017-work-report-1

[22] ReliefWeb. (2017b). *June 2017 landslides: Situation report.* https://reliefweb.int/report/bangladesh/june-2017-landslides-situation-report

[23] ReliefWeb. (2020). *Cyclone Amphan (2020) — Bangladesh.* https://reliefweb.int/disaster/tc-2020-000137-bgd

[24] ReliefWeb. (2024). *Cyclone Remal (2024) — Bangladesh.* https://reliefweb.int/disaster/tc-2024-000083-bgd

[25] Sarker, M., Chowdhury, R., & Ali, S. (2024). Field implementation of modular community facilities in post-flood Bangladesh. *Disaster Prevention and Management, 33*(1), 45–59.

[26] Smith, J. (2020). Cost-effectiveness of prefabricated construction in disaster-prone areas. *International Journal of Construction Management, 15*(4), 200–214. https://doi.org/10.1234/ijcm.2020.45678

[27] Smith, R. E. (2011). *Prefabrication and modular construction: Next-generation building technologies.* Wiley.

[28] Sultana, S., Ahmed, S. F., & Haque, A. K. E. (2022). Community-driven deployment of modular infrastructure for post-disaster resilience: Lessons from coastal Bangladesh. *International Journal of Disaster Risk Reduction, 75,* 103012.

[29] Tan, T. H., & Chen, F. (2014). Modular construction for high-rise buildings. *Journal of Construction Engineering and Management, 140*(3), 4014015. https://doi.org/10.1061/(ASCE)CO.1943-7862.0000803

[30] United Nations Development Programme. (2022). *Enhancing disaster resilience in Bangladesh: Innovative approaches to flood management.*

[31] UN-Habitat. (2022). *Sustainable modular construction: Guidelines for climate-adaptive housing.*

[32] UNICEF. (2024). *Bangladesh floods: Situation report.*

[33] World Bank. (2023). *Economic efficiency of modular solutions in disaster recovery.*

[34] ZahirulAlam. (2024, October 1). *Shelter Cluster: Eastern floods — shelter damage and needs assessment.* https://shelltercluster.org/bangladesh-floods-2024/documents/shelter-clustereastern-floodsshelter-damage-and-needs-assessment

PROFILES

MOHAMMAD ATIQUR RAHMAN SAKIB completed his Bachelor's degree in Civil Engineering from Ahsanullah University of Science and Technology (AUST), Bangladesh. He is currently pursuing a Master of Science (M.Sc.) in Civil and Structural Engineering at the University of Adelaide, Australia. His research interests include advanced structural analysis, earthquake-resistant design, and sustainable construction techniques. With strong academic excellence and a deep passion for research, he aims to contribute to internationally recognized studies in structural engineering.
Email address: arsakib22@gmail.com

NAFIS NIAZ CHOWDHURY completed his Civil Engineering degree from Ahsanullah University of Science and Technology in 2024. He is currently engaged in active research within the field, with particular focus on structural sustainability, smart infrastructure, and urban development. Inspired by the large-scale projects he has observed firsthand, he aims to connect advanced simulation techniques with real-world construction practices to enhance industry efficiency and innovation.
Email address: nafisnovo17@gmail.com

BADHON SINGHA is a graduate in Civil Engineering from Ahsanullah University of Science and Technology (AUST), Bangladesh. His academic and research interests include seismic performance of structures, base isolation systems, and modular construction in disaster-prone regions. He has authored and co-authored multiple research papers, including studies on fluid viscous dampers, lead rubber bearing isolators, and soft-story structural behavior, several of which are accepted or under review in peer-reviewed journals.
Email address: badhon10776@gmail.com

STUDY ON THE REINFORCEMENT EFFECT OF PROTECTIVE SURFACE REINFORCEMENT FOR CRACKED LINING IN RAILWAY TUNNELS

Qizhu Jiao[1], Yalong Shi[2*], Congwen Yan[3], Peng Chen[4], Kai Liu[5]

Abstract

Designers often express concern about resource wastage caused by excessive reinforcement of lining cracks and the limited effectiveness of conventional repair methods such as plastering mortar and crack sealing, when subjected to construction defects and environmental degradation. To address these limitations and suppress further crack propagation, this study proposes a protective reinforcement method and evaluates its performance under surrounding rock pressure using finite element analysis. The results show that: (1) the first principal stress within the protective reinforcement remains well below the material's design strength, ensuring structural integrity; (2) no tensile damage occurs in the lining under either single-crack or mesh-crack conditions, confirming that the reinforcement effectively inhibits crack development; (3) reinforcement bars reduce stress concentration at crack tips, lower tensile stress, and improve the structural safety factor; and (4) retaining bars are unsuitable for reinforcing deep cracks (≥0.5H) due to their weak shear resistance and the complexity of deep crack formation. These findings provide a basis for optimising reinforcement strategies for cracked lining structures.

Received: *26 March, 2025*
Revised: *9 October, 2025*
Accepted: *26 November, 2025*

[1,3]China Railway Siyuan Survey and Design Institute Group Co., Ltd., Wuhan 430063.

[2,4,5]China Railway Southwest Research Institute Co., LTD, Chengdu, 611731.

****Corresponding author:***
shiyalong_crsi@163.com

DOI:
https://doi.org/10.54552/V86I4.288

List of Notations:

γ	is unit weight for material
μ	is Poisson ratio
E_0	is the elastic modulus of the material
H	is the lining thickness
SF	is the safety factor
f_t	is the design value of concrete tensile strength
K	is the minimum allowable safety factor
MPa	Mega pascal

Keywords:
Cracks, Protective covering steel, Railway tunnels, Reinforcement effect, Safety evaluation

1.0 INTRODUCTION

As the operational lifespan of tunnels increases, lining cracks have become one of the main issues affecting the safe operation of tunnels (Li *et al.,* 2018; Wang *et al.,* 2016; Li, 2020). In response to remediation measures for cracked linings, both domestic and international scholars have conducted a certain amount of research.

For example, Wang *et al.* (2010) calculated the lining safety factor under the action of longitudinal cracks in the Anji Tunnel. They proposed that for cracks in plain concrete segments where the safety factor meets the regulatory requirements, reinforcement should be done using mortar plastering. For cracks that do not meet the regulatory requirements, reinforcement should be carried out using I20a@550m+steel mesh + sprayed concrete.

Yu *et al.* (2017) used finite element software to study the reinforcement effect of combined components formed by steel plates and anchoring devices. The results showed that the combined structure could improve the stress characteristics of the cracks and the surrounding areas, prevent stress concentration, and restore the load-bearing capacity to a state similar to the intact lining.

Chen *et al.* (2014) classified the cracks in a certain railway tunnel into four levels (AA, A1, B, and C) based on the crack's length and width. They used finite element software to analyze the reinforcement effects of W steel strips + steel mesh + sprayed concrete and cross-joint anchor grout. The results showed that the W steel strip + steel mesh + sprayed concrete could increase the safety factor of the structure with longitudinal cracks from 0.92 to 2.69, while the cross-joint anchor grout could raise the safety factor from 0.97 to 2.51, meeting the regulatory requirements.

In addition to the aforementioned measures, common crack remediation techniques also include concrete lining replacement, corrugated sheet lining, partial replacement, and full replacement (Su *et al.,* 2020; Fu *et al.,* 2021; Yu *et al.,* 2021; Shao *et al.,* 2019; Wang *et al.,* 2017), all of which are now relatively well established. However, in reinforcement design, some designers have raised two concerns: first, whether excessive reinforcement or replacement measures for defective cracks in plain concrete linings may result in unnecessary resource expenditure; and second, whether cracks repaired only with surface plastering or grouting will

continue to propagate if the grout quality is inadequate or if environmental factors alter the lining's stress state. In response to these concerns, this study adopts the approach of inhibiting crack initiation and propagation, using finite element software to evaluate the reinforcement performance of protective surface reinforcement. The aim is to provide guidance and support for similar remediation projects.

2.0 COMPUTATIONAL MODEL

2.1 Expansion and Prevention of Cracks

The core of tensile crack propagation is the change in material mechanical behaviour caused by stress concentration at the crack tip. The stress concentration at the tip of the crack leads to a sudden change in the mechanical properties of the material, which in turn promotes the continuous propagation of the crack. As shown in Figure 1, the crack tip includes three areas: Traction free macrocrack, Bridging zone, and Microcrack zone, among which the plastic damage characteristics of concrete materials need to be considered in the Bridging zone and Microcrack zone.

The stress-strain curve of materials considering concrete tensile damage is shown in Figure 2.

When the concrete material at the tip of the crack is in the post peak stage (D_t>0), the crack is in an unstable equilibrium state. Under the disturbance of the surrounding environment, the probability of crack propagation will greatly increase. Therefore, the core of suppressing the propagation of tensile cracks is to ensure that the stress at the crack tip is in a pre-peak state and has a certain safety margin, as show in

$$\begin{cases} D_t = 0 \\ SF = \dfrac{\sigma_1}{f_t} \geq K \end{cases} \quad (1)$$

Among them, K is the minimum allowable safety factor, and according to the *Railway Tunnel Design Code*, it is taken as 3.6.

2.2 Model Overview

Finite element software was used to study the stress characteristics of single-line tunnels (height 10.93m, width 10.67m, cross-sectional area 80.03m²) and double-line tunnels (height 10.98m, width 14.06m, cross-sectional area 118.80m²) with single and mesh cracks. A "load-structure" model was used for calculations, with a lining longitudinal length of 12m and thickness of 45cm. The lining was simulated using solid elements, the foundation spring was simulated with spring elements, and the protective surface reinforcement was simulated using shell elements. Cracks were simulated using contact surfaces, assuming that no tensile or shear stresses are transmitted at the crack location, but compressive stresses are transmitted.

Given that cracks have a more significant impact on the stress of plain concrete linings, and past experience shows that cracks located at the crown have the most significant effect on the structural stress, calculations were carried out for a single longitudinal crack and mesh crack at the crown of an IV-grade surrounding rock plain concrete lining. According to the Railway Tunnel Design Code (TB10003-2016) (hereinafter referred to as "Tunnel Code"), the vertical load for a single-line tunnel with IV-grade surrounding rock is taken as 86.940kPa, and for a double-line tunnel, it is 112.153kPa. The lateral pressure coefficient is taken as 0.25. The secondary lining load-bearing ratio is taken as 50%. The models for the longitudinal crack and mesh crack at the crown are shown in Figures 3 and 4.

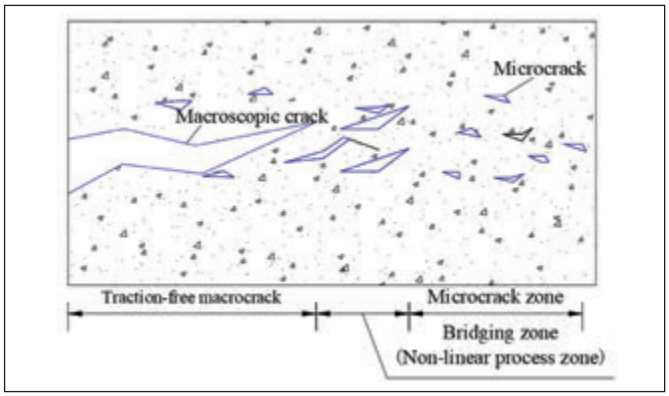

Figure 1: Schematic diagram of crack tip zoning

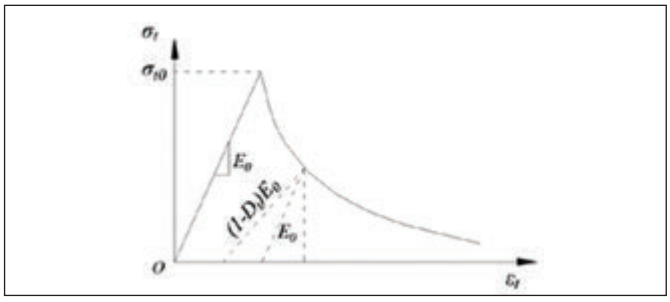

Figure 2: Uniaxial tensile stress-strain curve of concrete

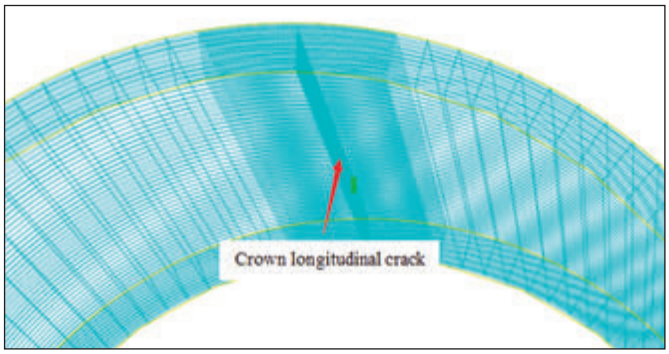

Figure 3: Numerical model of longitudinal crack in arch crown

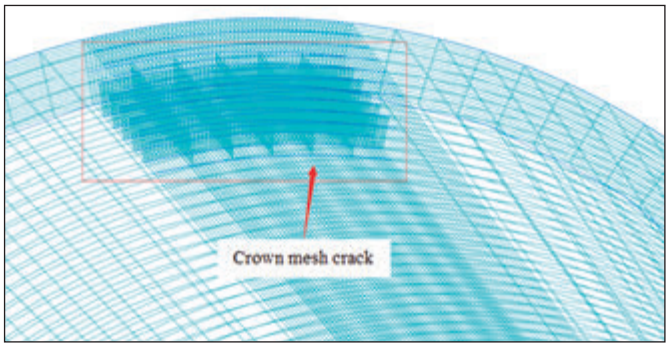

Figure 4: Numerical model of mesh crack in arch crown

Table 1: Physical and mechanical parameters of material

Material	γ (kN/m^3)	μ	E_0 (GPa)	Tensile Strength (MPa)	Compressive Strength (MPa)
Concrete	23	0.2	31.5	2.4	23.4
Reinforcement	7850	0.2	200	210	210

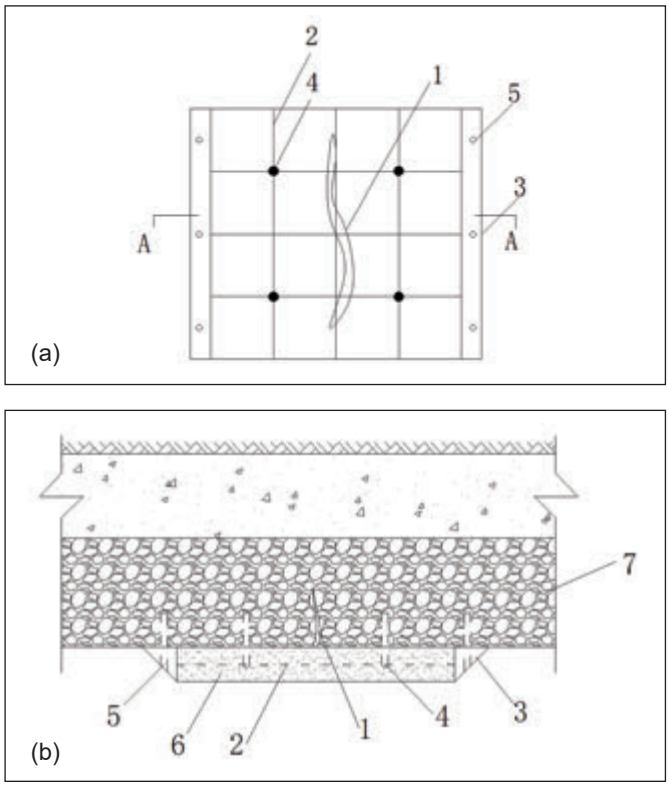

Figure 5: Structural diagram of face protection rebar
(a) Schematic diagram of the protective surface reinforcement in plan view;
(b) A-A sectional view
(1: Crack; 2: Protective Surface Reinforcement Steel;
3: Side Supporting Structure; 4: Reinforced Dowels;
5: Support Anchor Hole; 6: Mortar Protective Layer; 7: Lining)

The range of the protective surface reinforcement extends 1m beyond the crack range. In the stress analysis, the effect of the mortar protection layer is not considered, and the thickness of the shell elements is calculated equivalently based on the area. The schematic diagram of the reinforcement plan for the surface reinforcement is shown in Figure 5 (a), and the A-A cross-sectional view is shown in Figure 5 (b).

2.3 Material Physical and Mechanical Parameters

According to the *Railway Tunnel Design Code* (TB10003-2016), the elastic foundation parameters for IV-class surrounding rock are set to 350 MPa/m. The concrete strength grade is C35, and the type of reinforcement is HRB400. A plastic damage model is used for simulation. The damage evolution equation for concrete is determined based on the *Code for Design of Concrete Structures* (GB50010-2010) and (Li *et al.,* 2021; Zhang *et al.,* 2008). The material physical and mechanical parameters are shown in Table 1.

Table 2: Calculation Conditions

Crack Type	Characteristic Parameters
Single Longitudinal Crack	Length: 1m, 3m, 6m, 9m, 12m Depth: 0.1*H*, 0.5*H*, 0.9*H*
Mesh Cracks	Longitudinal Range: 0.5m, 1.0m, 1.5m Circumferential Range: 0.5m, 1.0m, 1.5m Depth: 0.5*H*

Note: H in the table indicates lining thickness

2.4 Calculation Conditions

First, the stress characteristics of single-line and double-line tunnel linings with a single longitudinal crack and mesh cracks at the vault are calculated and analysed. Then, based on the stress characteristics of the cracked linings, typical conditions are selected to analyse the reinforcement effect of the protective surface reinforcement. The calculation conditions are shown in Table 2.

3.0 THE STRESS CHARACTERISTICS OF CRACKED LINING STRUCTURES

The calculation results indicate that cracks have a negligible impact on the compressive load-bearing characteristics of the structure. Due to space limitations, only the tensile damage degree and the first principal stress calculation cloud diagrams for the conditions of a single longitudinal crack (9m long, 0.9H depth) and mesh cracks (1.5m longitudinal length, 1.5m circumferential width, 0.5H depth) at the crown of a single-line tunnel are presented here.

3.1 Single Longitudinal Crack

The calculation results of the tensile damage degree and the first principal stress of a single longitudinal crack (9m long and 0.5H depth) in a single-line tunnel are shown in Figure 6(a) and Figure 6(b).

The variation of the tensile damage degree of the lining in single-line and double-line tunnels with a single crack, as a function of crack length and depth, is shown in Figures 7 and 8.

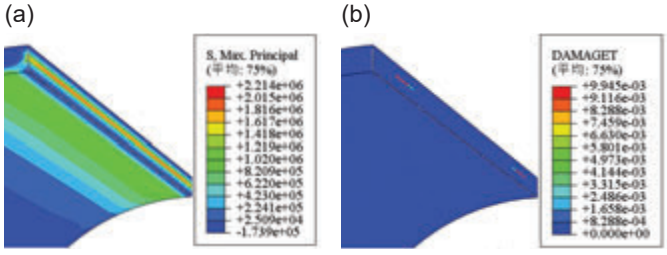

Figure 6: Calculation results of single line tunnel vault with longitudinal crack under typical working conditions
(a) the first principal stress of lining (Pa);
(b) lining tensile damage

As shown in Figure 6(a), the lining with a single longitudinal crack, under surrounding rock pressure, exhibits tensile damage at the crack tip along the crack's length, with a damage degree of 0.227. This indicates a tendency for the crack to propagate along its length. As shown in Figure 6(b), the first principal stress of the lining is 1.950MPa, which lies in the descending region of the stress-strain curve and is below the tensile strength of concrete. Therefore, in subsequent calculations and analyses, a tensile damage degree greater than 0 is used as the criterion for determining crack propagation.

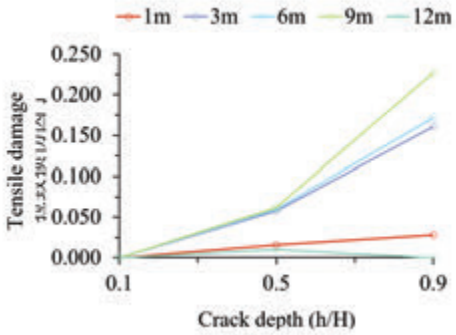

Figure 7: Relationship between tensile damage and longitudinal crack characteristic parameters of single track tunnel

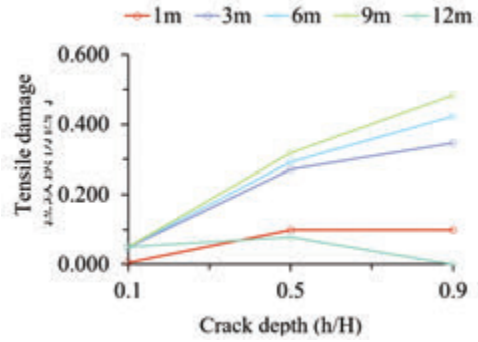

Figure 8: Relationship between tensile damage and longitudinal crack characteristic parameters of double track tunnel

As shown in Figures 7 and 8, for the single longitudinal crack scenario, increasing the crack depth results in a greater tensile damage degree, with damage concentrated at the crack tip. For cracks shorter than the lining's circumference (12m), longer cracks lead to a greater degree of tensile damage. When the crack length reaches 12m, stress release causes a reduction in the tensile damage degree of the structure. However, at this point, the crack significantly weakens the lining, and reinforcement measures equivalent to or stronger than those for non-longitudinal through cracks should be considered. For single-line tunnels, when the crack depth is 0.1H, the structural damage degree is 0, and the crack can be addressed with grouting closure or mortar surface treatment.

3.2 Mesh Crack

The tensile damage degree and the first principal stress calculation results for the condition of a mesh crack (1.5m longitudinal length, 1.5m circumferential width, 0.5H depth) in a single-line tunnel are shown in Figure 9(a) and Figure 9(b).

As shown in Figure 9 (a), for the lining structure with mesh cracks under the surrounding rock pressure, tensile damage occurs at the crack tips along the tunnel's direction, with a damage degree of 0.684, indicating that the mesh crack tends to propagate along the tunnel's direction. As shown in Figure 9 (b), the first principal stress of the lining is 1.929 MPa, which is in the descending part of the stress-strain curve and is below the tensile strength of concrete. The variation of the tensile damage degree of the lining in single-line and double-line tunnels with a single crack, as a function of crack length and depth, is shown in Figures 8 and 9.

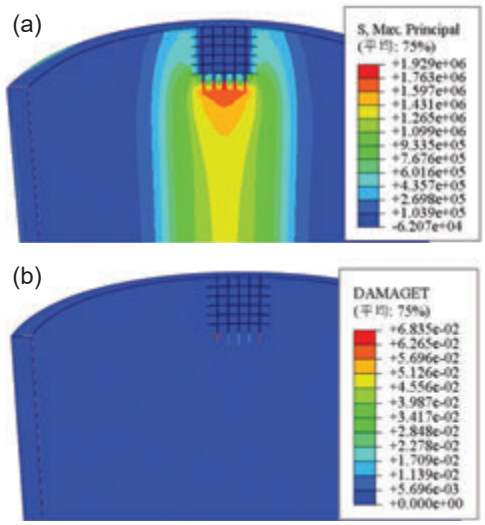

Figure 9: Calculation results of single line tunnel vault with mesh crack under typical working conditions (a) the first principal stress lining; (b) lining tensile damage

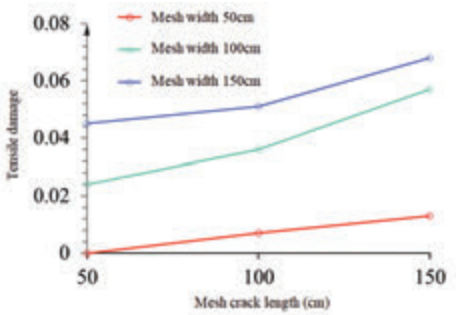

Figure 10: Relationship curve between tensile damage and mesh crack characteristic parameter of single track tunnel

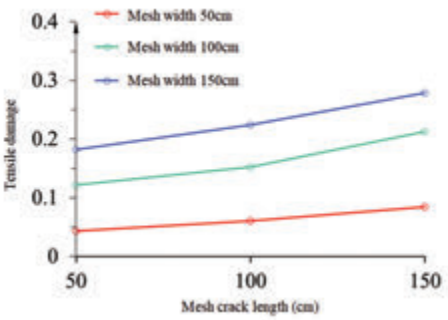

Figure 11: Relationship curve between tensile damage and mesh crack characteristic parameter of double track tunnel

As shown in Figures 10 and 11, for single-line and double-line tunnels with mesh cracks, the tensile damage degree of the lining is positively correlated with the longitudinal distribution length and circumferential distribution width of the mesh cracks. With an increase in the distribution range of the mesh cracks: The tensile damage degree of the lining structure with 0.5m×0.5m (longitudinal range × circumferential range) mesh cracks in single-line and double-line tunnels is 0 and 0.043, respectively. For a 1.5m×1.5m mesh crack, the tensile damage degree of the lining is 0.068 for single-line tunnels and 0.279 for double-line tunnels. In the case of single-line tunnels with a 0.5m×0.5m mesh crack, the tensile damage degree is 0, suggesting that the cracks can be treated with grouting or mortar coating alone.

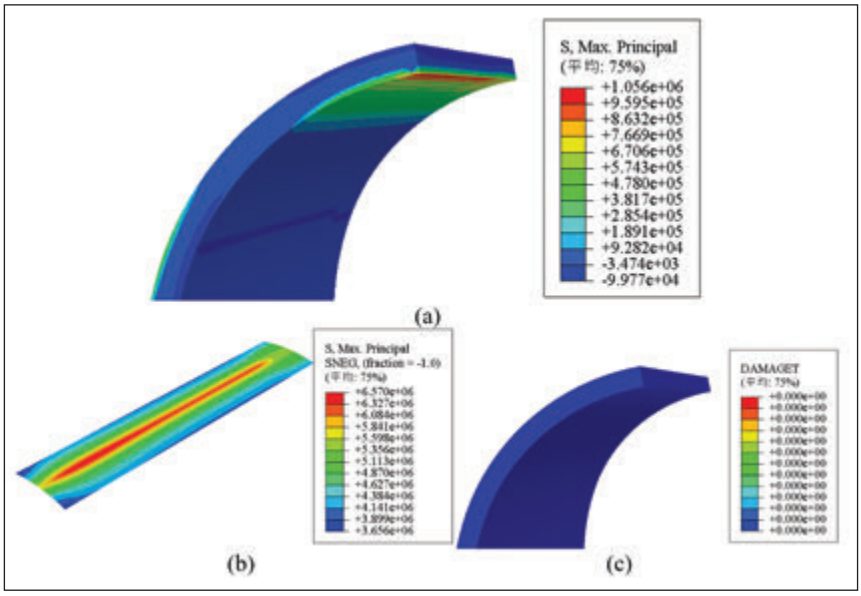

Figure 12: Calculation results of structural stress after surface reinforcement for typical single crack conditions
(a) the first principal stress of lining; (b) the first principal stress of the reinforcement; (c) lining tensile damage

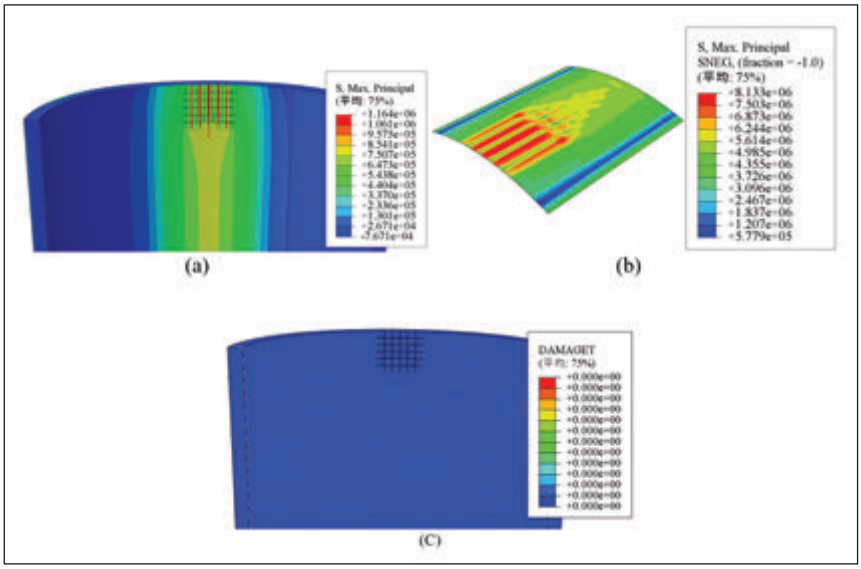

Figure 13: Calculation results of structural stress after surface reinforcement for typical mesh crack conditions
(a) the first principal stress of lining; (b) the first principal stress of the reinforcement; (c) lining tensile damage

4.0 THE REINFORCEMENT EFFECT OF SURFACE REINFORCEMENT MEASURES

Based on the results in Section 3, the structural damage degree of the lining under rock pressure is positively correlated with the crack length (<12m) and depth for single longitudinal cracks. For mesh cracks, the structural damage degree is positively correlated with the longitudinal and circumferential distribution ranges of the cracks. Therefore, for single longitudinal crack scenarios, simulations of the reinforcement effect of surface bars will be conducted for the most unfavourable and special conditions, with crack lengths of 9m and 12m, and depths of 0.1H, 0.5H, and 0.9H. For mesh crack scenarios, reinforcement effect simulations will be conducted for crack dimensions of 0.5m×0.5m, 1.0m×1.0m, and 1.5m×1.5m. The reinforcement bar diameter is set at φ10mm, with longitudinal and circumferential spacing both set at 150mm.

Due to space limitations, only the cloud diagrams of calculation results for the single-track tunnel with a single longitudinal crack (length 9m, depth 0.5H) and the single-track tunnel with mesh cracks (1.5m × 1.5m) are presented here, as shown in Figures 12 and 13 respectively.

As shown in Figures 12(a) and 13(a), for the single longitudinal crack condition (length 9m, depth 0.5H) and the mesh crack condition (1.5m × 1.5m) in the single-track tunnel, the application of surface reinforcement eliminates tensile damage in the lining. The maximum principal stress in the lining is 1.056 MPa and 1.164 MPa, respectively, located on the surface near the cracks. According to the *Railway Tunnel Design Code* (TB10003-2016), the structural safety factors are 3.977 and 3.608, respectively, meeting the code's requirements. As shown in Figures 12(b) and 13(b), the maximum principal stress in the surface reinforcement is 6.570 MPa and 8.133 MPa, which are far below the design strength of 210 MPa. Thus, the use of surface reinforcement effectively enhances the structural bearing capacity, and the reinforcement effect complies with the requirements of the *Railway Tunnel Design Code*. As shown in Figures 12(c) and 13(c), the tensile damage degree at the tip of the lining for both single cracks and mesh cracks is 0 after reinforcement with surface reinforcement.

Table 3: Calculation results of reinforcement effect of surface reinforcement on lining with single longitudinal crack

Section Type	Crack Length	Crack Depth	Unreinforced			Surface Reinforcement			
			Tensile Damage	Lining First Principal Stress (MPa)	SF	Tensile Damage	Lining First Principal Stress (MPa)	First Principal Stress of the Surface Reinforcement (MPa)	SF
Single Line	9	0.1*H*	0	1.58	2.658	0	0.806	5.444	5.211
	12	0.1*H*	0	1.58	2.658	0	0.802	5.823	5.237
	9	0.5*H*	0.062	2.218	—	0	1.056	6.57	3.977
	12	0.5*H*	0.01	2.214	—	0	0.995	6.187	4.221
	9	0.9*H*	0.227	1.95	—	0	1.061	6.565	3.959
	12	0.9*H*	0	1.33	—	0	1.061	6.564	3.959
Double Line	9	0.1*H*	0.05	1.782	—	0	0.994	6.628	4.225
	12	0.1*H*	0.05	1.782	—	0	0.964	6.629	4.357
	9	0.5*H*	0.319	2.044	—	0	1.221	7.593	3.440
	12	0.5*H*	0.078	1.958	—	0	1.221	7.593	3.440
	9	0.9*H*	0.484	2.041	—	0	1.227	7.591	3.423
	12	0.9*H*	0	1.512	—	0	1.227	7.591	3.423

Table 4: Calculation results of reinforcement effect of surface reinforcement on lining with mesh crack

Section Type	Longitudinal Range	Circumferential Range	Unreinforced			Surface Reinforcement			
			Tensile Damage	Lining First Principal Stress (MPa)	SF	Tensile Damage	Lining First Principal Stress (MPa)	First Principal Stress of the Surface Reinforcement (MPa)	SF
Single Line	0.5m	0.5m	0	1.981	2.120	0	1.028	7.782	4.086
	1.0m	1.0m	0.036	2.012	—	0	1.066	8.196	3.940
	1.5m	1.5m	0.068	1.929	—	0	1.164	8.133	3.608
Double Line	0.5m	0.5m	0.043	2.183	—	0	1.128	9.609	3.723
	1.0m	1.0m	0.153	2.234	—	0	1.247	8.923	3.368
	1.5m	1.5m	0.279	2.233	—	0	1.237	9.239	3.395

Note: "—" indicates that when there is tensile damage to the lining, the first principal stress is in the descending stage, so the value of the first principal stress and the safety factor is not of reference significance

The stress calculation results under rock pressure for single-track and double-track tunnel linings with single longitudinal cracks and mesh cracks after reinforcement with surface reinforcement are shown in Tables 3 and 4.

As shown in Tables 3 and 4, when 50% of the surrounding rock pressure is taken as the design load, the reinforced lining with φ10mm@150mm surface reinforcement does not exhibit any tensile damage in both the single longitudinal crack and the mesh crack cases, indicating that the surface reinforcement can effectively inhibit the further expansion of the cracks. For the most unfavourable condition of single cracks in both single-line and double-line tunnels, the tensile stress of the lining is 1.061 MPa and 1.227 MPa, respectively, distributed near the cracks on the inner surface of the lining. The safety factors are 3.959 and 3.423, respectively. Although some conditions do not meet the required safety factor of 3.6, the deviation is less than 10%, indicating that surface reinforcement can effectively reduce stress concentration at the crack tip and improve the structural bearing capacity.

For the most unfavourable condition of mesh cracks in both single-line and double-line tunnels, the tensile stress of the lining is 1.164 MPa and 1.237 MPa, respectively, distributed near the crack on the inner surface of the lining. The corresponding safety factors are 3.608 and 3.395. In some conditions, the safety factor does not meet the required 3.6, but it is less than 10% away from 3.6, indicating that the surface reinforcement can effectively improve the stress concentration at the crack tip and enhance the structural bearing capacity.

It should be noted that for cracks with a depth of 0.9H, from the perspective of inhibiting crack propagation, the surface reinforcement is beneficial. However, for cracks that are about to penetrate, it is necessary to consider potential failure modes such as shear failure and misalignment due to insufficient shear strength at that location. Surface reinforcement is suitable for

crack opening failure modes, but its effect on the lining's shear strength is relatively weak. Additionally, the load mode that results in a crack with a depth of 0.9H differs from the design load mode, making it difficult to analyse. Therefore, surface reinforcement is deemed unsuitable for cracks with a depth of 0.9H. For safety reasons, cracks with depths between 0.5H and 0.9H, as well as those with a depth of 0.9H, are grouped together, and in such cases, surface reinforcement is not considered applicable. The first principal stress of the surface reinforcement in the above-mentioned conditions ranges from 5.444 MPa to 9.609 MPa, which is far below the design strength of HRB400 steel bars (210 MPa), indicating that the surface reinforcement remains structurally sound.

5.0 CONCLUSIONS AND RECOMMENDATIONS

This paper uses finite element software to conduct a numerical analysis on the reinforcement effect of cracked lining with surface reinforcement under 50% surrounding rock load. The main conclusions are:

- The first principal stress distribution range of the surface reinforcement components is 5.444 MPa to 9.609 MPa, far lower than the design strength of 210 MPa, indicating that the surface reinforcement will not fail.
- No tensile damage was observed in any of the cracked lining conditions, indicating that the surface reinforcement effectively inhibits the expansion of cracks.
- For linings with single and mesh cracks, the surface reinforcement effectively improves the stress concentration at the crack tips, reduces the tensile stress in the structure, and increases the structure's safety factor, making it an effective crack reinforcement measure.
- Considering the shear failure mode of cracks deeper than 0.5H, the weaker shear resistance of the surface reinforcement, and the complexity of the formation mechanism, surface reinforcement is considered unsuitable for reinforcing cracks of this depth.

Additionally, this paper looks into the reinforcement effect of surface reinforcement in the repair of plain concrete cracks and confirms its effectiveness in crack remediation. However, the stability of surface reinforcement under train-induced wind in high-speed railway tunnels has not been studied yet. This will be further explored in subsequent research to determine the feasibility of surface reinforcement in the remediation of lining cracks in high-speed railway tunnels. ■

AUTHORS' CONTRIBUTIONS

- **Qizhu Jiao:** Conceptualisation, study design, and supervision.
- **Yalong Shi:** Writing original draft preparation and literature review.
- **Congwen Yan:** Data collection, methodology, and formal analysis.
- **Peng Chen:** Data validation, visualisation, and software implementation.
- **Kai Liu:** Writing review, editing, and final manuscript approval.

REFERENCES

[1] Cangshu, L. (2018). *Research on distribution and safety evaluation in lining split of high speed railway tunnel based on statistical analysis* (Doctoral dissertation). Beijing Jiaotong University.

[2] Wei, W., Jun, D., & Juntao, Y. (2016). Research on safety of lining structure in railway tunnel under spatial crack disease. *Journal of Safety Science and Technology, 12*(1), 33–37. https://doi.org/10.11731/j.issn.1673-193x.2016.01.006

[3] Hualao, W., Xuezeng, L., Ning, L., & Dongwu, X. (2010). Safety evaluation of tunnel lining with longitudinal cracks and reinforcement design. *Chinese Journal of Rock Mechanics and Engineering, 29*(Z1), 2651–2656. CNKI:SUN:YSLX.0.2010-S1-013

[4] Jingwen, Y., Lun, G., Zichao, X., Shifu, W., Xingxing, L., & Xuhao, C. (2017). Analysis of stress state of assembly structure for rapid repair of lining cracking in traffic tunnels. *Subgrade Engineering, (4)*, 123–127. https://doi/10.13379/j.issn.1003-8825.2017.04.25

[5] Jiang, C., Junsheng, Y., Nengxue, C., & Xiaowen, X. (2014). Study on crack remediation and reinforcement of lining in railway tunnel. *Journal of Safety Science and Technology, 10*(9), 134–139. https://doi.org/10.11731/j.issn.1673-193x.2014.09.023

[6] Chenhong, S., Nannan, A., & Zhifeng, W. (2020). Study on crack remediation and reinforcement of lining in railway tunnel. *Journal of Architecture and Civil Engineering, 37*(5), 203–213. https://doi.org/10.19815/j.jace.2020.08029

[7] Hongqian, Y., Jun, Q., Huairong, L., Zhigang, H., & Deiwu, L. (2021). Study on causes and treatment of concrete cracking of the secondary lining of Qilianshan Tunnel. *Modern Tunnelling Technology, 58*(1), 217–222. https://doi.org/10.13807/j.cnki.mtt.2021.01.029

[8] Donghua, S. (2019). Study on defect correction technology for tunnel lining in high-speed rail line. *Railway Construction Technology, (Z1),* 113–117. https://doi.org/10.3969/j.issn.1009-4539.2019.S1.027

[9] Zhijie, W., Haiyan, X., Ping, Z., Qichao, Z., &Xiao, G. (2017). Study on the treatment of lining defects of highway tunnel. *Railway Standard Design, 61*(10), 125–132. https://doi.org/10.13238/j.issn.1004-2954.2017.10.025.

[10] Ministry of Housing and Urban-Rural Development of the People's Republic of China. (2010). *GB 50010-2010 code for design of concrete structures.* China Architecture Publishing & Media Co., Ltd.

[11] Qingfu, L., Yihang, K., & Wei, G. (2021). CDP model parameters calculation and value method verification. *Journal of Zhengzhou University (Engineering Science), 42*(2), 43–48. https://doi.org/10.13705/j.issn.1671-6833.2020.06.002

[12] Jin, Z., Qing, W., Shouying, H., & Chuanjia, W. (2008). Parameter verification of concrete damage plasticity model in ABAQUS. *Building Structure, 38*(8), 127–130. https://xueshu.baidu.com/usercenter/paper/show?paperid=99ceb6e61f30a4480852d4b35e3735cf

PROFILES

QIZHU JIAO is currently employed by China Railway Fourth Survey and Design Institute Group Co., Ltd. He obtained a Bachelor's degree in Underground Engineering and Tunnel Engineering from Tongji University in 1992, and a Master's degree in Architecture and Civil Engineering from Huazhong University of Science and Technology in 2006. Since 1992, he has been long engaged in the design and research of tunnel engineering. He has presided over multiple railway, highway and municipal tunnel projects with a total length of more than 2,000 kilometers. His projects have won one FIDIC Project Award, one China National Science and Technology Progress Award, and five Provincial/Municipal Science and Technology Progress Awards.
Email address: 415884709@qq.com

YALONG SHI is a Senior Engineer at the China Railway Southwest Research Institute. He received his Master's degree from the China Academy of Railway Sciences in 2014. His work focuses on tunnel and underground engineering, as well as advanced monitoring and measurement technologies for urban rail transit. He has made significant contributions to the development and application of intelligent monitoring technologies, and his research achievements have been recognized with the Second Prize of the Science and Technology Progress Award of China Railway Group and the Second Prize of the Chengdu Municipal Science and Technology Progress Award.
Email address: shiyalong_crsi@163.com

CONGWEN YAN is employed by China Railway Fourth Survey and Design Institute Group Co., Ltd. He obtained a Master's degree in Architecture and Civil Engineering from Southwest Jiaotong University in 2020, and a Bachelor's degree in Civil Engineering from the same university in 2017. Currently, he is engaged in the design of railway tunnel engineering.
Email address: 1162719639@qq.com

PENG CHEN is an Engineer at China Railway Southwest Research Institute Co., Ltd. He obtained his master's degree from Southwest Jiaotong University in 2018. His main research focuses on structural safety assessment and defect remediation of tunnels and underground engineering.
Email address: chenpeng_crsi@163.com

KAI LIU is an Engineer at China Railway Southwest Science Research Institute Co., Ltd. He obtained a master's degree in Architecture and Civil Engineering from Southwest Jiaotong University in 2019. He is now engaged in research and consulting work on the detection and remediation of tunnel defects in operation, which is one of the key areas of research in the industry. He has unique insights and research on tunnel lining cracks and voids in operational tunnels.
Email address: 513290132@qq.com

MANUSCRIPT PREPARATION GUIDELINES FOR IEM JOURNAL AUTHORS

The aim of publishing the Journal of the Institution of Engineers Malaysia (or IEM Journal) is to promote the advancement of science, engineering, and technology; disseminate new and current knowledge; share novel findings among practising engineers, researchers and other interested colleagues. Hence, the IEM Journal covers a wide range of practical and diversified engineering disciplines, including publishing papers on any subjects relevant to the engineering and technology of today. As in other journals, all paper submissions to the IEM journal will be peer-reviewed by professionals.

Submission of a contribution is taken to manifest the fact that the submission has not been submitted, accepted, published, or copyrighted elsewhere. To avoid publication delays, please send all manuscripts to the Editor (via the Online Journal Submission) and observe the following guidelines. Each paper is independently peer-reviewed.

Types of Papers

IEM Journal will accept any submissions that fall within the three types of papers shown below:

- **Research Paper**

Significant research and development or applications in any field of engineering and/or technology. Submissions should be about 8-14 pages.

- **Review Paper**

Articles which summarises the state-of-the-art of a specific area of research. Submissions should be about 10-20 pages.

- **Brief Paper**

A concise description of new technical concepts or applications within the scope of the journal. Submission should be about 4 pages

Together with the paper submission, at least four (4) reviewers complete with their contact details (official postal and email address, and telephone number) are to be proposed by authors. Reviewers should be the experts in their research areas.

Plagiarism Policy

IEM Journal strictly prohibits any form of Plagiarism.

If the manuscript has been presented, published, or submitted for publication elsewhere, please inform the Editor. Our primary objective is to publish technical materials not available elsewhere.

Format and Elements of Submitted Texts

a) Initial Submission

For initial submission and reviewing, ALL papers are accepted regardless of the formatting used.

b) Final Submission

Upon final submission of paper, authors are required to follow the manuscript instruction guidelines and paper template as presented below.

Please prepare your main text document in Microsoft Word and PDF format, text should be single line spaced, line numbered and pages should be numbered. You can download the paper template here.

Please note that the style that you submit your paper in (e.g. any additional italics or bold fonts, bullet points, etc.) may be changed on publication to accommodate our publication style.

Manuscript Style

Language:

- The language of the IEM Journal is in English. However, a paper in Bahasa Melayu is also accepted. For accepted papers, an abstract in English and Bahasa Melayu must be included.
- The manuscript should be able to be readily understood by an engineer and researchers alike and should avoid any colloquialisms.
- The terms, including nomenclature and abbreviations, and style should be consistent throughout your journal paper. If you collaborate with other writers, please communicate clearly with them.
- Avoid referring directly to the names of individuals, organisations, products, or services unless essential to the comprehension of the manuscript. Gratuitous flattery or derogatory remarks about a person or organisation should not be included.
- Symbols and Units: SI and derived units should be used, if possible.
- Abbreviations: the use of internationally recognised abbreviations is allowed in the text. The abbreviations should be defined on first use. Abbreviations should not be used in the title.

Manuscript Guide

The following is a detailed manuscript preparation guide for articles submitted to IEM Journal; however, they can, in the most part, be used as a basis for other article types amending to concur with the page limit and premise of the formats, as appropriate.

The manuscript should be typewritten using single-spacing, font of 12 Times Roman; on one side of sheet only and in a single column format.

Title

Titles are limited to 150 characters, including spaces. Please avoid the use of any abbreviations, acronyms, or formulae. Titles should clearly reflect the content of the manuscript and any search terms that readers may use should be considered and incorporated.

List of Authors Name

List down all the names of authors (who has contributed to the paper) and the respective affiliations. From the list of authors, place an asterisk (*) next to the corresponding author's name. Provide an official email address of the corresponding author. **Please DO NOT include your personal telephone number on the title page.**

Abstract

Provide an informative 100 to 250 words abstract at the head of the manuscript. This should be a concise reflection of the aims, findings, conclusions and any interesting or important results. Carefully incorporate any terms that may be used by potential interested readers to improve the article's discoverability online (search engine optimisation). The abstract should contain no reference. Abbreviations that are not commonly used should be defined (for the benefit of the non-specialist reader) at first use.

Keywords

These are used for indexing. Please include between 3-5 keywords.

List of Notations

Please provide a list of symbols and definitions used in the text. This will ease our readers.

Introduction

A concise summary of current background knowledge, with reference to relevant previous works in the field should be presented. Please also describe the objectives of and justification for the work contained in the submitted manuscript.

Main Text

The methods and processes applied to investigate and achieve the objectives should be communicated in sufficient detail that readers could repeat the work successfully. The results should be reported clearly and interpreted accurately and analysed thoroughly. Figures/tables can be used to support these results.

It is important that all research articles include a section at the end of the main text that highlights the novelty of the results to the engineering field and any potential applications.

All sections should be numbered in Arabic such as 1, 2, etc. with the title in capitals. Sub-sections should be numbered such as 1.1, 2.3, etc. Numbered all equations in round brackets ( ) flush to the right. The equation should be in the centre.

Style for Illustrations (Tables and Figures)

Try to include the illustrations in between the text. Each illustration must be numbered such as "Figure 1, Figures 2-3, etc." and have a meaningful caption at the bottom. For tables, the caption must be at the top.
On graphs, show only the coordinate axes, or at most the major grid lines, to avoid a dense hard-thread result.

All lettering should be large enough to permit legible reduction of the figure to column width. Typing on figures is not acceptable. Photographs should be glossy prints, of good contrast and gradation and any reasonable size.

Conclusions

A concise summary of the results of case studies or research project papers and the lessons learned should be discussed. If necessary, please elaborate the applicability / relevance of your article to readers in other countries.

Research journals must discuss the practical relevance and potential applications of the engineering work described. This is important to readers working in engineering related practice.

Please also include relevant references to demonstrate how previous engineering research work has been used. These references could be standards, codes or relevant past journal papers.

Appendices

Additional information, such as tables or mathematical derivations can be included. These will be included in the article.

Acknowledgements

Please provide acknowledgement details to those persons or organization that contributed to the paper. Additional details required by funding bodies can be included.

References

The references to other literature that you have cited in your main text should be based on the APA style of referencing (Author, Date) as described below. Please refer https://apastyle.apa.org/ for a detailed guide on the referencing style.

- Single author: (Author, Year) or Author (Year)
- Two authors: (Author 1 & Author 2, Year) or Author 1 and Author 2 (Year)
- Three and more authors: (Author 1 et al., Year) or Author 1 et al. (Year)

In the text, the author and year of the reference should be put in parentheses immediately after the work referred to, for example 'Controlled tests on the Millennium Bridge (Chapman et al., 2005; Murray & Geddes, 1987; Wilby et al., 2011) during which.....' or 'as mentioned by Lim et al. (2018), the NCA derived from the agricultural wastes...'

All references must be listed, in full, at the end of the paper in alphabetical order, irrespective of where they are cited in the text.

In the reference section, the references should be written in full, as follows:

Books: Author 1 surname, author 1 initials, & Author 2 surname, author 2 initials. (Year of publication). Book title. Publisher, City, Country. doi reference. For example:

Kobayashi, K., Khairuddin, A. R., Ofori, G. & Ogunlana, S. (Eds.). (2009). *Joint ventures in construction*. Thomas Telford, London, UK.

Owen, G. & Totterdill, B. (2008). *The dispute board hearing. In Dispute Boards: Procedures and Practice*. Thomas Telford, London, UK.

Journal, magazine and newspaper articles: Author 1 surname, author 1 initials, & Author 2 surname, author 2 initials. (Year of publication). Paper title. Journal title, Volume (Issue number), First page-Last page. doi reference. Unpublished papers and theses should not be cited as they are not readily available.

Lim, J. L. G., Raman, S. N., Lai, F. C., Zain, M. F. M., & Hamid, R. (2018).

Synthesis of nano cementitious additives from agricultural wastes for the production of sustainable concrete. *Journal of Cleaner Production*, 171, 1150-1160. https://doi.org/10.1016/j.jclepro.2017.09.143.

Soon, F. C., Khaw, H. Y., Chuah, J. H., & Kanesan, J. (2018). Hyper-

parameters optimisation of deep CNN architecture for vehicle logo recognition. *IET Intelligent Transport System*, 12(8), 939-946. https://doi.org/10.1049/iet-its.2018.5127.

Conference proceedings: Author 1 surname, author 1 initials, & Author 2 surname, author 2 initials. (Year of publication). Paper title. Proceedings title, Volume (Issue number), First page-Last page. doi reference. Unpublished conference proceedings (i.e. that were only given to delegates) should not be cited as they are not generally available.

Chuah, J. H., Khaw, H. Y., Soon, F. C., & Chow, C. (2017). Detection of Gaussian noise and its level using deep convolutional neural network. *Proceedings of the TENCON 2017 - 2017 IEEE Region 10 Conference*, 2447-2450. https://doi.org/10.1109/TENCON.2017.8228272.

Unpublished material should not be included in the Reference list.

Please refer to https://apastyle.apa.org/ for a detailed guide on the referencing style. Authors should strictly adhere to the referencing style specified herein.

Mathematical Equations

Only relevant equations should be included in the main text and should be numbered. An equation editor program can be used to type in a formula.

Figures and tables caption list: Please supply a figure caption list at the end of your journal paper. Figures and tables must be put in the text in consecutive order. All figures must have a brief title accompanied with a short description.

Brief Profile

At the end of the manuscript, each author should provide a brief profile (less than 150 words), together with recent photographs (preferable less than 3 MB).

Corresponding Authors

We only permit one corresponding author per submission.

Conflict of Interest

Conflict of interest occurs when an author (or the author's institution) has personal or financial relationships that inappropriately influence the statements in the publication. Authors should ensure that publications will be written in an unbiased, ethical and responsible manner. The authors working on any sponsored engineering work or publications should declare such work under Conflict of Interest during submission.

Submission of Paper

Authors are required to submit via the IEM Online Journal Submission

(OJS) through the following link:

https://iemjournal.com.my/index.php/iem/about/submissions.

Together with the manuscript, the corresponding author should

enclose a cover letter containing the significance of the paper, the postal and email address, and telephone number for correspondence. In the cover letter, kindly provide four (4) names as reviewers. The selected reviewers must have the relevant knowledge and research experience. Provide the reviewers postal and email addresses and telephone numbers (if possible).

Further Enquiries

For further enquires, please contact Secretariat at the address shown below:

The Institution of Engineers, Malaysia
Bangunan Ingenieur, Lots 60 & 62, Jalan 52/4
Peti Surat 223 (Jalan Sultan), 46720 Petaling Jaya, Selangor Darul Ehsan
Tel: 03–78900130 Fax: 03–79577678
E-mail: pub@iem.org.my or iemjournal@gmail.com

The Institution of Engineers, Malaysia

Bangunan Ingenieur, Lots 60/62, Jalan 52/4, Peti Surat 223 (Jalan Sultan), 46720 Petaling Jaya, Selangor Darul Ehsan
Tel: 03-78900130 Fax: 03-79577678 E-mail: sec@iem.org.my IEM Homepage: http://www.myiem.org.my

REFEREES FOR VETTING OF IEM PUBLICATIONS

Dear IEM Members/Readers,

The Standing Committee on Information and Publications is revising the list of referees to assist in the vetting of articles received from members and non-members. The referees should preferably be at least Corporate Members of The Institution or graduates with higher degrees.

The aim of appointing the referee is to ensure and maintain a standard in the IEM Publications namely the bulletin and the Journal.

Members who are interested to be placed in the database of referees are to return the registration form to the IEM Secretariat, providing details of their degrees and particular expertise and experience in the engineering fields.

We need your services to look into the vetting of articles received for Publications and due acknowledgement would be announced yearly in the Bulletin. Referees must be committed to return the papers within a month from date of appointment.

Chairman
Standing Committee on Information and Publications

All correspondences are to be addressed to: -

The Chief Editor
Standing Committee on Information and Publications
The Institution of Engineers, Malaysia
Bangunan Ingenieur, Lots 60 & 62, Jalan 52/4
P.O. Box 223 (Jalan Sultan)
46720 Petaling Jaya
Selangor Darul Ehsan

Email: pub@iem.org.my

AREAS OF INTEREST FOR VETTING OF PAPERS

Please tick (√) the appropriate area of interest that you are able to vet the papers.

- □ Acoustics
- □ Engineering Education
- □ Military Vehicles
- □ Room Temperature
- □ Aerodynamics
- □ Environmental Engineering
- □ Mini Pressure Meters
- □ Safety Engineering
- □ Air Conditioning
- □ Fine Chemical
- □ Mining Engineering
- □ Scaffolding Works
- □ Air Pollution Control
- □ Finite Element
- □ Naval Architecture
- □ Seepage
- □ Aircraft
- □ Fire Detection
- □ Navigation
- □ Sewerage
- □ Airport Engineering
- □ Fire Engineering
- □ Oil & Gas Engineering
- □ Shipbuilding
- □ Aluminium Design
- □ Floods
- □ Operation Research
- □ Signal Processing
- □ Arbitration
- □ Food Processing
- □ Palm Oil Industries
- □ Solar Energy Technology
- □ Automation
- □ Foundation Engineering
- □ Petrochemicals
- □ Steelworks Design
- □ Automotive Engineering
- □ Fuzzy Logic
- □ Petroleum Engineering
- □ Stream Turbine Power Plant
- □ Biochemical Engineering
- □ Gas Engineering
- □ Pharmaceuticals
- □ Sructural Analysis
- □ Biotechnology
- □ Geotechnical
- □ Piling
- □ Structural Rehabilitation
- □ Boiler Engineering
- □ Heat Exchanger
- □ Plumbing Engineering
- □ Survey Engineering
- □ Bridge Engineering
- □ Highway
- □ Pollution Control
- □ Taligates
- □ Building Services
- □ Hydraulics
- □ Ports & Harbour Engineering
- □ Telecommunication
- □ Coastal Engineering
- □ H.V. Electrical Distribution
- □ Power Electronics
- □ Thermal Engineering
- □ Co-Generation
- □ Industrial Engineering
- □ Power Generation
- □ Timber Design
- □ Computer Engineering
- □ Industrial Transport
- □ Pressure Vessels
- □ Tool Engineering
- □ Concrete Design
- □ Industrial Ventilation
- □ Prestressed Concrete
- □ Transfer Tunnels
- □ Concrete Technology
- □ Information Technology
- □ Project Management
- □ Transportation Engineering
- □ Construction Management
- □ Instrumentation
- □ Public Administration
- □ Urban Planning
- □ Control Engineering
- □ Lighting System
- □ Public Health Engineering
- □ Vehicles
- □ Drainage Engineering
- □ L.V. Electrical Distribution
- □ Quarry Engineering
- □ Vertical Transportation
- □ Dynamics Design
- □ Manufacturing
- □ Railways
- □ Waste Treatment
- □ Earthworks
- □ Mass Transit
- □ Reclamation Works
- □ Waste Water
- □ Edible Oil Refining
- □ Mechanical Handling Equipment
- □ Refrigeration
- □ Water Resources Engineering
- □ Electrical Transmission
- □ Management
- □ Reinforced Concrete Beams
- □ Water Pollution Control
- □ Electrochemical
- □ Metal Fabrication
- □ Road Transport
- □ Wind Engineering
- □ Electrotechnology
- □ Metallurgy
- □ Robotics
- □ Others (please specify)
- □ Energy Technology
- □ Micro Electronics
- □ Roof Structures

DISCIPLINES / SUB-DISCIPLINES OF VETTER

Please tick (√) the appropriate boxes.

- □ Aerospace
- □ Electrical
- □ Marine
- □ Petroleum
- □ Aeronautical
- □ Electronics
- □ Mechanical
- □ Production
- □ Agricultural
- □ Environmental
- □ Mining
- □ Structural
- □ Chemical
- □ Industrial
- □ Naval Architecture
- □ Others (Please specify)

VETTER'S DETAILS

Name : _____

Membership No. : _____ *(if applicable)*

Grade : ☐ Graduate ☐ Member ☐ Fellow ☐ Affiliate ☐ Others

(please specify) _____

Qualifications : _____

Addresses : *(Office)* _____

_____

(Residence) _____

_____

Contact No. : _____ *(Handphone)* _____ *(Office)* _____ *(Residence)*

E-mail Address : _____

Please mail all correspondences to the below. Please tick (√) the appropriate boxes.

Mail to : ☐ Office ☐ Residence

Brief Biodata (not longer than 50 words) (to be appended with this Reply Slip).

_____

_____

_____

_____

_____

Have you ever reviewed submissions for publication in any Journal(s) before? ☐ Yes ☐ No

If YES, name the Journal(s) _____

Do you have papers published in any Journal(s)? ☐ Yes ☐ No

If YES, name the Journal(s) _____

Date: _____ Signature : _____

IEM BRANCHES

PENANG	IEM PENANG BRANCH SECRETARIAT 1-04-02 E-Gate, Lebuh Tunku Kudin 2, 11700 Gelugor, Pulau Pinang	Tel: 04-606 599 iempenangbranch@gmail.com http://iempenang.org
SOUTHERN	IEM SOUTHERN BRANCH SECRETARIAT 24-B, Jalan Abiad, Taman Tebrau Jaya, 80400 Johor Bahru, Johor Darul Takzim	Tel: 07-331 9705 Fax: 07-331 9710 iemsouthern@gmail.com www.iemsb.org.my
PERAK	IEM PERAK BRANCH SECRETARIAT No. 60B, Jalan Lapangan Siber 1, Bandar Cyber (Business Centre), 31350 Ipoh, Perak Darul Ridzuan	Tel: 05-313 8459 iemperakbranch@gmail.com
TERENGGANU	IEM TERENGGANU BRANCH SECRETARIAT 23-05, KT Business Centre, Padang Hiliran, Jalan Sultan Mohamad, 21100 Kuala Terengganu	Tel: 09-620 4500 Fax: 09-620 4502 iemterengganu@gmail.com
NEGERI SEMBILAN	IEM NEGERI SEMBILAN BRANCH SECRETARIAT No. 77-A-1, Lorong Haruan 5/3, Oakland Commerce Square, 70300 Seremban, Negeri Sembilan	Tel: 06-631 1011 Fax: 06-631 4619 iemnsembilan@gmail.com www.iemns.org.my
MELAKA	IEM MELAKA BRANCH SECRETARIAT C/O Sri Perunding Consulting Engineers, No. 2, Jalan Malinja 2, Taman Malinja Bukit Baru, 75150 Melaka	Tel: 06-284 8028 Fax: 06-283 8919 spcesb@gmail.com
SARAWAK	IEM SARAWAK BRANCH SECRETARIAT International Engineering Centre (IntEC), A2-G-19 & A2-1-19, Isthmus Raintree Square, Lot 3249, MTLD Block 7, Jalan Keruing, 93450 Kuching, Sarawak	Tel: 06-284 8028 Fax: 06-283 8919 spcesb@gmail.com
SABAH	IEM SABAH BRANCH SECRETARIAT Lot 25, 3rd Floor, Block C, Damai Point Commercial Centre, Lorong Damai Point, Off Jalan Damai, 88100 Kota Kinabalu, Sabah	Tel: 088-259 122 Fax: 088-236 749 iemsabah@gmail.com www.iemsabah.org.my
MIRI	IEM MIRI BRANCH SECRETARIAT 2nd Floor, Unit 14 (906-3-14), Soon Hup Tower Complex, (Mega Hotel), Jalan Merbau, 98000 Miri Sarawak	Tel: 085-423 718 Fax: 085-424 718 iem.miri@gmail.com www.iem-miri.org.my
KEDAH / PERLIS	IEM KEDAH / PERLIS BRANCH SECRETARIAT No. 164, Tingkat 2, Kompleks Alor Setar, Lebuhraya Darul Aman, 05100 Alor Setar, Kedah Darul Aman	Tel: 04-734 3420 Fax: 04-733 3962 iemckps@gmail.com
PAHANG	IEM PAHANG BRANCH SECRETARIAT No. 114, Block F, Lorong Seri Teruntum, Medan Warisan, 25100 Kuantan, Pahang Darul Makmur	Tel: 019-855 6509 Fax: 09-514 6493 iempahang@gmail.com
KELANTAN	IEM KELANTAN BRANCH SECRETARIAT Lot 5139, Kompleks Niaga INOtrus Kawasan Perindustrian Pengkalan Chepa II, 6100 Kota Bharu, Kelantan	Tel: 09-773 0899 Fax: 04-733 3962 iemckps@gmail.com

IEM
The Institution of Engineers, Malaysia

THE INSTITUTION OF ENGINEERS, MALAYSIA
Bangunan Ingenieur, Lots 60 & 62, Jalan 52/4, P.O. Box 223 (Jalan Sultan),
46720 Petaling Jaya, Selangor Darul Ehsan.
Tel: 03-7890 0130 | Fax: 03-7957 7678 | E-mail: sec@iem.org.my

www.myiem.org.my